

Review

# Titania-Clay Mineral Composites for Environmental Catalysis and Photocatalysis

Ewa M. Serwicka 

Jerzy Haber Institute of Catalysis and Surface Chemistry, Polish Academy of Sciences, Niezapominajek 8, 30-239 Krakow, Poland; ncserwic@cyf-kr.edu.pl; Tel.: +48-12-6395-118

**Abstract:** The use of titania-based composite materials in the field of heterogeneous catalysis and photocatalysis has a long and rich history. Hybrid structures combining titania nanoparticles with clay minerals have been extensively investigated for nearly four decades. The attractiveness of clay minerals as components of functional materials stems primarily from their compositional versatility and the possibility of using silicate lamellae as prefabricated building blocks ready to be fitted into the desired nanoconstruction. This review focuses on the evolution over the years of synthetic strategies employed for the manufacturing of titania–clay mineral composites with particular attention to the role of the adopted preparative approach in shaping the physical and chemical characteristics of the materials and enabling, ultimately, tuning of their catalytic and/or photocatalytic performance.

**Keywords:** titania; clay; composite; catalysis; photocatalysis; catalyst design; air pollution; water pollution



**Citation:** Serwicka, E.M.

Titania-Clay Mineral Composites for Environmental Catalysis and Photocatalysis. *Catalysts* **2021**, *11*, 1087. <https://doi.org/10.3390/catal11091087>

Academic Editors: Lucjan Chmielarz and Roman Dziembaj

Received: 26 July 2021

Accepted: 4 September 2021

Published: 9 September 2021

**Publisher's Note:** MDPI stays neutral with regard to jurisdictional claims in published maps and institutional affiliations.



**Copyright:** © 2021 by the author. Licensee MDPI, Basel, Switzerland. This article is an open access article distributed under the terms and conditions of the Creative Commons Attribution (CC BY) license (<https://creativecommons.org/licenses/by/4.0/>).

## 1. Introduction

The use of titania-based composite materials in the field of heterogeneous catalysis and photocatalysis has a long and rich history. The importance of titania in industrial catalyst design was recognized at the end of the 1960s, when the patent assigned to BASF [1] marked a successful application of a TiO<sub>2</sub>-supported vanadia system for the synthesis of phthalic anhydride by the selective oxidation of *o*-xylene. A large number of related patents and open literature studies followed in the next decades [2]. Several other processes of industrial interest, employing TiO<sub>2</sub>-based catalysts, have been identified, including the selective catalytic reduction (SCR) of NO<sub>x</sub>, which is a reaction of major importance for air pollution control, enabling the removal of NO<sub>x</sub> from combustion flue gases [3–5]. The mixed oxide catalytic formulations for this process, with NH<sub>3</sub> as a reductant, first developed by Japanese scientists in the 1970s, contained titania as the dominant component and at least one other oxide such as, e.g., V<sub>2</sub>O<sub>5</sub>, MoO<sub>3</sub>, WO<sub>3</sub>, or Fe<sub>2</sub>O<sub>3</sub>. SCR catalysts of this type are widely applied worldwide and continue to be a subject of scientific studies [6–8]. Another worth mentioning field of titania application emerged after discovery, by Haruta et al. [9], of the remarkable catalytic activity displayed by gold nanoparticles supported on metal oxides. Such catalysts can oxidize CO at subambient temperature, and the Au/TiO<sub>2</sub> system, which belongs to the most active catalysts for this reaction, is the most studied one [10,11].

Photocatalysis is another major field of titania application. Following the breakthrough report by Fujishima and Honda in 1972 [12] on water splitting upon the illumination of TiO<sub>2</sub> photoelectrode, the photocatalytic reactions based on the interaction of a solid, semi-conducting catalyst and solar light have attracted great interest as an efficient, economical, and green technology with enormous future potential [13]. The target reactions range from hydrogen generation to hydrocarbon synthesis from CO<sub>2</sub>, to abatement of pollutants and bacteria in a variety of environments [14–18]. TiO<sub>2</sub> is by far the most widely studied photocatalyst because it displays high photocatalytic activity, and it is also chemically and thermally stable, nontoxic, and inexpensive.

It should be noted that in the catalytic applications, titania is generally used as a catalyst support. This is primarily due to the unique combination of relative chemical inertness and resistance to poisoning, with the ability to interact with the supported active phase [19,20]. On the other hand, in photocatalysis, titania acts as the actual catalyst, because the photocatalytic action depends on the intrinsic semiconducting characteristics of  $\text{TiO}_2$ , enabling the generation of charge carriers (holes and electrons) upon the band-gap illumination.

It is known that oxide nanoparticles can exhibit physical and chemical properties different from those of a bulk solid [21]. This is, essentially, due to the high surface to volume ratio and a high density of coordinatively unsaturated corner or edge surface centers. As a consequence, oxide stoichiometry, structural and electronic characteristics, the degree of metal–oxygen bond covalency, arrangement of surface atoms, and related properties, such as, e.g., acido-basicity, may all be modified. These features render nanoparticles extremely attractive for the use in catalysis and photocatalysis.

However, there are challenges in the practical application of nanoscale particles associated with the difficulty in their separation and recovery from the reaction medium, the tendency to form agglomerates at higher concentrations, or enhanced susceptibility to sintering at elevated temperatures [22,23]. These obstacles can be overcome by the immobilization of nanoparticles onto appropriate supports, which is the approach extensively explored in the design of titania-based systems.

Among the variety of inorganic and organic matrices that have been investigated as carriers for  $\text{TiO}_2$  nanoparticles, such as, e.g., silica, zeolites, glass, carbonaceous materials, or organic polymers [24], clay minerals have attracted particular attention as components of  $\text{TiO}_2$ -based composites, and various aspects of their catalytic and photocatalytic applications have been reviewed over the years [25–34]. First, the natural clay minerals display an excellent combination of advantageous properties, such as non-toxicity, low cost, and easy availability, and they are particularly desirable from the point of view of green chemistry-oriented processes. Second, the materials are characterized by unique structures consisting of stacked nanometer-thick layers, which may be used in advanced materials syntheses as prefabricated building blocks, ready to be fitted into a desired construction. Third, clay mineral surfaces may physisorb and/or chemisorb the reactants [35], increasing thereby their concentration in the vicinity of immobilized nanoparticles and, as a consequence, enhancing the efficiency of the catalytic or photocatalytic process.

The fact, that appropriate manipulation of the clay mineral lamellae enables the engineering of sophisticated functional nanostructures fits into the most recent trend in materials design referred to as nanoarchitectonics [36]. The approach touts a resourceful manipulation of nanoscale building blocks, which is backed by in-depth understanding of the interactions between the employed structural elements. Noteworthy, the preparation of metal oxide–clay nanocomposites in the 1970s [37], known as pillared interlayered clays (PILC) and described in detail further, is very likely the earliest example of such an approach, which was accomplished long before the term “nanoarchitectonics” was coined.

Air and water pollution is not only a serious environmental concern of today, but it also casts a long shadow over the future generations. Among various remediation efforts, the use of catalytic and photocatalytic methods is recognized as a particularly powerful tool, making research and development in this area a worldwide imperative. This review focuses on the aspect related to the evolution of strategies employed for the manufacturing of titania–clay mineral composites for the catalytic and photocatalytic removal of environmental contaminants, with particular attention to the role of the adopted preparative approach in shaping the physical and chemical characteristics of the materials, and in enabling, ultimately, tuning of their catalytic and/or photocatalytic performance. The discussed catalytic applications concentrate on the selective catalytic reduction of nitrogen oxides and the total oxidation of volatile organic compounds. The reviewed photocatalytic processes encompass the decontamination of water polluted with dyes,

phenolic compounds, and emerging pollutants, as well as the photodegradation of volatile organic compounds and  $\text{NO}_x$ .

## 2. Clay Mineral Components

The clay minerals considered in this review belong to the family of phyllosilicates, which are the most abundant silicates formed at the Earth's surface. "Phyllo" in Greek means "leaf", so the term phyllosilicate reflects the most characteristic feature of these minerals—the layered structure. Phyllosilicate layers are built of an Si-based tetrahedral (T), and an Al(Mg, Fe)-based octahedral (O) sheet combined in either a 1:1 (TO layer type) or 2:1 (TOT layer type) proportion (Figure 1) [38]. In TO clay minerals, the layer charge is commonly close to zero, but in TOT structures, the isomorphous substitution of a T and/or an O cation by a lower valent cation may occur, resulting in a negative layer charge. In such cases, structure neutrality is ascertained by the presence of compensating cations in the interlayer space. Short descriptions of the selected clay minerals most frequently used in the design of nanocomposites are given below.

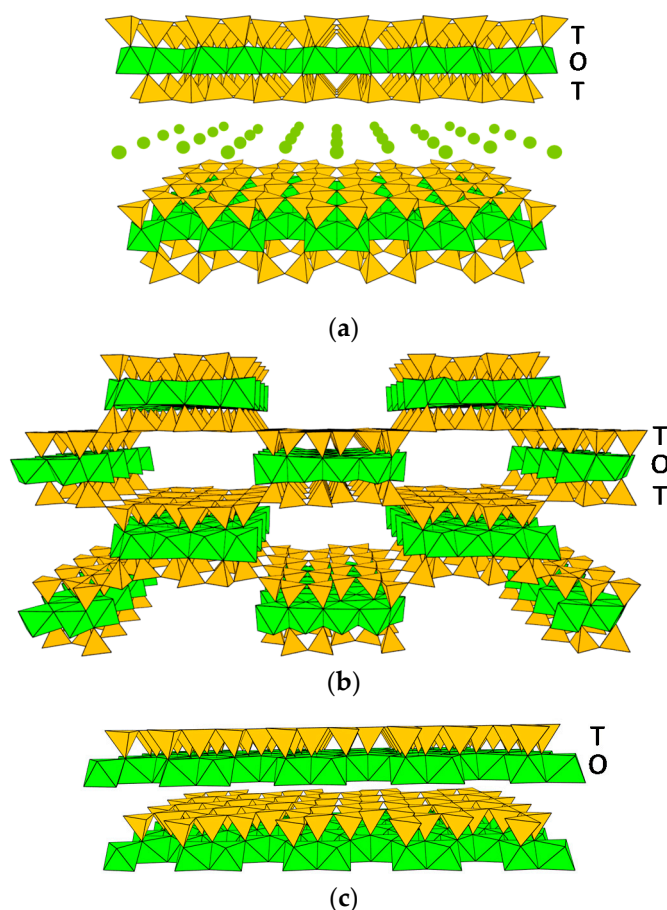


**Figure 1.** Structures of selected phyllosilicates: (a) montmorillonite; (b) sepiolite; (c) kaolinite; TOT or TO sheet arrangements are indicated.

The clay minerals most frequently used in the design of nanocomposites belong to the group of smectites, which are characterized by the TOT layer type. The smectite unit cell contains six octahedral and eight tetrahedral sites. When an octahedral sheet is based on trivalent Al cations, only two-thirds of the octahedral sites are occupied, and the corresponding structures are referred to as dioctahedral. If divalent Mg is the structure-forming element, then all six octahedral sites are occupied, and the smectite is called trioctahedral. As a result of isomorphous substitution, the smectite layers are negatively charged and carry 0.2–0.6 elementary charge per half unit cell. Two features make smectites

particularly attractive for structural modifications: (a) the presence of easily exchangeable hydrated cations in the interlayer and (b) the ability to swell, i.e., to increase the interlayer distance, due to the adsorption of water in the interlayer, leading, in the extreme, to clay mineral disassembly into single layers.

Montmorillonite, which is the most investigated member of the smectite group, consists of layers built of two tetrahedral Si sheets sandwiching an octahedral Al-based sheet (Figure 1a) [39]. The silicon–oxygen tetrahedra in the T sheet are linked by sharing three corners with neighboring tetrahedra, resulting in a hexagonal network. The fourth corner of each tetrahedron is shared with an octahedron in the adjacent O sheet. Thus, two of the six coordination sites in each octahedron are taken by oxygens, while the four remaining positions are occupied by hydroxyl groups. Partial isomorphous substitution of  $\text{Al}^{3+}$  by  $\text{Mg}^{2+}$  in the octahedral sheet generates a negative charge on the clay layers, which is balanced by the presence of cations in the interlayer space. Electrostatic attraction between the layers and interlayer cations is the primary force responsible for the assembly of a layered structure. In untreated montmorillonite, the interlayer is occupied mainly by hydrated  $\text{Na}^+$  and/or  $\text{Ca}^{2+}$ . As a result of the relatively low layer charge (ca. 0.2 e), montmorillonite can easily swell with the influx of water into the interlayer. The layered structure of montmorillonite is reflected in the morphology of its grains (Figure 2a). Montmorillonite is the dominant mineral component of the clay rock known as bentonite.

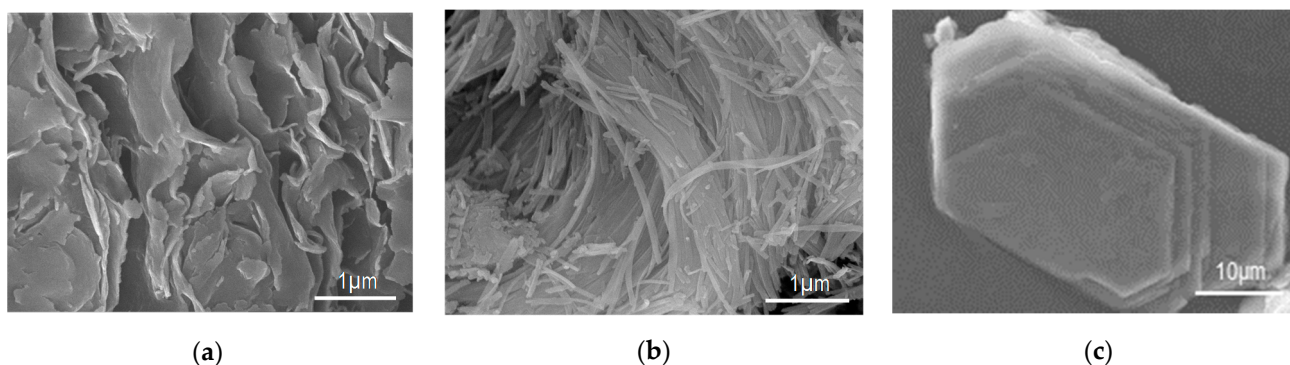


**Figure 2.** SEM images of: (a) montmorillonite; (b) sepiolite; (c) kaolinite.

Other smectites that have been used in the preparation of  $\text{TiO}_2$ –clay mineral composites include beidellite, hectorite (natural and synthetic), or saponite. Their structure is similar to that of montmorillonite as far as TOT sheet arrangement and the presence of interlayer cations is concerned, but they differ in layer composition and the localization of the isomorphous substituents responsible for the negative layer charge [40]. Thus, in beidellite, which, similarly to montmorillonite, contains an Al-based octahedral sheet, the layers acquire a negative charge due to the partial replacement of  $\text{Si}^{4+}$  in the tetrahedral sheet with  $\text{Al}^{3+}$ . In hectorite and saponite, the octahedral sheet is based on Mg, but in the former, the layer charge stems from the replacement of some octahedral  $\text{Mg}^{2+}$  with  $\text{Li}^+$ , while in the latter, it originates from the substitution of certain amount of tetrahedral  $\text{Si}^{4+}$  with  $\text{Al}^{3+}$ . In reality, some tetrahedral substitution occurs also in montmorillonite and hectorite, as well as the octahedral one in beidellite and saponite, so that mineral classification depends on the prevailing type of isomorphous replacement.

In some cases, vermiculite, a hydrous phyllosilicate mineral that undergoes significant expansion and exfoliation when heated, was used for the synthesis of composites with titania [40]. As in smectite, the 2:1 layers of vermiculite are separated by interlayer hydrated cations, but the layer charge is larger than in smectite. Occasionally, the composites design was based on the use of non-swelling TOT phyllosilicates, with still higher layer charge and  $\text{K}^+$  in the interlayer, such as micas or illite [40].

Another group of TOT-type clay minerals, which are perhaps less known but very attractive for materials design, consists of sepiolite and palygorskite (also known as att-

pulgite). Both minerals are built of 2:1 phyllosilicate ribbons with a Mg-based octahedral sheet arranged in staggered rows separated by tunnels, as illustrated in Figure 1b by the example of sepiolite [41]. The ribbon width is made up of six tetrahedra in sepiolite and of four tetrahedra in palygorskite, so that the effective cross-section of the tunnels is  $10.6 \times 3.7 \text{ \AA}$  and  $6.4 \times 3.7 \text{ \AA}$ , respectively. Neighboring ribbons are connected to each other through an inverted Si–O–Si bond, which results in a continuity of the tetrahedral sheet, as opposed to the discontinuous octahedral sheet. The unique tunnel structures are the cause of the fibrous morphology (Figure 2b), microporosity, and high specific surface area of both minerals.

In addition to the TOT-type clay minerals, also the TO 1:1-type structures, such as kaolinite and halloysite, have been investigated as components of hybrids with titania. Kaolinite, an abundant soil constituent, has a structure composed of stacked layers built of one tetrahedral silicate sheet condensed with one aluminium octahedral sheet (Figure 1c). Layers are held together by hydrogen bonding between octahedral basal oxygen and tetrahedral hydroxyl in the opposite layer [40]. The layered structure impacts the morphology, and kaolinite is characterized by plate-like particles (Figure 2c). Halloysite, which has the same layer composition and 1:1 structure, may be regarded as a hydrated kaolinite, with a monolayer of water occupying the interlayer [40]. As a result, hydrated halloysite has a basal spacing larger than that of kaolinite (ca. 10 and 7 Å, respectively). In a TO layer, there is a misfit between the smaller octahedral and larger tetrahedral sheet. In the case of halloysite, where interlayer bonding is weakened by the presence of water, layers show the tendency to roll. For this reason, in nature, most of the hydrated halloysite shows a unique tubular morphology.

In the composite synthesis, the clay mineral components may be used either in their natural form, or they may be the subject of pretreatment, which is usually aimed at (a) homogenizing the mineral composition, (b) maximizing the surface area available for TiO<sub>2</sub> nanoparticles deposition, (c) making the interlayer more available for intercalation of Ti precursor, or (d) modification of the clay surface to promote the anchoring of Ti species. The most common methods enabling realization of the above goals include the preparation of a homoionic form, preswelling/delamination of clay mineral, transformation into organo-derivatives, acid activation, and functionalization of the clay mineral surface [26,29,30,33,34,42].

### 3. Titania Nanoparticles

Titanium dioxide occurs in nature in three polymorphic forms: rutile (tetragonal), anatase (tetragonal), and brookite (orthorhombic). Their crystal lattices are built of TiO<sub>6</sub> octahedra, which in anatase are connected by edge-sharing, while in rutile and brookite, both corner- and edge-sharing co-exist (Figure 3). Under ambient conditions, macrocrystalline rutile is the most stable form, while anatase and brookite are metastable and transform to rutile upon thermal treatment. However, Zhang and Banfield [43] demonstrated that the thermodynamic stability is particle-size dependent, and for crystallites of less than ca. 14 nm diameter, anatase becomes more stable than rutile. In accordance with this finding, TiO<sub>2</sub> nanoparticles tend to crystallize in the anatase structure.

There are, essentially, two major approaches to the incorporation of TiO<sub>2</sub> nanoparticles into the clay mineral matrix. The more common one consists of a one-pot synthesis, in which TiO<sub>2</sub> nanoparticles are generated in situ, in the presence of clay mineral suspension. In the other procedure of TiO<sub>2</sub>–clay mineral hybrid preparation, the pre-formed TiO<sub>2</sub> nanoparticles (either laboratory synthesized or commercial) are mixed with appropriately pretreated clay mineral component.

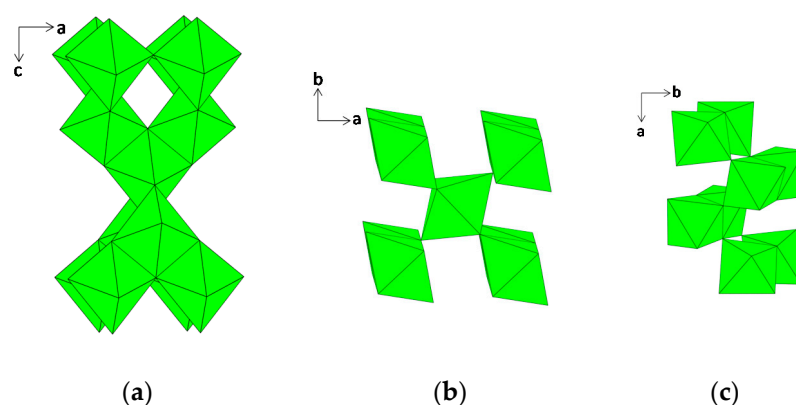


**Figure 3.** Structures of titania polymorphs: (a) anatase; (b) rutile; (c) brookite.

The most widespread method of  $\text{TiO}_2$  nanoparticles preparation involves a sol–gel method based on the controlled hydrolysis of Ti(IV) compounds. Although currently the majority of works describe the use of titanium alkoxides as precursors of titania species, the first reported synthesis of  $\text{TiO}_2$ –clay mineral composite, a Ti-pillared montmorillonite, involved the hydrolysis of an inorganic precursor,  $\text{TiCl}_4$ , for the generation of Ti pillars [44]. The first use of Ti alkoxide hydrolysis for the preparation of titania pillars was reported one year later [45]. From the very beginning, it was noted that the course of hydrolysis and the properties of the resulting composites were very sensitive to the reaction conditions, such as temperature, pH, concentration of the reactants, aging, etc. On one hand, this variability represented a challenge in the materials synthesis, but on the other, it enabled the optimization of physicochemical characteristics of composites for the purpose of potential applications.

#### 4. $\text{TiO}_2$ –Clay Mineral Composites

The nature of the clay mineral component plays a key role in determining the final nanoarchitecture of the composite. When smectite clay minerals, such as montmorillonite or hectorite, are used in the preparation of  $\text{TiO}_2$ -bearing hybrids, and the cation exchange and swellability are the driving forces in composite formation, two essentially different types of structures may arise. In the first case, the  $\text{TiO}_2$  nanoparticles or Ti precursor species enter the interlayer, and the layers are pushed apart, sometimes very significantly, but the stacked arrangement of layers is retained. Such materials are referred to as pillared interlayered clays (PILC). The other type of structure develops when the smectite layers become exfoliated and lose their long-range spatial order, while  $\text{TiO}_2$  nanoparticles adhere to the surfaces of separated lamellae. This type of nanoarchitecture is referred to as a house of cards arrangement. When non-swelling clay minerals are used, e.g., kaolinite or palygorskite, yet another type of structure is the usual outcome. There, the interlayer is not easily accessible for guest species, the layers are not prone to exfoliation, and titania nanoparticles become attached to the external surfaces of clay mineral. This type of structure may also be formed with the participation of smectites, either in addition to the interlayer loading, or exclusively, if the synthesis conditions prevent involvement of the interlayer. All three types of  $\text{TiO}_2$ –clay mineral composites have been investigated for their catalytic and photocatalytic properties. The overwhelming majority of works addressed the smectite-derived hybrids, and in this area, the most creative synthetic approaches have been developed.

#### 5. $\text{TiO}_2$ –Clay Mineral Composites for Catalytic Applications

The innovative idea of clay pillaring, also referred to as cross-linking, appeared in the 1970s as a result of market-driven research in the field of catalysis. The rocketing oil prices caused by the 1973 oil crisis forced the petrochemical industry to search for catalysts capable of cracking heavy fractions of oil, for which the conventional FCC (fuel catalytic

cracking) zeolitic catalysts were not suitable due to too narrow pores [38]. As an alternative to designing large-pore zeolite systems, the ingenious idea of engineering porous structures from two-dimensional silicate building blocks emerged. The essence of this discovery has been described in a series of patents, of which the first one, by Vaughan et al. [46], defined the synthetic approach leading to a new class of porous solids, called pillared interlayered clays (PILC). The concept of pillaring is based on the finding that large inorganic polymeric oxy-hydroxy cationic species, derived from the partial hydrolysis of multivalent cations, e.g.,  $\text{Al}^{3+}$ ,  $\text{Zr}^{4+}$ , or  $\text{Ti}^{4+}$ , can replace the common interlayer cations by means of cation exchange. The resulting solids have expanded interlayers and, after thermal treatment, form rigid structures in which metal oxide species referred to as “pillars” hold the layers apart and generate thereby zeolite-like pore network in the interlayer. The pillaring process is schematically illustrated in Figure 4.

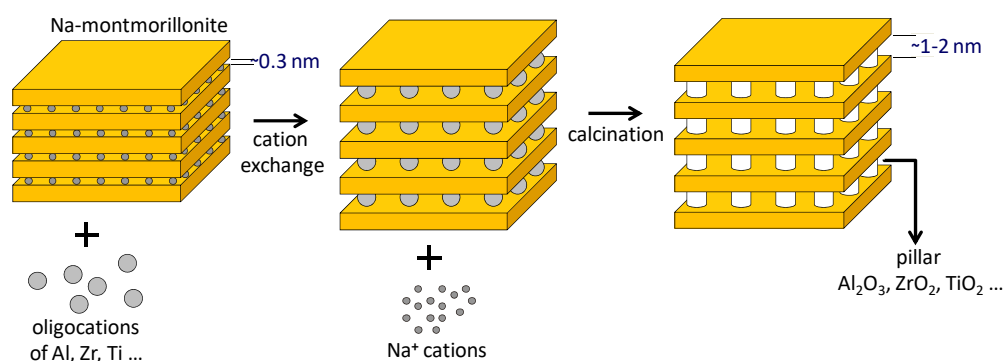


**Figure 4.** Schematic illustration of clay pillaring process.

The pillaring of montmorillonite with Ti species has been first described by Sterte [44], who used for intercalation polymeric Ti cations formed by the partial hydrolysis of  $\text{TiCl}_4$  in HCl. The  $\text{TiO}_2$  pillars formed upon calcination were poorly crystalline, but nucleation of the anatase structure was indicated. The prepared Ti-PILC solids possessed significant specific surface areas (SSA) of 200–350  $\text{m}^2/\text{g}$  and an interlayer gallery height of 1.8 nm, i.e., considerably larger than reported for other PILC systems, based on, e.g., the intercalation of Al or Zr polycations. Shortly afterwards, an alternative synthetic methodology has been described by Yamanaka et al. [45]. The major difference consisted in the use of titanium tetraisopropoxide as a precursor of the pillaring species. The alkoxide was subjected to hydrolysis followed by peptization with HCl solution, and the obtained titania sol underwent facile ion exchange with montmorillonite interlayer cations, which indicated that the sol particles were positively charged. The SSA of the pillared products were about 300  $\text{m}^2/\text{g}$ , i.e., similar as in the method of Sterte, but the pillar height in the range 1.4–1.7 nm was somewhat lower, and the pillars themselves appeared amorphous to X-rays. Both papers proved truly seminal, because up to the present time, most syntheses of Ti-pillared clays involve either the hydrolysis of  $\text{TiCl}_4$  e.g., [46–57] or an alkoxide e.g., [58–69]. The authors of both works pointed to the possibility of tailoring the materials’ SSA and porosity by adjusting such synthesis parameters as, e.g., the concentration of Ti precursor, the amount of HCl, aging of the pillaring solution, or the temperature of heat treatment. Later, it was recognized that the nature of alkoxide is also an important variable [60]. In general, the conditions of the Ti precursor hydrolysis are of paramount importance; hence, over the years, a number of procedural modifications related mainly to this step have been proposed for both synthetic routes. For instance, the synthesis variant designed by Lin et al. [47], consisting of the preparation of  $\text{TiCl}_4$  solution in ethanol and inducing hydrolysis with a solution of glycerin and water, found a number of followers e.g., [49,56,57]. On the other hand, an undoubtedly resourceful but technically more demanding approach, consisting of the intercalation of titanium isopropoxide dissolved in supercritical  $\text{CO}_2$  into an organoclay interlayer followed by hydrolysis with adsorbed water present in the interlayer space, proposed by Yoda et al. [70], failed to gain widespread popularity. The nature of polymeric

Ti pillaring species is still not exactly established. Einaga [71] suggested that during  $\text{TiCl}_4$  hydrolysis in a strongly acidic environment, a polymeric  $[(\text{TiO})_8(\text{OH})_{12}]^{4+}$  complex is formed, while Comba and Merbach [72] postulated the existence of trimeric and tetrameric species. Yamanaka et al. [45] described the polycondensed Ti species as positively charged sol particles and suggested that their size may be controlled by the extent of sol peptization. More recently, Bahranowski et al. [54] argued that the amount of intercalated  $\text{TiO}_2$  was higher than would be expected for complete exchange of the parent clay with Einaga's complex, and that polycondensed Ti cations larger than octamers were likely to act as pillaring species.

Of the two preparation routes, the one based on  $\text{TiCl}_4$  hydrolysis is more cumbersome, because the reaction is highly exothermic and releases fumes of HCl upon contact of the reactant with atmospheric moisture. Moreover, the pillaring solution is strongly acidic, which causes the leaching of metal elements from the clay layer, mainly Mg and Al [73]. The hydrolysis of alkoxides is carried out in less acidic conditions, but the reactants are also prone to hydrolysis upon contact with humid air. These aspects of Ti-clay composites synthesis prompted Binitha and Sugunan [74] to use titanyl sulfate ( $\text{TiOSO}_4$ ), which is an inorganic precursor stable in humid air and soluble in water, for the preparation of the pillaring agent. The synthesis of titania sol was technically simpler, and it involved the hydrolysis of  $\text{TiOSO}_4$  solution with ammonium hydroxide followed by the peptization of precipitate with  $\text{HNO}_3$ . The sol was further reacted with commercial acid montmorillonite KSF in a standard pillaring procedure. The textural parameters of the obtained Ti-PILC solid, i.e., an interlayer distance of 1.3 nm and SSA of  $133 \text{ m}^2/\text{g}$ , were significantly lower than those generally reported for samples prepared with  $\text{TiCl}_4$  or alkoxide-derived pillaring agents, which is the effect likely to be associated, at least in part, with the fact that KSF is a commercial clay, subjected, during manufacturing, to compositional and structural modification.

From the very beginning, Ti-PILC solids were recognized as materials with high surface acidity, of both the Brønsted and the Lewis type, surpassing that of other pillared clays, such as Al-PILC or Zr-PILC [44,54,75]. Brønsted acid sites stem from the structural hydroxyl groups present on clay layers and from protons released upon the transformation of intercalated oligomeric cations into metal oxide pillars, while Lewis acid centers are associated with pillar oxide clusters. Physicochemical study combining UV-Vis and XPS spectroscopies shed light on the origin of the exceptional acidic properties of Ti-PILC [54]. The data showed that titanium sites involved in the linkage of pillars with the silica sheet of montmorillonite assume tetrahedral coordination. As such, they may expand the coordination sphere to an octahedral or pyramidal one and act as Lewis acid sites toward molecules possessing lone electron pairs. Alternatively, Ti–O–Si bridges may undergo hydrolysis and form the titanol (Ti–OH) and silanol (Si–OH) Brønsted acid centers [76]. The type of acidity determines which type of reaction can be catalyzed. It should be remembered that development of the Brønsted acid function was of key importance for the original idea of designing alternative FCC catalysts. However, already early on, it became apparent that this avenue of exploration failed, because the hydrothermal stability of PILC solids was insufficient for industrial requirements, the PILC tended to lose Brønsted acidity at elevated temperature, and the prevailing Lewis acidity accelerated the formation of coke deposit and catalyst deactivation [38]. Nevertheless, research in the area of acid catalysis by pillared clays continued, and a number of studies have been published as shown by the relevant reviews [77,78]. Surprisingly, despite the strong acid functionality characterizing Ti-pillared clays, the bulk of research concerned Al- or Zr-pillared clays, pure or mixed with other elements, while works addressing typical acid-catalyzed processes (e.g., cracking, isomerization, alkylation, etc.) by Ti-PILC were few and far between [78]. Investigated reactions included the dehydration of alcohols, cumene cracking, and alkylations [49,59,74,77–81]. Interesting results were obtained by Binitha and Sugunan [74], who investigated the ethylation of benzene with ethanol, to yield ethylbenzene, which is a valuable substrate for the manufacture of styrene, an important industrial

monomer. The reaction was carried out in the gas phase at 350 °C, over commercial KSF montmorillonite, the sodium-exchanged form of KSF, and Ti-PILC obtained from sodium-exchanged clay by the above-described simplified pillaring procedure using easy-to-handle  $\text{TiOSO}_4$  precursor. The authors found good correlation between the activity of the catalysts and their acidity, which was determined by the temperature-programmed desorption of ammonia. The latter increased in the order  $\text{KSF} < \text{Na-KSF} < \text{Ti-PILC}$ , and so did the conversion of ethanol. It is noteworthy that a spectacular improvement of selectivity toward ethylbenzene was observed over the Ti-pillared clay catalyst. While the selectivity over non-pillared samples was in the range of 40–60%, on Ti-PILC catalyst, ethylbenzene was the only reaction product, and the effect was attributed to the shape selectivity exerted by the constraints of the pore network of Ti-PILC.

In contrast to the limited data on acid catalysis by Ti-PILC, the examples of Ti-pillared clays applications to redox catalytic processes are plentiful. However, here, the Ti-PILC materials were predominantly used as supports for the catalytically active transition metal species, which, due to the existence of multiple oxidation states and a range of possible coordinations, readily underwent redox interactions with the incoming reagents.

Ti-pillared clays are especially attractive for designing catalysts for reactions known to be catalyzed by  $\text{TiO}_2$ -supported systems. The nanometer size of the individual pillars offers a surface-to-bulk ratio unattainable with conventional titania supports, while the firm anchoring of pillars at the silicate layers holds titania nanoclusters apart and hinders deactivation by sintering. Additionally, the Brønsted and Lewis acidity displayed by Ti-PILC system may be beneficial for the catalytic reaction. This review focuses on examples concerning catalytic processes vital for the air pollution control, for which titania–clay mineral composites have been most widely tested, i.e., the selective catalytic reduction (SCR) of  $\text{NO}_x$ , and combustion of toxic volatile organic compounds (VOCs).

### 5.1. Selective Catalytic Reduction of Nitrogen Oxides

The efficient removal of nitrogen oxides escaping to the atmosphere from combustion flue gases emitted by stationary (power stations, factories) and mobile (vehicles) sources is one of the major environmental concerns of our times [82,83]. Selective catalytic reduction, converting nitrogen oxides to nitrogen, is a very efficient method of  $\text{NO}_x$  abatement, with ammonia being the most commonly used reducing agent. The pollutants are converted to nitrogen and water, but at higher temperatures, secondary pollution with  $\text{NO}_x$  may occur due to the oxidation of ammonia (Figure 5).

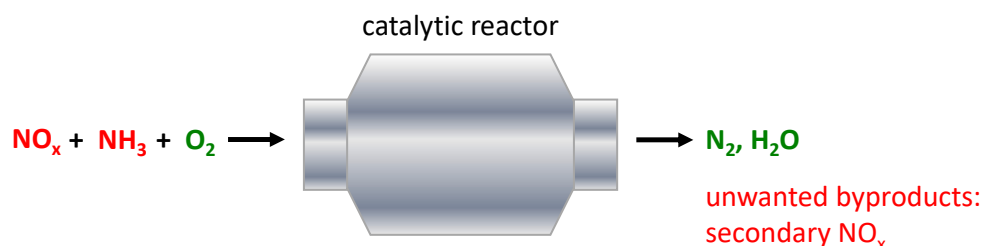


**Figure 5.** Schematic illustration of the catalytic  $\text{NH}_3$  SCR de $\text{NO}_x$  process.

Alternatively, the use of hydrocarbons as reductants has also been widely explored. As indicated in the Introduction, the currently used method of  $\text{NO}_x$  removal at an industrial scale is the selective catalytic reduction with ammonia over vanadia-based  $\text{TiO}_2$ -supported catalysts, because of their excellent thermal stability and lower oxidation activity for the undesired oxidation of  $\text{SO}_2$  to  $\text{SO}_3$ . The latter reacts with  $\text{NH}_3$  and  $\text{H}_2\text{O}$ , yielding ammonium sulfates and  $\text{H}_2\text{SO}_4$ , which cause corrosion and plugging of the reactor system. Therefore, it is not surprising that the attention of many researchers focused on de $\text{NO}_x$  catalysts based on Ti–clay mineral composites, in particular those doped with vanadium, as potential catalysts in the  $\text{NH}_3$  SCR de $\text{NO}_x$  process [84,85].

### 5.1.1. V-TiO<sub>2</sub>-Clay Mineral Composites

The first attempt to use Ti-pillared clays in the capacity of SCR catalyst was reported by Yang et al. [86], who compared the performance of a series of montmorillonite catalysts with different pillars in the SCR of NO with NH<sub>3</sub> and found that Ti-PILC, prepared by the method of [44] from TiCl<sub>4</sub> precursor, was less active than Fe- and Cr-pillared clays. The preparation of a V-doped Ti-PILC system, attempting to emulate the composition of industrial deNO<sub>x</sub> catalyst, was first described in open literature by Bahranowski et al. [87]. The authors synthesized a series of V-containing Ti-pillared montmorillonites from TiCl<sub>4</sub> precursor and inserted vanadium either by post-synthesis cation exchange with aqueous solution of VOSO<sub>4</sub>, followed by calcination, or by the addition of vanadyl sulfate to the pillaring solution in the procedure referred to as co-pillaring. The V content ranged from 0.8 to 5.3 wt %. The parent Ti-PILC showed a long-range order characterized by interlayer spacing of 2.6 nm. The SSA of the carrier was 345 m<sup>2</sup>/g and decreased upon loading with vanadium, indicating that the dopant was located within the pore network of the support. Moreover, characterization of the materials by electron spin resonance [88,89] led to the conclusion that the observed ESR signals of vanadium were characteristic of vanadyl species attached to the titania pillars, so that a resemblance to the commercial deNO<sub>x</sub> catalysts, in terms of direct contact between vanadium and titania, was indeed achieved. The catalysts proved very active in the SCR of NO with ammonia, with the V-exchanged samples reaching maximum activity at lower temperature than the co-pillared clay (≤300 °C and 350 °C, respectively), thus emphasizing the importance of an appropriate manner of V incorporation. The best result was obtained for the post-synthesis doped sample with medium V content (3.4 wt %), which in a broad temperature window (between ca. 250 and 350 °C) converted 90–100% NO, at 97–100% selectivity to N<sub>2</sub>, thus surpassing the performance of the conventional vanadia–titania reference catalyst. Indication as to the reason for the observed trends in activity was provided by ESR analysis. It was shown that depending on the synthesis conditions, different vanadyl species were formed. The poorer performance of the co-pillared sample was related to the more covalent nature of the V-O in-plane π bonding, which affected adversely the strength of surface V-OH Brønsted acid centers, essential for the deNO<sub>x</sub> catalytic cycle. On the other hand, the optimum performance of post-synthesis doped sample with intermediate V content was attributed to the onset of formation, at higher V loading, of polymeric surface vanadates.

Later, the findings concerning the high activity of post-synthesis VO<sup>2+</sup>-exchanged Ti-PILC catalysts in the SCR of NO with ammonia were confirmed by Long and Yang [90], who prepared their catalysts from a different montmorillonite but used the same pillaring method and a similar exchange procedure. However, their Ti-PILC support exhibited no (001) reflection and was therefore described as delaminated, i.e., characterized by non-parallel ordering of the clay layers. The SSA of the parent Ti-PILC was 310 m<sup>2</sup>/g and decreased upon the incorporation of vanadium. The best catalysts contained 3.5 wt % V and performed as well as the commercial V<sub>2</sub>O<sub>5</sub>/WO<sub>3</sub>/TiO<sub>2</sub> deNO<sub>x</sub> catalyst. Importantly, the authors carried out tests of the catalysts' stability in the reaction feed containing H<sub>2</sub>O and SO<sub>2</sub>, common components of combustion flue gases, which could poison the catalyst by blocking its active sites, and/or due to the formation of ammonium sulfate deposits. At low temperature, inhibiting effects on the performance of V-Ti-PILC were observed, but they became negligible when the temperature was above 375 °C. A thorough physico-chemical characterization indicated that vanadium was present as vanadia species well dispersed on TiO<sub>2</sub> pillars. The consistency of the data obtained by two different laboratories regarding the optimum V loading and the manner of V distribution confirmed that the post-synthesis method of doping Ti-PILC by cation exchange was an easy, efficient, and reliable preparative procedure for the synthesis of V-containing Ti-pillared clay catalysts. However, it should be remembered that the amount of dopant that can be introduced in a single exchange experiment is limited by the cation exchange capacity of the support, and, frequently, the treatment has to be performed multiple times in order to achieve higher degree of doping [87,90]. In that respect, impregnation of the support with a solution of

the compound containing the active metal, which enables loading of the desired quantity of the dopant in one experiment simply by adjusting its concentration in the impregnating solution, has a practical advantage over the exchange method.

Long and Yang, in their studies of V-doped titania-pillared clay deNO<sub>x</sub> catalysts, investigated also materials obtained by the incipient wetness impregnation of Ti-PILC with aqueous solutions of ammonium metavanadate [50], and they found that the maximum SCR activity on catalysts prepared by impregnation was almost the same as that on the samples obtained by exchange. In the presence of H<sub>2</sub>O and SO<sub>2</sub>, the high-temperature activity slightly improved, which was attributed to the increased acidity of the PILC support due to the formation of surface sulfate species. Impregnation offered a facile way of introducing the tungsten component by adding ammonium metatungstate to the impregnating solution, thus enabling the preparation of a material with composition as close as possible to that of the commercial V<sub>2</sub>O<sub>5</sub>/WO<sub>3</sub>/TiO<sub>2</sub> reference. In fact, the co-impregnation of V<sub>2</sub>O<sub>5</sub> and WO<sub>3</sub> further increased the activity of the PILC catalyst. The later study by Chae et al. [91] of vanadia supported on Ti-PILC, which was prepared by impregnation in a manner similar to that used by Long and Yang [50], concentrated on the detailed characterization of surface vanadia species and their evolution with increasing V content (2–20 wt %). The authors found that the optimum SCR activity was reached for intermediate V contents, corresponding to the abundant formation of two-dimensional polyvanadate species, while monomeric V centers and three-dimensional vanadia particles displayed lower activity, which is in agreement with the findings concerning the conventional vanadia–titania catalysts [92]. Vanadium-doped Ti-PILC catalysts prepared by impregnation were also studied by Zang et al. [93]. In accordance with previous studies, the best catalyst showed higher catalytic activity with a broader operating temperature window and higher N<sub>2</sub> selectivity, as well as higher tolerance to SO<sub>2</sub> and H<sub>2</sub>O than the reference V/TiO<sub>2</sub> catalyst with similar vanadium content.

One of the key steps in the mechanism of SCR of NO with ammonia over the vanadia–titania system is the adsorption of NH<sub>3</sub> on Brønsted acid centers [92]. In view of this, efforts have been made to improve this function in the pillared clay catalysts by appropriate modification of the preparative procedure. A common method of enhancing the Brønsted acidity of an oxide is sulfation, i.e., the anchoring of SO<sub>4</sub> species at the surface of the solid. Upon exposure to water vapor, surface sulfates convert to acidic S–OH groups. This approach has been adopted by Del Castillo et al. [94,95] in their studies of Ti-PILC and continued in later works on Ti-PILC-supported vanadia catalysts obtained by impregnation [96–99]. Sulfation was carried out in a simple manner by using H<sub>2</sub>SO<sub>4</sub> for the acid hydrolysis of TiCl<sub>4</sub>. The results showed that sulfation of the pillared clay support was beneficial for the catalyst performance and that the activity in the SCR of NO with NH<sub>3</sub> was directly related to the extent of sulfation due to the generation of strong Brønsted acidity. A study of Arfaoui et al. [100] showed that sulfation had a positive effect on the SCR activity of vanadia supported on Ti-PILC also in the case of carrier obtained from the alkoxide precursor. The same authors studied also the effect of the nature of Ti precursor on the performance of Ti-PILC-supported vanadia catalysts by preparing PILC supports using titanium methoxide, ethoxide, or chloride, and they found that alkoxides yielded the most efficient catalysts [101]. The effect was attributed to the improved textural properties of alkoxide-derived supports, i.e., higher SSA and enhanced mesoporosity, which favored the good dispersion of vanadia.

Recently, Cheng et al. [102], following the report that the addition of ceria to conventional vanadia–titania deNO<sub>x</sub> catalyst had a spectacular effect on the catalyst performance by enhancing its low temperature activity [103], synthesized a series of V-Ce/Ti-PILC samples and tested the materials in the SCR of NO with ammonia. Ceria is known to be an active promoter of SCR of NO due to its exceptional ability to store and release oxygen via the redox shift between Ce<sup>4+</sup> and Ce<sup>3+</sup> [104]. The Ti-pillared support was prepared from acid-treated montmorillonite, using a pillaring agent obtained by acid hydrolysis of Ti tetrabutoxide. However, it should be noted that the reported d<sub>001</sub> basal spacing of

the starting clay was 0.96 nm; i.e., it was much less than expected for the acid-treated montmorillonite under common humidity conditions (1.2–1.5 nm). On the other hand, the value of 0.96 nm corresponds to the thickness of an individual montmorillonite layer; hence, the observed  $d_{001}$  spacing points to the thermal collapse of the clay mineral used in this study, which was an aspect not discussed by the authors. Deposition of the mixed V-Ce oxide phase was carried out by sequential impregnation, using aqueous solutions of ammonium metavanadate and cerium nitrate as sources of active phase components. All Ce-doped pillared clays, including the one without vanadium, performed significantly better than the undoped V/Ti-PILC catalyst, with optimum composition corresponding to the Ce:V weight ratio of 4. The best catalyst converted >90%  $\text{NO}_x$  between 280 and 450 °C; i.e., the temperature window has been significantly broadened with respect to Ce-free catalysts. Unfortunately, this work lacked the assessment of the reaction selectivity to  $\text{N}_2$ , which is essential for the proper evaluation of the proposed catalytic formulations.

It is noteworthy that subsequently published research carried out by the same group on the SCR of NO with  $\text{NH}_3$  over Zr-PILC-supported ceria catalysts proved unequivocally the superior properties of Ti-PILC as the support for  $\text{CeO}_2$  active phase, ensuring a wider temperature window for >90% NO conversion (ca. 320–410 °C vs. 380–420 °C for Ti-PILC and Zr-PILC, respectively) [103,105].

#### 5.1.2. $\text{TiO}_2$ -Clay Mineral Composites Doped with Other Transition Metal Elements

Other transition metal cations have also been investigated as redox components of the active phase, with most studies addressing the use of Fe or Cu, as elements to be combined with titania–clay support. Both iron and copper are known to display catalytic activity in de $\text{NO}_x$  reactions, and, as compared to vanadium, they are characterized by a lack of toxicity, and, in the case of iron, substantially lower cost.

Yang et al. [86], already in their first report on the use of montmorillonite pillared with various transition metal oxides such as  $\text{NH}_3$  SCR catalyst, identified the Fe-PILC sample as one of the most active. In a series of further works, the same group carried out an extensive investigation of catalysts prepared by the doping of Ti-pillared clay with an Fe-based active phase, either by incipient wetness impregnation [106] or by ion exchange [107–112]. As in the case of V-doped catalysts, the investigated Ti-PILC materials, prepared from  $\text{TiCl}_4$  precursor, were delaminated. The choice of Ti-PILC as a carrier was due to the set of useful properties: large SSA, high thermal and hydrothermal stability, large micropore sizes that enabled further doping with active ingredients without causing a significant blockage of the pore network, high acidity, and advantageous interaction of  $\text{TiO}_2$  with the deposited active phase. Moreover, Ti-PILC itself, although not particularly active in the  $\text{NH}_3$  SCR of NO, proved resistant to poisoning by  $\text{SO}_2$  [86].

Ti-PILC impregnated with  $\text{Fe}_2\text{O}_3$  was found to be by one order of magnitude more active than Ti-PILC on its own, both in the absence and in the presence of  $\text{H}_2\text{O}$  and  $\text{SO}_2$ . Moreover, the activity of the  $\text{Fe}_2\text{O}_3$ -Ti-PILC system could be significantly enhanced by the addition of chromia. By adjusting the Fe/Cr ratio within a fixed total oxide loading (10 wt %), it was possible to optimize the performance so that in the presence of  $\text{H}_2\text{O}$  and  $\text{SO}_2$ , the best catalyst, with Fe/Cr = 3, outperformed the commercial  $\text{V}_2\text{O}_5/\text{WO}_3/\text{TiO}_2$  reference by nearly 40% [106].

Subsequent work demonstrated that even higher activities could be achieved over Fe-exchanged Ti-PILC catalysts, which, also in the presence of  $\text{H}_2\text{O}$  and  $\text{SO}_2$ , were about twice as active as the commercial reference catalyst [108]. In addition, the Fe/Ti-PILC catalysts showed higher  $\text{N}_2$  selectivity and lower activity for the oxidation of  $\text{SO}_2$  than the vanadium-based reference. The Fe content varied in the range 4.3–20.1 wt %, the higher loading being achieved by multiple exchange and/or increase in the exchange temperature. Optimum performance was observed for intermediate Fe content of 5.9 wt %. Physicochemical characterization of the catalysts showed that the FeOx phase was well dispersed at lower Fe loading present predominantly as isolated Fe ions and at higher Fe content as amorphous iron oxide aggregates. The evolution of catalysts' activity with

Fe content indicated that the isolated Fe sites were more active than the oxide clusters. It is noteworthy that this observation can explain the superiority of an Fe-exchanged catalyst as compared to an Fe<sub>2</sub>O<sub>3</sub>-impregnated one, since ion exchange favors a more homogeneous distribution of the dopant than impregnation, thus facilitating the formation of dispersed isolated ions. Interestingly, the high-temperature activity of the samples grew in the presence of H<sub>2</sub>O and SO<sub>2</sub>; the effect was attributed to the increased Brønsted acidity resulting from sulfation of the FeO<sub>x</sub> active species. In accordance with the key role of Brønsted acid sites in the SCR of NO with ammonia, the authors demonstrated that the acid function of the Fe/Ti-PILC composite catalyst could be enhanced by acid activation of montmorillonite prior to pillaring, and that such a treatment resulted in an increase in catalytic activity with respect to the catalyst prepared from the untreated clay [109].

Further improvement of Fe-exchanged catalysts could be achieved by adding certain rare earth elements as promoters [108,111,112]. For instance, doping with cerium at the level of 0.5–1.0 wt %, carried out either by cation exchange or by impregnation, enhanced significantly the SCR performance. The former manner of doping proved more efficient and the best catalyst, obtained by the sequential cation exchange of Ti-PILC with Ce and Fe, was over three times more active than the commercial reference [108,111]. The authors argued that cerium dopant did not affect the catalyst acidity but improved its redox function, thus enhancing the oxidation of NO to NO<sub>2</sub>, which is an intermediate in the SCR of NO over Fe/Ti-PILC catalysts [112].

A very interesting contribution has been provided by Chmielarz et al. [53,113,114], who investigated the SCR of NO with ammonia over two types of Fe-doped Ti-clay mineral composites—PILC and so-called porous clay heterostructures (PCH)—and demonstrated that the manner of preparation of the Ti-clay composite was an important tool in the design of supported catalysts. PCH, first described by Galarneau et al. [115], are obtained from clay minerals by the surfactant-directed method. In this approach, clay mineral is first intercalated with a cationic surfactant, which acts as a template, directing the interlayer hydrolytic transformation of the Si precursor species. As a result, a porous silica framework is formed within the interlayer spaces of clays, with pore sizes in the range of large micropores–small mesopores. The authors used TiCl<sub>4</sub> precursor for the synthesis of Ti-PILC, while a mixture of tetraethylorthosilicate and titanium isopropoxide was employed as precursor of the silica–titania interlayer skeleton of Ti-PCH. The SSA of supports was 212 and 573 m<sup>2</sup>/g for Ti-PILC and Ti-PCH, respectively, with some evidence of thermal collapse visible in the former after treatment at 700 °C and in the latter at 800 °C. Fe was introduced into Ti-clay composites by the cation exchange procedure. Along with Fe-doped Ti-clay mineral composites, the authors investigated also Ti-PILC and Ti-PCH supports exchanged with copper. It turned out that the nature of the Ti-clay mineral support had an important effect on the distribution of the active phase, and, as a consequence, on the catalyst performance in SCR of NO with ammonia. Thus, Fe/Ti-PILC converted more NO in the low-temperature range, whereas Fe/Ti-PCH was more active at higher temperatures. The selectivity to nitrogen was better over Fe/Ti-PCH catalyst. The differences were attributed to the different degree of dispersion of Fe species at both supports. In Fe/Ti-PILC, the Fe active phase existed mainly as bulky Fe oxide clusters and Fe oligomers, while in Fe/Ti-PCH, large oxide clusters were absent, and the surface was covered with isolated Fe monomers and oligomeric species. The authors argued that Fe oxide agglomerates were active in the low temperature deNO<sub>x</sub> and in the oxidation of ammonia (responsible for the fall of N<sub>2</sub> selectivity), while Fe monomers showed deNO<sub>x</sub> activity at a higher temperature range and were less active in ammonia oxidation. Cu-doped catalysts showed similar trends in deNO<sub>x</sub> activities. In this case, differences in the dispersion of copper species were considered the key factor, as oligomeric Cu oxide clusters, known to effectively catalyze the reaction at lower temperatures, dominated on Ti-PILC, and monomeric Cu ions, active in the medium- and high-temperature DeNO<sub>x</sub>, prevailed on Ti-PCH. The reported higher SSA and thermal stability of Ti-PCH supports,

in combination with the ability to better disperse the transition metal oxide active phase, reveal the potential of such solids as in catalyst design.

In a recent study, Xu et al. [116] reported a new method of preparation of Fe-doped Ti-PILC by using a mixed Fe-Ti pillaring agent for the intercalation of montmorillonite. The catalyst obtained in such a way showed better activity in the SCR of NO with ammonia than the one synthesized with pillaring solution containing only Fe oligocations. Moreover, it showed remarkable resistance to poisoning by alkali and heavy metals. Unfortunately, the lack of key details of the synthetic procedure, such as, e.g., the manner of preparation of mixed Fe-Ti pillaring solution, makes attempts at reproduction of the catalytic formula a formidable challenge. Nevertheless, the idea of co-pillaring of Fe and Ti species may provide an inspiration for further research into pillared clay-derived deNO<sub>x</sub> catalysts.

Although the SCR of NO with ammonia is currently the most widespread deNO<sub>x</sub> treatment, there are drawbacks associated with its use, such as the toxicity and corrosive properties of NH<sub>3</sub>. A widely explored alternative is the SCR of NO<sub>x</sub> with hydrocarbons as reducing agents (HC SCR) [117], yielding nitrogen, CO<sub>2</sub>, and H<sub>2</sub>O as the desired reaction products (Figure 6).

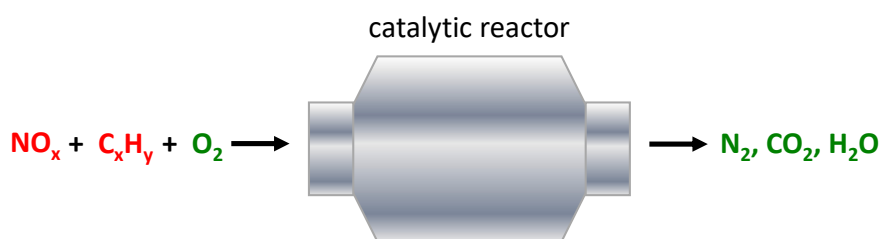


**Figure 6.** Schematic illustration of the catalytic HC SCR deNO<sub>x</sub> process.

The process is of particular interest for application in mobile sources, due to the presence of all necessary reactants in the exhaust streams from car engines. The interest in this technology was prompted by 1990 reports indicating that Cu-ZSM-5 and other Cu-exchanged zeolites were active in the selective catalytic reduction of NO with hydrocarbons [118]. It was only natural that copper-containing pillared clay composites became the focus of research with respect to the HC SCR of NO. Yang et al. [107,119] were the first to report the use of copper-exchanged Ti-PILC catalysts, obtained from TiCl<sub>4</sub> precursor, in the SCR of NO with ethylene as a reductant. The pillared clay-based catalyst proved significantly more active (ca. 55% maximum NO conversion) than the Cu-ZSM-5 zeolite (ca. 46% maximum NO conversion) [119]. The activity of Cu-Ti-PILC could be further increased by promoting with a small amount of ceria (ca. 60% maximum NO conversion). Moreover, H<sub>2</sub>O and SO<sub>2</sub> only slightly deactivated the SCR activity of Cu-Ti-PILC, whereas severe deactivation was observed for Cu-ZSM-5. The authors studied a series of Cu-Ti-PILC catalysts with Cu content in the range 1.0–7.6 wt % and found that the catalytic activity increased with copper loading until 5.9 wt % (245% ion-exchange capacity). Comparison of two methods of preparation of Cu-doped Ti-PILC, cation exchange, and incipient wetness impregnation demonstrated that the former resulted in a much more active HC SCR catalyst. The effect was attributed to the different degree of copper species dispersion at the support surface, the active phase being present predominantly as isolated Cu sites in cation-exchanged catalyst, and as clusters of CuO in the impregnated sample. In addition, impregnation resulted in a lower SSA due to partial pore blockage. It is noteworthy that the Cu-exchanged Ti-PILC proved more active than Ti-PILC exchanged with a number of other cations, such as Fe, Co, Ce, Ag, or Ga. The superiority of Cu-based Ti-PILC catalysts has been confirmed by the work of Valverde et al. [120], who studied Ti-PILC cation exchanged or impregnated with Cu as well as cation exchanged with Fe or Ni in the SCR of NO with propylene as a reductant. At variance with previous studies, the pillaring agent for Ti-PILC synthesis was prepared from Ti methoxide. Cu-exchanged Ti-PILC proved more active in the SCR process than catalysts containing other transition metal ions. As to the method of

copper insertion, again, cation exchange was found to yield the most active catalyst. In accordance with previous studies [121,122], the existence of three types of copper species has been proposed: isolated  $\text{Cu}^{2+}$  ions anchored at the titania pillars, clustered  $\text{Cu}^{2+}$  ions, and CuO particles. The  $\text{Cu}^{2+}$  ions dominated in Cu-exchanged samples, while CuO aggregates prevailed in impregnated catalysts. The authors argued that low coordinated  $\text{Cu}^{2+}$  ions were active sites for SCR reaction; therefore, cation exchange, which ensured their high population, resulted in more efficient catalysts. The key role of isolated  $\text{Cu}^{2+}$  as active sites for the SCR of NO with propylene has been confirmed in later works by Li et al. [123] and Lu et al. [124], who demonstrated that the catalytic activity of Cu-exchanged Ti-PILC in the SCR of NO by  $\text{C}_3\text{H}_6$  increased with the relative share of  $\text{Cu}^{2+}$  in the spectrum of formed copper species. The authors showed that the content of cupric ions may be controlled during catalyst synthesis by an appropriate choice of the Ti/clay ratio and/or adjustment of pH during the Cu exchange procedure.

It should be noted that the maximum NO conversions reported for Cu-doped Ti-PILC catalysts oscillated around 45–55% and occurred in the ca. 240–260 °C range [120–124]. At higher temperatures, a fall of NO conversion was observed due to the increasing combustion of the hydrocarbon reductant. In search for the active phase providing higher activity on the Ti-PILC support, Dong et al. [125], basing on the earlier work by this group [126], which identified Fe-exchanged Al-PILC as highly active catalysts for  $\text{C}_3\text{H}_6$ -SCR, prepared a series of Ti-PILC catalysts loaded with Fe. Ti-PILC was synthesized from  $\text{TiCl}_4$  precursor, and Fe was incorporated by cation exchange with aqueous solution of  $\text{Fe}(\text{NO}_3)_3$  at 70 °C. The content of Fe introduced in such a way ranged from 5 to 22 wt %. The effect of other synthesis parameters, such as Ti/clay ratio and the temperature of calcination, were explored in a recent paper from this group [127]. The catalysts showed remarkable  $\text{C}_3\text{H}_6$ -SCR activity, and the efficiency of more heavily loaded catalysts ( $\geq 13$  wt %) reached 100% NO conversion at  $\geq 400$  °C, with  $\text{N}_2$  selectivity over 90%. The optimum performance was observed for the catalyst with 19 wt % Fe and a Ti/clay ratio equal to 10 mmol/g. The impact of the temperature of calcination was very small. UV-Vis analysis identified three types of Fe species existing in the catalysts: isolated  $\text{Fe}^{3+}$  ions, small  $\text{Fe}_x\text{O}_y$  oligomers, and  $\text{Fe}_2\text{O}_3$  particles. The best catalyst contained the highest share of  $\text{Fe}_x\text{O}_y$  oligomers; hence, these species were assumed to be the active sites for the SCR reaction. In view of the earlier reports from two laboratories [119,120], showing a rather low efficiency of Fe-Ti-PILC catalysts in the SCR of NO with ethylene (Ti-PILC synthesized from  $\text{TiCl}_4$ , cation exchanged at room temperature, 6.8 wt % Fe, maximum NO conversion around 30% at 450 °C) and propylene (Ti-PILC synthesized from Ti methoxide, cation exchanged at room temperature, 5.8–15.5 wt % Fe, maximum NO conversion around 30% at 400 °C), the observed high activity of Fe-Ti-PILC was a striking result. Understanding the cause of such a dramatic improvement with respect to previous studies would be of immense importance for catalyst design, but this aspect was not addressed by the authors.

The data on the use of  $\text{TiO}_2$ -clay mineral composites in combination with active phase based on elements other than V, Fe, or Cu are rare and often considered as a background for the presentation of more active materials. Thus, in the already discussed papers, Yang et al. [107] and Valverde et al. [120], who studied the SCR of NO with hydrocarbons over Cu-exchanged Ti-PILC, also tested catalysts exchanged with Co, Ce, Ag, Ga [107], and Ni [120]. All these materials proved inferior to Cu-Ti-PILC. Co-exchanged Ti-PILC investigated by Chmielarz and al. [128] in the SCR of NO with  $\text{NH}_3$  performed poorer than Cu-Ti-PILC in the low-temperature region (250–450 °C) but showed superior SCR properties above 400 °C, because, in contrast to Ti-clays modified with Cu, no oxidation of ammonia was observed at high temperature range. Several works addressed titania-clay composites containing Mn-based active phase. Thus, Shen et al. [129,130] synthesized Ti-pillared montmorillonite supports loaded with Mn oxide deposited by means of incipient wetness impregnation of  $\text{Mn}(\text{NO}_3)_2$  solution. The authors investigated the materials activity in the SCR of NO with  $\text{NH}_3$ , looking at such variables as precursors of Ti-pillaring agents ( $\text{TiCl}_4$ ,  $\text{Ti}(\text{OC}_4\text{H}_9)_4$ , or  $\text{TiOSO}_4$ ), Mn content (2–10 wt %), and doping with ceria.

The tests were carried out only up to 240 °C. The catalysts with intermediate Mn content (6–8 wt %) showed appreciable SCR activity, especially after doping with cerium. The best catalyst, prepared from  $\text{TiOSO}_4$  precursor and containing 4.2 wt % Mn and 4.9 wt % Ce, converted > 90% NO from 190 °C upwards and showed good resistance to  $\text{SO}_2$  and  $\text{H}_2\text{O}$ . Unfortunately, no data on the selectivity to nitrogen were provided. Pillaring was found essential for developing high activity, as the Mn,Ce-doped un-pillared clay converted at most 40% NO. It was shown that the beneficial influence of ceria was due to its ability to improve the dispersion of the Mn oxide phase.

Recently, several reports described the preparation of  $\text{TiO}_2$ -clay mineral supports by non-pillaring procedures [131–133]. In a very recent work, Wang et al. [131] proposed a different synthesis method of ceria-titania-montmorillonite composites. Instead of the impregnation of the previously prepared Ti-PILC support with ceria, the authors mixed montmorillonite powder with the ethanol solution containing both the Ti tetrabutoxide and the cerium nitrate and then induced a sol-gel transformation by the addition of water. The solid product was subjected to drying and calcination. Modification of the synthesis procedure resulted in a composite consisting of disordered clay mineral and anatase particles interacting with nano  $\text{CeO}_x$  species rather than in an ordered Ti-PILC structure. However, the structural considerations presented in this work should be treated with caution. In the XRD patterns, the  $2\theta$  scale started from ca.  $7.5^\circ$ , which might have cut off the area with the (001) reflection of raw montmorillonite. The authors interpreted the barely visible peak at  $2\theta = 9.6^\circ$  ( $d_{001} = 9.2$  nm) as a basal reflection of parent clay. The peak position and intensity point rather to the presence of an impurity TOT clay mineral with closely adhering layers, for instance traces of mica. In addition, the conclusion on calcination-induced increase in the basal spacing of montmorillonite disagrees with the known thermal behavior of this mineral. Nevertheless, the proposed synthetic approach brought about a great improvement of the catalytic performance of the Ce-Ti-montmorillonite system, which attained >90% NO conversion in a very broad temperature window (260–475 °C). It was argued that the preparation procedure resulted in the formation of highly dispersed  $\text{CeO}_x$  particles of improved reducibility. Unfortunately, the work lacked discussion of the selectivity to nitrogen. In two cases, deNO<sub>x</sub> catalysts were prepared using palygorskite (Pal), a fibrous, non-swelling clay mineral with intrinsic microporosity, for the preparation of titania-clay mineral composite [132,133]. In both works, a  $\text{TiO}_2$  component and clay mineral were present as mixtures rather than intergrown structures of the PILC type. Luo et al. [132] obtained  $\gamma$ - $\text{MnO}_2$ - $\text{TiO}_2$ -palygorskite composites by adding the suspension of titania, prepared by base hydrolysis of  $\text{TiCl}_4$ , to the slurry of Pal, and using the resulting mixture as a medium for the synthesis of  $\gamma$ - $\text{MnO}_2$  from  $\text{MnSO}_4$  and  $(\text{NH}_4)_2\text{S}_2\text{O}_8$  solutions. A series of  $\gamma$ - $\text{MnO}_2$ / $\text{TiO}_2$ -Pal catalysts with  $\gamma$ - $\text{MnO}_2$  content ranging from 1 to 7 wt % were prepared and tested in the SCR of NO with ammonia. The best catalyst, containing 5 wt %  $\gamma$ - $\text{MnO}_2$ , showed very good activity and converted >90% NO between 190 and 400 °C. However, above 300 °C, the selectivity to  $\text{N}_2$ , which at lower temperature exceeded 95%, fell quite rapidly; hence, the actual temperature window of good catalytic performance was 190–300 °C. Deterioration of the SCR selectivity at high temperature was most likely related to the limited thermal stability of the  $\gamma$ - $\text{MnO}_2$ / $\text{TiO}_2$ -Pal composite. Above 300 °C, the structure of Pal collapsed, the anatase component became more crystalline, and the  $\gamma$ - $\text{MnO}_2$  reflections disappeared from the XRD pattern, pointing to a substantial modification of the Mn-bearing phase. In the work by Xie et al. [133], supported ceria-tungsta catalysts were prepared by adding  $\text{TiO}_2$  and Pal, in various relative quantities, to the impregnating solution containing  $\text{Ce}(\text{NO}_3)_3$  and  $(\text{NH}_4)_6\text{H}_2\text{W}_{12}\text{O}_{40}$ . After drying and calcination, the catalysts were tested in the SCR of NO with ammonia. All showed high activity, with the best one, containing 20 wt % Pal, converting over 90% of NO in the 270–410 °C range. However, the authors provided no information on the selectivity to  $\text{N}_2$ , which made the proper evaluation of the prepared catalysts impossible.

An overview of the main characteristics of the most relevant TiO<sub>2</sub>–clay mineral composites employed as catalysts for the removal of nitrogen oxides by NH<sub>3</sub> SCR is presented in Table 1 and by HC SCR is presented in Table 2.

**Table 1.** Summary of the main synthesis and catalysis data for the most relevant examples of TiO<sub>2</sub>–clay mineral composites used as catalysts for the NH<sub>3</sub> SCR of NO<sub>x</sub> (Mt—montmorillonite, Pal—palygorskite, HDTMA—hexadecyltrimethylammonium cation, CE—cation exchange, GHSV—gas hourly space velocity).

TiO <sub>2</sub> –Clay Mineral Composite	Synthesis	Reaction Conditions	Maximum NO Conversion/Selectivity to N <sub>2</sub>	Ref.
V/Ti-pillared Mt	TiCl <sub>4</sub> precursor + Mt, calcination 400 °C, Ti-PILC SSA = 346 m <sup>2</sup> g <sup>-1</sup> ; V-doping by cation exchange or co-pillaring, calcination 400 °C; best catalyst 3.4 wt % V by cation exchange	200–450 °C, NO = NH <sub>3</sub> = 1000 ppm, O <sub>2</sub> = 2%; balance = He; GHSV = 10,000 h <sup>-1</sup>	100% conversion at 275 °C, 100% selectivity (for the best catalyst)	[87]
V/Ti-pillared Mt	TiCl <sub>4</sub> precursor + Mt, calcination 350 °C, Ti-PILC SSA = 310 m <sup>2</sup> g <sup>-1</sup> ; V-doping by cation exchange, calcination 400 °C; best catalyst 3.5 wt % V	200–400 °C, NO = NH <sub>3</sub> = 1000 ppm, O <sub>2</sub> = 2%; 1000 ppm SO <sub>2</sub> (when used), 8% H <sub>2</sub> O vapor (when used); balance = He; GHSV = 75,000 h <sup>-1</sup>	94.5% conversion at 375 °C, 98.8% selectivity, negligible inhibition by SO <sub>2</sub> and H <sub>2</sub> O (for the best catalyst)	[90]
V/Ti-pillared Mt	TiCl <sub>4</sub> precursor + Mt, calcination 350 °C, Ti-PILC SSA = 310 m <sup>2</sup> g <sup>-1</sup> ; V-doping by impregnation, calcination 500 °C; best catalyst 4.4 wt % V <sub>2</sub> O <sub>5</sub>	200–450 °C, NO = NH <sub>3</sub> = 1000 ppm, O <sub>2</sub> = 2%; 1000 ppm SO <sub>2</sub> (when used), 8% H <sub>2</sub> O vapor (when used); balance = He; GHSV = 75,000 h <sup>-1</sup>	93.0% conversion at 400 °C, 98.9% selectivity (for the best catalyst); slight improvement upon exposure to SO <sub>2</sub> and H <sub>2</sub> O and co-doping with W	[91]
V/Ti-pillared Mt	TiCl <sub>4</sub> precursor + Mt, calcination 400 °C, Ti-PILC SSA = 223 m <sup>2</sup> g <sup>-1</sup> ; V-doping by impregnation, calcination 500 °C; best catalyst 3.47 wt % V <sub>2</sub> O <sub>5</sub>	120–480 °C, NO = NH <sub>3</sub> = 1000 ppm, O <sub>2</sub> = 8%; 500 ppm SO <sub>2</sub> (when used), 10% H <sub>2</sub> O vapor (when used); balance = He; GHSV = 75,000 h <sup>-1</sup>	ca. 99.0% conversion at 260 °C, ca.98% selectivity, (for the best catalyst); moderate loss of activity upon time-on-stream exposure to SO <sub>2</sub> and H <sub>2</sub> O	[93]
V,Ce/Ti-pillared Mt	Ti(OC <sub>4</sub> H <sub>9</sub> ) <sub>4</sub> precursor + Mt, acid treated Mt, calcination 400 °C, V,Ce-doping by sequential impregnation, calcination 400 °C; best catalyst 1 wt % V + 4 wt % Ce	100–450 °C, NO = 1000 ppm, NH <sub>3</sub> = 1100 ppm, O <sub>2</sub> = 4%; 5% H <sub>2</sub> O; balance = N <sub>2</sub> ; GHSV = 50,000 h <sup>-1</sup>	97% conversion at 370 °C	[102]
S,Ti-pillared Mt	TiCl <sub>4</sub> precursor + Mt, H <sub>2</sub> SO <sub>4</sub> as sulfating agent, S,Ti-PILC SSA = 152 m <sup>2</sup> g <sup>-1</sup> ;	100–400 °C, NO = NH <sub>3</sub> = 1000 ppm, O <sub>2</sub> = 2.5%; balance = He; GHSV = 46,000 h <sup>-1</sup>	91.6% conversion at 400 °C, 71% selectivity	[97]
V/S,Ti-pillared Mt	TiCl <sub>4</sub> precursor + Mt, H <sub>2</sub> SO <sub>4</sub> as sulfating agent, S,Ti-PILC SSA = 152 m <sup>2</sup> g <sup>-1</sup> ; V-doping by impregnation, calcination 400 °C; best catalyst 3.0 wt % V, SSA = 131 m <sup>2</sup> g <sup>-1</sup>	100–400 °C, NO = NH <sub>3</sub> = 1000 ppm; O <sub>2</sub> = 2.5%; balance = He; GHSV = 46,000 h <sup>-1</sup>	99.9% conversion at 300 °C, 79% selectivity (for the best catalyst)	[97]

Table 1. Cont.

TiO <sub>2</sub> -Clay Mineral Composite	Synthesis	Reaction Conditions	Maximum NO Conversion/ Selectivity to N <sub>2</sub>	Ref.
Fe/Ti-pillared Mt	TiCl <sub>4</sub> precursor + Mt, calcination 350 °C, Ti-PILC SSA = 310 m <sup>2</sup> g <sup>-1</sup> ; Fe-doping by CE, calcination 400 °C; best catalyst 5.9% wt % Fe, SSA = 245 m <sup>2</sup> g <sup>-1</sup>	300–450 °C, NO = NH <sub>3</sub> = 1000 ppm, O <sub>2</sub> = 2%; 1000 ppm SO <sub>2</sub> (when used), 8% H <sub>2</sub> O vapor (when used); balance = N <sub>2</sub> ; GHSV = 113,000 h <sup>-1</sup>	92.5% conversion at 400 °C, 99.5% selectivity (for the best catalyst), activity enhancement (98%) upon exposure to SO <sub>2</sub> and H <sub>2</sub> O	[108]
Fe/Ti-pillared Mt	TiCl <sub>4</sub> precursor + Mt, calcination 400 °C, Ti-PILC SSA = 212 m <sup>2</sup> g <sup>-1</sup> ; Fe-doping by CE, calcination 550 °C, 8.90 wt % Fe <sub>2</sub> O <sub>3</sub> , SSA = 195 m <sup>2</sup> g <sup>-1</sup>	100–550 °C, NO = NH <sub>3</sub> = 2500 ppm, O <sub>2</sub> = 2.5%; balance = He; 0.1 g catalyst, 40 mL/min <sup>-1</sup> flow rate	98% conversion at 450 °C, 94% selectivity	[53]
Fe,Cr/Ti-pillared Mt	TiCl <sub>4</sub> precursor + Mt, calcination 300 °C, Ti-PILC SSA = 308 m <sup>2</sup> g <sup>-1</sup> ; Fe,Cr-doping by impregnation, calcination 400 °C; best catalyst 7.5% wt % Fe <sub>2</sub> O <sub>3</sub> + 2.5% wt % Cr <sub>2</sub> O <sub>3</sub>	175–425 °C, NO = NH <sub>3</sub> = 1000 ppm, O <sub>2</sub> = 2%; 1000 ppm SO <sub>2</sub> (when used), 8% H <sub>2</sub> O vapor (when used); balance = N <sub>2</sub> ; GHSV = 60,000 h <sup>-1</sup>	99% conversion at 375 °C, >99% selectivity (for the best catalyst), ca. 40% activity loss upon exposure to SO <sub>2</sub> and H <sub>2</sub> O	[106]
Fe,Ce/Ti-pillared Mt	TiCl <sub>4</sub> precursor + Mt, calcination 350 °C, Ti-PILC SSA = 310 m <sup>2</sup> g <sup>-1</sup> ; Ce and Fe-doping by sequential CE, calcination 400 °C; 5.45 wt % Fe, 0.51 wt % Ce	300–450 °C, NO = NH <sub>3</sub> = 1000 ppm, O <sub>2</sub> = 2%; 1000 ppm SO <sub>2</sub> (when used), 8% H <sub>2</sub> O vapor (when used); balance = N <sub>2</sub> ; GHSV = 226,000 h <sup>-1</sup>	91.5% conversion at 400 °C, 100% selectivity (for the best catalyst), activity enhancement (96%) upon exposure to SO <sub>2</sub> and H <sub>2</sub> O	[108]
Cu/Ti-pillared Mt	TiCl <sub>4</sub> precursor + Mt, calcination 400 °C, Ti-PILC SSA = 212 m <sup>2</sup> g <sup>-1</sup> ; Cu-doping by CE, calcination 550 °C, 1.51 wt % CuO, SSA = 198 m <sup>2</sup> g <sup>-1</sup>	100–550 °C, NO = NH <sub>3</sub> = 2500 ppm, O <sub>2</sub> = 2.5%; balance = He; 0.1 g catalyst, 40 mL/min <sup>-1</sup> flow rate	93% conversion at 500 °C, 94% selectivity	[53]
Co/Ti-pillared Mt	TiCl <sub>4</sub> precursor + Mt, calcination 350 °C, Ti-PILC SSA = 279 m <sup>2</sup> g <sup>-1</sup> ; Co-doping by CE, calcination 350 °C, best catalyst SSA = 296 m <sup>2</sup> g <sup>-1</sup>	75–475 °C, NO = NH <sub>3</sub> = 2500 ppm, O <sub>2</sub> = 2.5%; balance = He; 0.1 g catalyst, 40 mL/min <sup>-1</sup> flow rate	100% conversion at 450 °C, 99% selectivity	[128]
Mn/Ti-pillared Mt	Ti(OC <sub>4</sub> H <sub>9</sub> ) <sub>4</sub> precursor + Mt, drying 80 °C, Mn-doping by impregnation, calcination 550 °C, best catalyst 8 wt % Mn, SSA = 134 m <sup>2</sup> g <sup>-1</sup>	80–240 °C, NO = NH <sub>3</sub> = 600 ppm; O <sub>2</sub> = 3%; balance = N <sub>2</sub> ; GHSV = 50,000 h <sup>-1</sup>	100% conversion at 240 °C	[129]
Fe/Ti,Si-PCH	HDTMA-Mt + Si(OC <sub>2</sub> H <sub>5</sub> ) <sub>4</sub> + Ti(OC <sub>3</sub> H <sub>7</sub> ) <sub>4</sub> , calcination 600 °C, Fe-doping by CE, calcination 600 °C; best catalyst 7.61 wt % Fe <sub>2</sub> O <sub>3</sub> , SSA = 525 m <sup>2</sup> g <sup>-1</sup>	100–550 °C, NO = NH <sub>3</sub> = 2500 ppm, O <sub>2</sub> = 2.5%; 2000 ppm SO <sub>2</sub> (when used), 5% H <sub>2</sub> O vapor (when used); balance = He; 0.1 g catalyst, 40 mL/min <sup>-1</sup> flow rate	100% conversion at 400 °C, 98% selectivity (for the best catalyst), slight deactivation upon exposure to SO <sub>2</sub> and H <sub>2</sub> O	[114]

Table 1. Cont.

TiO <sub>2</sub> –Clay Mineral Composite	Synthesis	Reaction Conditions	Maximum NO Conversion/Selectivity to N <sub>2</sub>	Ref.
Cu/Ti,Si-PCH	HDTMA-Mt + Si(OC <sub>2</sub> H <sub>5</sub> ) <sub>4</sub> + Ti(OC <sub>3</sub> H <sub>7</sub> ) <sub>4</sub> , calcination 600 °C, Cu-doping by CE, calcination 600 °C; best catalyst 1.97 wt % CuO, SSA = 541 m <sup>2</sup> g <sup>-1</sup>	100–550 °C, NO = NH <sub>3</sub> = 2500 ppm; O <sub>2</sub> = 2.5%; 2000 ppm SO <sub>2</sub> (when used), 5% H <sub>2</sub> O vapor (when used) balance = He; 0.1 g catalyst, 40 mL/min <sup>-1</sup> flow rate	97% conversion at 500 °C, 90% selectivity (for the best catalyst), slight deactivation upon exposure to SO <sub>2</sub> and H <sub>2</sub> O	[114]
Ce,Ti/Mt	Ti(OC <sub>4</sub> H <sub>9</sub> ) <sub>4</sub> precursor + Ce precursor + Mt, sol–gel, calcination 400 °C; disordered structure, best catalyst 10.27 wt % CeO <sub>2</sub> , SSA = 109 m <sup>2</sup> g <sup>-1</sup>	100–400 °C, NO = NH <sub>3</sub> = 500 ppm; O <sub>2</sub> = 3%; balance = N <sub>2</sub> ; GHSV = 100,000 h <sup>-1</sup>	ca. 95% conversion in 260–475 °C range (for the best catalyst), selectivity not discussed	[131]
Mn/TiO <sub>2</sub> /Pal	Pal slurry + TiO <sub>2</sub> from TiCl <sub>4</sub> precursor (2:1 mass ratio) + in situ synthesized γ-MnO <sub>2</sub> ; best catalyst 5 wt % MnO <sub>2</sub> , calcination 300 °C	50–400 °C, NO = NH <sub>3</sub> = 1000 ppm; O <sub>2</sub> = 3%; balance = N <sub>2</sub> ; GHSV = 25,000 h <sup>-1</sup>	98% conversion at 300 °C, 95% selectivity (for the best catalyst)	[132]
Ce,W/TiO <sub>2</sub> /Pal	TiO <sub>2</sub> + Pal + Ce,V impregnating solution, drying 110 °C, calcination 500 °C; best catalyst 10 wt % CeO <sub>2</sub> , 5 wt % WO <sub>3</sub> , 20 wt % Pal, SSA = 102 m <sup>2</sup> g <sup>-1</sup>	50–400 °C, NO = NH <sub>3</sub> = 500 ppm; O <sub>2</sub> = 5%; balance = N <sub>2</sub> ; GHSV = 30,000 h <sup>-1</sup>	98.4% conversion at 360 °C	[133]

**Table 2.** Summary of the main synthesis and catalysis data for the most relevant examples of TiO<sub>2</sub>–clay mineral composites used as catalysts for the HC SCR of NO<sub>x</sub> (Mt—montmorillonite, CE—cation exchange, GHSV—gas hourly space velocity).

TiO <sub>2</sub> –Clay Mineral Composite	Synthesis	Reaction Conditions	Maximum NO Conversion/Selectivity to N <sub>2</sub>	Ref.
Cu/Ti-pillared Mt	TiCl <sub>4</sub> precursor + Mt, calcination 300 °C, Ti-PILC SSA = 383 m <sup>2</sup> g <sup>-1</sup> ; Cu-doping by CE or impregnation, calcination 400 °C; best catalyst CE 5.9 wt % Cu, SSA = 346 m <sup>2</sup> g <sup>-1</sup>	250–500 °C, NO = C <sub>2</sub> H <sub>4</sub> = 1000 ppm, O <sub>2</sub> = 2%; 500 ppm SO <sub>2</sub> (when used), 5% H <sub>2</sub> O vapor (when used), balance = He; 0.5 g catalyst, flow rate 250 mL/min <sup>-1</sup>	55% conversion at 300 °C (for the best catalyst), slight inhibition by SO <sub>2</sub> and H <sub>2</sub> O	[119]
Ga/Ti-pillared Mt	TiCl <sub>4</sub> precursor + Mt, calcination 300 °C, Ti-PILC SSA = 383 m <sup>2</sup> g <sup>-1</sup> ; Ga-doping by CE, calcination 400 °C, 5.6 wt % Ga	250–500 °C, NO = C <sub>2</sub> H <sub>4</sub> = 1000 ppm, O <sub>2</sub> = 2%; balance = He; 0.5 g catalyst, flow rate 250 mL/min <sup>-1</sup>	37% conversion at 450 °C	[119]
Fe/Ti-pillared Mt	TiCl <sub>4</sub> precursor + Mt, calcination 300 °C, Ti-PILC SSA = 383 m <sup>2</sup> g <sup>-1</sup> ; Fe-doping by CE, calcination 400 °C, 6.8 wt % Ga	250–500 °C, NO = C <sub>2</sub> H <sub>4</sub> = 1000 ppm, O <sub>2</sub> = 2%; balance = He; 0.5 g catalyst, flow rate 250 mL/min <sup>-1</sup>	31% conversion at 450 °C	[119]

Table 2. Cont.

TiO <sub>2</sub> -Clay Mineral Composite	Synthesis	Reaction Conditions	Maximum NO Conversion/ Selectivity to N <sub>2</sub>	Ref.
Cu/Ti-pillared Mt	Ti(OCH <sub>3</sub> ) <sub>4</sub> precursor + Mt, calcination 500 °C, Ti-PILC SSA = 295 m <sup>2</sup> g <sup>-1</sup> ; Cu-doping by CE or impregnation, calcination 400 °C; best catalyst CE 5.9 wt % Cu, SSA = 234 m <sup>2</sup> g <sup>-1</sup>	220–450 °C, NO = C <sub>3</sub> H <sub>6</sub> = 1000 ppm; O <sub>2</sub> = 5%; 5% H <sub>2</sub> O vapor (when used); balance = He; GHSV = 15,000 h <sup>-1</sup>	55% conversion at 260 °C (for the best catalyst)	[120]
Fe/Ti-pillared Mt	Ti(OCH <sub>3</sub> ) <sub>4</sub> precursor + Mt, calcination 500 °C, Ti-PILC SSA = 295 m <sup>2</sup> g <sup>-1</sup> ; Fe-doping by CE, calcination 400 °C; best catalyst 8 wt % Fe, SSA = 218 m <sup>2</sup> g <sup>-1</sup>	220–450 °C, NO = C <sub>3</sub> H <sub>6</sub> = 1000 ppm; O <sub>2</sub> = 5%; balance = He; GHSV = 15,000 h <sup>-1</sup>	31% conversion at 300 °C (for the best catalyst)	[120]
Ni/Ti-pillared Mt	Ti(OCH <sub>3</sub> ) <sub>4</sub> precursor + Mt, calcination 500 °C, Ti-PILC SSA = 295 m <sup>2</sup> g <sup>-1</sup> ; Ni-doping by CE, calcination 400 °C; best catalyst 3.4 wt % Ni, SSA = 236 m <sup>2</sup> g <sup>-1</sup>	220–450 °C, NO = C <sub>3</sub> H <sub>6</sub> = 1000 ppm; O <sub>2</sub> = 5%; balance = He; GHSV = 15,000 h <sup>-1</sup>	30% conversion at 400 °C (for the best catalyst)	[120]
Fe/Ti-pillared Mt	TiCl <sub>4</sub> precursor + Mt calcination 500 °C, Ti-PILC SSA = 203 m <sup>2</sup> g <sup>-1</sup> ; Fe-doping by CE, calcination 500 °C; best catalyst 19.2 wt % Fe, SSA = 190 m <sup>2</sup> g <sup>-1</sup>	150–600 °C, NO = C <sub>3</sub> H <sub>6</sub> = 1000 ppm; O <sub>2</sub> = 1%; 200 ppm SO <sub>2</sub> (when used), 10% H <sub>2</sub> O (when used); balance = He; GHSV = 12,000 h <sup>-1</sup>	100% conversion at 400 °C, (for the best catalyst), 95% selectivity; slight inhibition by SO <sub>2</sub> and H <sub>2</sub> O	[125]

### 5.2. Total Oxidation of Volatile Organic Compounds

Widespread emission of volatile organic compounds (VOCs) to the atmosphere is considered a major global environmental hazard due to the toxic, mutagenic, and carcinogenic nature of the organic pollutants and their involvement in the formation of the photochemical smog [134]. The main sources of VOCs pollution are industrial processes and transportation activities. Among different techniques for the abatement of VOCs, neutralization based on catalytic combustion is regarded as particularly attractive, owing to its low operational costs and high destruction efficiency [135,136]. As a result of catalytic combustion, the hydrocarbon or oxygen-containing hydrocarbon compounds should be converted to CO<sub>2</sub> and H<sub>2</sub>O, while VOCs containing heteroatoms other than oxygen are expected to yield, beside CO<sub>2</sub> and H<sub>2</sub>O, easily absorbable or nontoxic products (Figure 7). In the case of the most frequently encountered chlorinated VOCs, the desired Cl-containing product is HCl, readily scrubbed with a caustic solution, and for N-containing VOCs, it is crucial to avoid the secondary pollution by NO<sub>x</sub> and convert the nitrogen from the organic compound to N<sub>2</sub>.

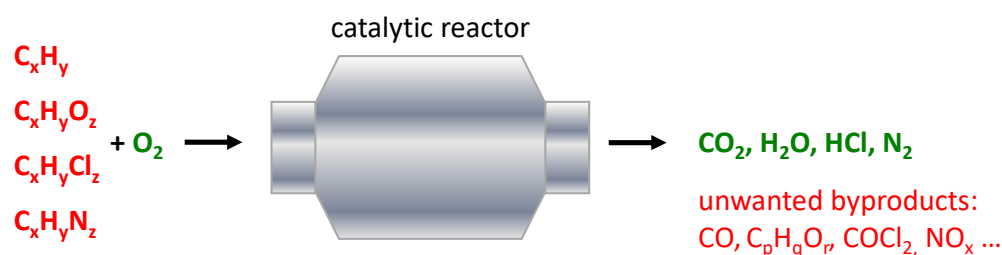


Figure 7. Schematic illustration of catalytic combustion of VOCs.

Pillared clays have been since long tested as catalysts for VOCs abatement [137], but most of the works addressed the use of Al- and Zr-pillared materials rather than the Ti-pillared ones. Nevertheless, reports on the combustion of organic air contaminants over catalysts based on titania–clay mineral composites cover a broad spectrum of pollutants, ranging from hydrocarbons to Cl- and N-containing VOCs.

Among the most widespread hydrocarbon pollutants are aromatics such as benzene, toluene, and xylenes (collectively known as BTX), whose emission stems mainly from their use as industrial solvents and from the uncontrolled combustion of biomass. Liang et al. [138] studied the deep oxidation of toluene, a model BTX compound, using  $\text{FeO}_x$  active phase supported on Ti-pillared montmorillonite obtained with the use of  $\text{TiCl}_4$ . Although the authors referred to the method of Fe deposition as impregnation, description of the procedure clearly shows that the Ti-PILC support, after treatment with  $\text{Fe}(\text{NO}_3)_3$  solution, was subjected to a thorough washing. Impregnation is a procedure that precludes washing prior to drying of the product; therefore, in fact, cation exchange has been used for Fe loading. Obviously, during ion exchange, a degree of precipitation of Fe oxy-hydroxy species may occur as a result of  $\text{Fe}^{3+}$  cation hydrolysis [108]. The lack of (001) reflection in the Ti-PILC XRD pattern pointed to the delamination of the clay mineral component. The content of introduced Fe ranged from 2.7 to 9.5 wt %, but no reflections due to iron oxides were seen even in the most heavily loaded catalyst, indicating good dispersion of the cation-exchanged Fe species. The best catalytic activity was observed for the catalyst of intermediate Fe loading, which was characterized by  $T_{90}$  (temperature at which 90% of toluene was converted) equal to 348 °C. Moreover, the catalyst showed good long-term stability. The authors carried out physicochemical characterization, which assessed the catalysts' reducibility, acidity, and the nature of surface oxygen, and they found that the latter, in particular the surface-adsorbed O species, played the key role in determining the catalyst activity.

A novel approach to the preparation of titania–clay composites for the design of combustion catalysts has been proposed recently by Napruszewska et al. [139]. The authors synthesized MnAl/TiO<sub>2</sub>/clay composites, but rather than using conventional Ti-pillared clay as a support, they employed TiO<sub>2</sub>–montmorillonite systems obtained from exfoliated organo-montmorillonite and inverse (water in oil) microemulsion containing Ti oxo-hydroxy species in aqueous cores of surfactant micelles [140], as schematically illustrated in Figure 8.

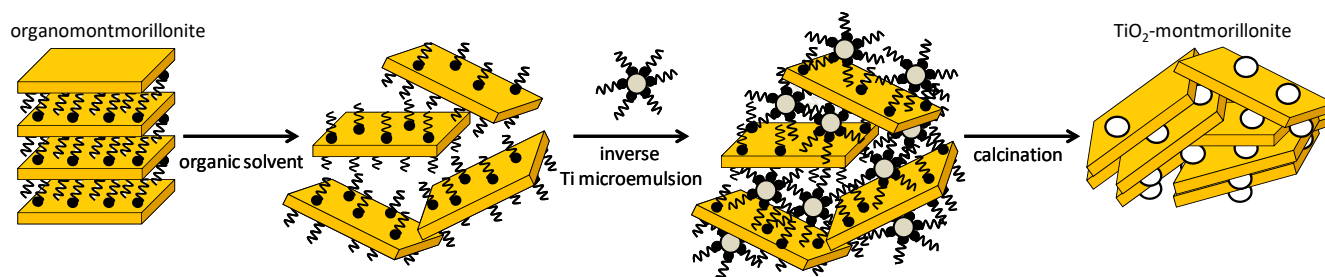


Figure 8. Schematic illustration of the use of inverse Ti microemulsion for the preparation of TiO<sub>2</sub>–montmorillonite composite.

After calcination, such composites contain larger  $\text{TiO}_2$  particles and are therefore mesoporous, which makes them texturally more suitable as hosts for insertion of the catalytically active phase. Ti pillaring solution from  $\text{TiCl}_4$  precursor was used for the preparation of Ti-microemulsion, using 1-hexanol as an oil phase and cetyltrimethylammonium bromide as a surfactant. The microemulsion was added to the organoclay dispersion in 1-hexanol and neutralized by the addition of NaOH or  $\text{NH}_3$  (aq). MnAl hydrotalcite-like compound, chosen as the precursor of the active phase, was also prepared in inverse micelles and intermixed with organo-montmorillonite loaded with titania microemulsion. After washing and drying, the catalysts were calcined at 450 and 600 °C in order to assess their thermal stability. Catalytic tests of toluene combustion revealed that the MnAl/ $\text{TiO}_2$ /clay composites prepared with the use of ammonia showed excellent activity, with  $T_{90}$  of 239 and 252 °C for catalysts calcined at 450 and 600 °C, respectively. Comparison with the literature data showed that the novel catalysts performed considerably better in deep oxidation of toluene than any of the other previously described pillared clay–transition metal oxide composite catalysts. The superior performance of catalysts obtained with the use of ammonia, with respect to those prepared with NaOH, was attributed to the more uniform and thermally stable mesoporous network, coupled with a high abundance of more reducible Mn species.

Several reports focused on the application of titania–clay composites for the destruction of Cl-containing VOCs [141–144]. Chlorinated organics are widely used as solvents in many industrial activities, such as the manufacturing of chemicals (e.g., vinyl chloride) and pharmaceuticals, degreasing of metal surfaces, dry cleaning, or printing. Catalysts for the deep oxidation of chlorinated VOCs should be characterized by an enhanced resistance to hydrogen chloride, since HCl is the desired chlorine-containing product of catalytic combustion. Bahranowski et al. [141] pointed out that montmorillonites intercalated with Ti-, Zr-, or mixed Ti,Zr- pillars represent chemically robust porous structures that are well suited for designing catalysts for the combustion of chlorinated VOCs. Pd and/or Cr active phase (1 wt %) was deposited on such supports by means of incipient wetness impregnation. In a separate work, the authors found that impregnation of calcined support resulted in a more active catalyst than impregnation carried out prior to the support calcination [142]. Detailed physicochemical characterization showed that the catalysts were porous solids with high surface area (240–390  $\text{m}^2/\text{g}$ ). Pd was spread over the surface in the form of fine  $\text{PdO}_x$  nanoparticles of  $\leq 10$  nm size, while Cr was present chiefly as monomeric  $\text{CrO}_x$  species. Co-impregnation of Pd and Cr improved the dispersion of palladium. Both the Pd- and the Cr-containing catalysts were most reducible when supported on Ti-PILC, and they showed the highest acidity, predominantly of the Lewis type, on the [Ti,Zr]-PILC carrier. The materials were tested in combustion of dichloromethane (DCM) and trichloroethylene (TCE) and proved remarkably active, selective, and durable, vastly outperforming the commercial Pd,Pt/ $\text{Al}_2\text{O}_3$  reference. The excellent catalytic properties were attributed to the combination of highly porous structure of PILC supports, enabling multiple contacts of reactants with active centers on the catalyst surface, good dispersion of the active phase, and an appropriate blend of redox and acid–base functions of the catalysts. The influence of the nature of the PILC support on the catalyst activity varied, depending on the type of chlorinated hydrocarbon. In DCM combustion, Ti-PILC supported catalysts showed superior performance, due to the much better reducibility of active phases deposited on this carrier, which pointed to the determining role of the lattice oxygen insertion step in the chain of transformations leading to DCM destruction. In the oxidation of TCE, the best activity was observed for catalysts supported on [Ti,Zr]-PILC, which are characterized by the highest Lewis acidity and indicated that TCE interaction with the catalysts was governed by the Lewis base character of the TCE double bond. For both studied reactions, the Pd-only catalysts showed 100% selectivity to HCl and  $\text{CO}_2$  at  $T_{90}$ . The Cr-only catalysts were most active but least selective and emitted substantial amounts of  $\text{Cl}_2$  and CO. Mixed (Pd,Cr)-containing samples represented an attractive, cheaper alternative to purely Pd systems, as at  $T_{90}$  their selectivity to  $\text{CO}_2$  was 100%, while selectivity to HCl ranged from 87 to 100%, depending on the oxidized chlorohydrocarbon and type of PILC

support. Longevity tests demonstrated that PILC-supported catalysts were very stable in the reaction environment both in terms of the catalytic performance and the chemical and structural identity.

Catalysts based on titania–clay mineral composites were also investigated for their activity in the total oxidation of chlorobenzenes, which are widely studied model reactions of dioxin destruction [143,144]. Zuo et al. [143] prepared a series of Cr-based Ti-PILC-supported catalysts doped with various amounts of cerium (10 wt % Cr+Ce). Ti-PILC was synthesized using  $\text{Ti}(\text{OC}_4\text{H}_9)_4$  as a titanium source for montmorillonite pillaring. Active phase was deposited by impregnation with mixed solutions of  $\text{Cr}(\text{NO}_3)_3$  and  $\text{Ce}(\text{NO}_3)_3$ , with a molar ratio of Cr/Ce equal to 3:1, 6:1, and 9:1. The catalyst with Cr:Ce = 6:1 enabled the complete oxidation of a low concentration of chlorobenzene at approximately 250 °C, and  $\text{H}_2\text{O}$ ,  $\text{CO}_2$ , and HCl were the only reaction products. The result placed the Ti-PILC-supported Cr,Ce catalyst among the most active described in the literature. Another type of catalyst active in the removal of chlorinated aromatics was prepared by He et al. [144], who studied the combustion of 1,2-dichlorobenzene over  $\text{TiO}_2$ –palygorskite composites doped with vanadium and tungsten. The catalysts were prepared in a simple manner by impregnating a physical mixture of palygorskite and titania powders with solution of  $\text{NH}_4\text{VO}_3$  and  $(\text{NH}_4)_{10}\text{H}_2(\text{W}_2\text{O}_7)_6$ . The authors optimized the content of clay mineral in the composite and found that the highest catalytic activity, corresponding to 90% 1,2-dichlorobenzene conversion, was obtained with the catalyst containing 33 wt % of palygorskite. The reference catalyst, without palygorskite component, showed similar activity, which made the clay-containing formula more attractive as a cheaper and more benign option.

N-containing VOCs such as, e.g., amines, nitro compounds, and/or nitriles, generated mainly by textile, agricultural, pharmaceutical, and chemical industries, represent yet another type of toxic atmosphere pollutants. The first report on the neutralization of nitrogen-containing VOCs with the aid of Ti-PILC supported catalyst has been published by Huang et al. [145], who compared the performance of Cr–Ce active phase deposited on Al-PILC, Zr-PILC, Ti-PILC, and  $\text{Al}_2\text{O}_3/\text{Ti-PILC}$  in deep oxidation of n-butylamine, ethylenediamine, and acetonitrile. Ti-PILC was obtained from  $\text{Ti}(\text{OC}_4\text{H}_9)_4$  precursor. The  $\text{Al}_2\text{O}_3/\text{Ti-PILC}$  support was prepared by treatment of the non-calcined Ti-PILC with Al-pillaring solution, which was followed by drying and calcination. All supports were impregnated with mixed solutions of  $\text{Cr}(\text{NO}_3)_3$  and  $\text{Ce}(\text{NO}_3)_3$  to give the total content of Cr and Ce equal 8 wt % and a Cr/Ce atomic ratio of 6:1. CrCe/Ti-PILC and CrCe/ $\text{Al}_2\text{O}_3/\text{Ti-PILC}$  exhibited higher catalytic activity than other catalysts. All catalysts showed good selectivity to  $\text{N}_2$ , with a yield of  $\text{NO}_x$  not exceeding 2%. In a later work [146], the authors investigated the influence of the Ti-PILC synthesis conditions on the CrCe/Ti-PILC catalyst efficiency in the destruction of n-butylamine and found that the appropriate choice of the aging time of the pillaring solution and/or of the temperature of pillaring enabled optimization of the catalytic performance. The effect was attributed to the enhancement of the support textural parameters, which favored synergetic interaction between the  $\text{CrO}_x$ – $\text{CeO}_2$  phase and the Ti-PILC support.

The most relevant data on the synthesis and catalytic performance of  $\text{TiO}_2$ –clay mineral composites in the elimination of volatile organic pollutants are gathered in Table 3.

**Table 3.** Summary of main synthesis and catalysis data for the most relevant examples of TiO<sub>2</sub>–clay mineral composites used as catalysts for the combustion of VOCs (T<sup>X</sup> = temperature at X% conversion), Ht—hydrotalcite, Mt—montmorillonite, Pal—palygorskite, HDTMA—hexadecyltrimethylammonium cation, IM—inverse microemulsion, CE—cation exchange, GHSV—gas hourly space velocity).

TiO <sub>2</sub> –Clay Mineral Composite	Synthesis	Reaction Conditions	T <sup>X</sup>	VOC	Ref.
Fe/Ti-pillared Mt	TiCl <sub>4</sub> precursor + Mt, calcination 500 °C, SSA = 230 m <sup>2</sup> g <sup>−1</sup> ; Fe-doping by CE, calcination 500 °C; best catalyst 3.8% Fe <sub>2</sub> O <sub>3</sub> wt %, SSA = 185 m <sup>2</sup> g <sup>−1</sup>	250–450 °C, toluene = 1000 ppm, air; 0.1 g catalyst, flow rate 100 mL/min <sup>−1</sup>	T <sup>90</sup> = 347 °C (for the best catalyst)	Toluene	[138]
Mn/TiO <sub>2</sub> /Mt	HDTMA-Mt + TiO <sub>2</sub> IM + MnAl Ht IM, calcination 450 and 600 °C, best catalyst calcination 450 °C, 17.5 wt % MnO, SSA = 178 m <sup>2</sup> g <sup>−1</sup>	100–400 °C, toluene = 500 ppm, air; GHSV = 10,000 h <sup>−1</sup>	T <sup>90</sup> = 239 °C (for the best catalyst)	Toluene	[139]
Pd,Cr/Ti-pillared Mt	TiCl <sub>4</sub> precursor + Mt, calcination 400 °C, Ti-PILC SSA = 379 m <sup>2</sup> g <sup>−1</sup> ; Pd,Cr-doping by impregnation, calcination 500 °C, best catalyst 1 wt % Pd, SSA = 392 m <sup>2</sup> g <sup>−1</sup>	200–550 °C, DCM = 530 ppm, air; 10% H <sub>2</sub> O vapor; GHSV = 10,000 h <sup>−1</sup>	T <sup>90</sup> = 339 °C (for the best catalyst)	Dichloromethane (DCM)	[141]
Pd,Cr/Ti,Zr-pillared Mt	TiCl <sub>4</sub> + ZrOCl <sub>2</sub> precursor + Mt, calcination 400 °C, Ti,Zr-PILC SSA = 379 m <sup>2</sup> g <sup>−1</sup> ; Pd,Cr-doping by impregnation, calcination 500 °C, best catalyst 1 wt % Pd, SSA = 342 m <sup>2</sup> g <sup>−1</sup>	200–550 °C, DCM = 530 ppm, air; 10% H <sub>2</sub> O vapor; GHSV = 10,000 h <sup>−1</sup>	T <sup>90</sup> = 395 °C (for the best catalyst)	Dichloromethane (DCM)	[141]
Pd,Cr/Ti-pillared Mt	TiCl <sub>4</sub> precursor + Mt, calcination 400 °C, Ti-PILC SSA = 379 m <sup>2</sup> g <sup>−1</sup> ; Pd,Cr-doping by impregnation, calcination 500 °C, best catalyst 0.5 wt % Pd + 0.5 wt % Cr, SSA = 378 m <sup>2</sup> g <sup>−1</sup>	200–550 °C, TCE = 340 ppm, air; 10% H <sub>2</sub> O vapor; GHSV = 10,000 h <sup>−1</sup>	T <sup>90</sup> = 338 °C (for the best catalyst)	Trichloroethylene (TCE)	[141]
Pd,Cr/Ti,Zr-pillared Mt	TiCl <sub>4</sub> + ZrOCl <sub>2</sub> precursor + Mt, calcination 40, 0 °C, Ti,Zr-PILC SSA = 379 m <sup>2</sup> g <sup>−1</sup> ; Pd,Cr-doping by impregnation, calcination 500 °C, best catalyst 0.5 wt % Pd + 0.5 wt % Cr, SSA = 352 m <sup>2</sup> g <sup>−1</sup>	200–550 °C, TCE = 340 ppm, air; 10% H <sub>2</sub> O vapor; GHSV = 10,000 h <sup>−1</sup> .	T <sup>90</sup> = 328 °C (for the best catalyst)	Trichloroethylene (TCE)	[141]
Cr,Ce/Ti-pillared Mt	Ti(OC <sub>4</sub> H <sub>9</sub> ) <sub>4</sub> precursor + Mt, calcination 550 °C, Ti-PILC SSA = 225 m <sup>2</sup> g <sup>−1</sup> ; Cr,Ce-doping by impregnation, calcination 500 °C, best catalyst 8.6 wt % Cr + 1.4 wt % Ce, SSA = 179 m <sup>2</sup> g <sup>−1</sup>	200–550 °C, CB = 500 ppm, air; GHSV = 20,000 h <sup>−1</sup>	T <sup>100</sup> = 250 °C (for the best catalyst)	Chlorobenzene (CB)	[143]

Table 3. Cont.

TiO <sub>2</sub> -Clay Mineral Composite	Synthesis	Reaction Conditions	T <sup>x</sup>	VOC	Ref.
V,W/TiO <sub>2</sub> -Pal	TiO <sub>2</sub> and Pal mixture, V,W-doping by impregnation, calcination 500 °C, best catalyst mass ratio (VO <sub>x</sub> +WO <sub>y</sub> +TiO <sub>2</sub> ):Pal = 2	200–350 °C, <i>o</i> -DCB = 3%, air; GHSV = 28,000 h <sup>-1</sup>	T <sup>90</sup> = 300 °C (for the best catalyst)	<i>o</i> -Dichlorobenzene ( <i>o</i> -DCB)	[144]
Cr,Ce/Ti-pillared Mt	Ti(OC <sub>4</sub> H <sub>9</sub> ) <sub>4</sub> precursor + Mt, calcination 500 °C, Ti-PILC SSA = 207 m <sup>2</sup> g <sup>-1</sup> ; Cr,Ce-doping by impregnation, calcination 500 °C, 6.9 wt % Cr + 1.1 wt % Ce, SSA = 183 m <sup>2</sup> g <sup>-1</sup>	120–340 °C, <i>n</i> -butylamine = 1000 ppm, air; GHSV = 20,000 h <sup>-1</sup>	T <sup>90</sup> = 231 °C	<i>n</i> -Butylamine	[145]
Cr,Ce/Ti-pillared Mt	Ti(OC <sub>4</sub> H <sub>9</sub> ) <sub>4</sub> precursor + Mt, calcination 500 °C, Ti-PILC SSA = 207 m <sup>2</sup> g <sup>-1</sup> ; Cr,Ce-doping by impregnation, calcination 500 °C, 6.9 wt % Cr + 1.1 wt % Ce, SSA = 183 m <sup>2</sup> g <sup>-1</sup>	140–340 °C, ethylenediamine = 1000 ppm, air; GHSV = 20,000 h <sup>-1</sup>	T <sup>90</sup> = 254 °C	Ethylenediamine	[145]
Cr,Ce/Ti-pillared Mt	Ti(OC <sub>4</sub> H <sub>9</sub> ) <sub>4</sub> precursor + Mt, calcination 500 °C, Ti-PILC SSA = 207 m <sup>2</sup> g <sup>-1</sup> ; Cr,Ce-doping by impregnation, calcination 500 °C, 6.9 wt % Cr + 1.1 wt % Ce, SSA = 183 m <sup>2</sup> g <sup>-1</sup>	200–340 °C, acetonitrile = 1000 ppm, air; GHSV = 20,000 h <sup>-1</sup>	T <sup>90</sup> = 277 °C	Acetonitrile	[145]

## 6. TiO<sub>2</sub>-Clay Mineral Composites for Photocatalytic Applications

Photocatalytic reactions proceed on the surface of a metal oxide semiconductor under light irradiation according to the scheme presented in Figure 9. The process starts with the absorption of a photon with energy greater than the band gap of the semiconducting catalyst, which causes the excitation of a valence band electron to the conduction band, leaving behind a positively charged electron hole. The photogenerated charge carriers may migrate to the surface and participate in the interfacial charge transfer reactions with the available molecules and/or ions of acceptor or donor character, which is the essence of photocatalytic transformations.

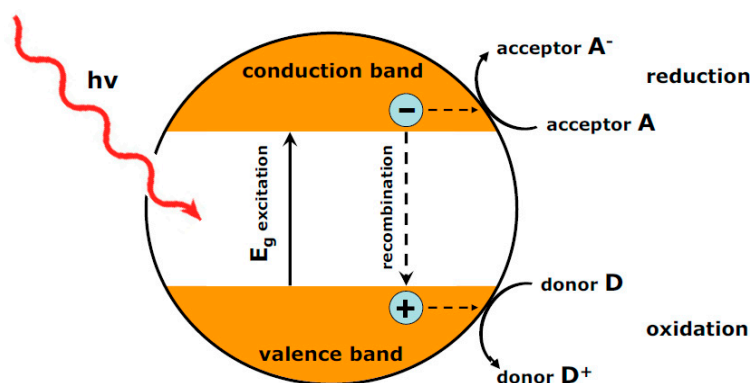
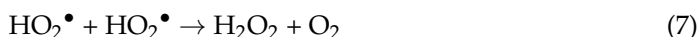
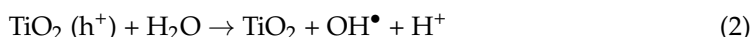


Figure 9. Schematic illustration of a photocatalytic effect on the surface of a semiconductor.

Since the seminal work of Fujishima and Honda [12], titania is the semiconductor on which most of the attention has been focused. When  $\text{TiO}_2$  is illuminated with light of appropriate energy, reactions of photogenerated holes and electrons with donors and acceptors present at the photocatalyst surface produce reactive species of high oxidation potential. The basic mechanism of their formation during photocatalytic reactions with the use of aqueous suspensions of  $\text{TiO}_2$  may be illustrated by the set of the following equations [30,31]:



The process starts with the reaction of photogenerated holes with surface  $\text{OH}^-$  groups or water molecules, to yield hydroxyl radicals  $\text{OH}^\bullet$ , and with the reaction of photogenerated electrons with adsorbed dioxygen molecules to give  $\text{O}_2^{\bullet-}$  superoxide radical anions, as described by Equations (1)–(4). The subsequent protonation of a superoxide anion yields hydroperoxyl radical  $\text{HO}_2^\bullet$ , which may trap a photoelectron and transform to hydroperoxide anion, as indicated by Equations (5) and (6). Eventually, both intermediates form  $\text{H}_2\text{O}_2$  (Equations (7) and (8)). The photogenerated holes, as well as  $\text{OH}^\bullet$ ,  $\text{O}_2^{\bullet-}$ ,  $\text{HO}_2^\bullet$ , and  $\text{H}_2\text{O}_2$ , are highly reactive powerful oxidants playing a key role in heterogeneous photocatalysis at the  $\text{TiO}_2$  surface. The species are capable of oxidative decomposition of even the most refractory organic molecules. Many organic contaminants of the environment, especially the ones with low molecular weight, cannot be easily eliminated by conventional methods, such as, e.g., filtration. Some of them, while not dangerous themselves, cause a serious concern because they facilitate the growth of bacteria. This makes disinfection a necessary step in water treatment. If the disinfection of water involves chlorination, some low molecular weight organic compounds may change into very toxic products. For example, acetic acid, safe at low concentrations, transforms upon chlorination into trichloroacetic acid, which is a very hazardous and hard to remove environmental toxin. It is noteworthy that the organic contaminants in water stem not only from the industrial and household sewage but also from the decomposition of natural matter, e.g., that ever present in nature humic substances. Photocatalysis based on  $\text{TiO}_2$  is of key importance in the design of advanced oxidation technologies aimed at the elimination of organic pollutants from the environment [13,16,17,30].

Anatase and rutile are the most studied titania polymorphs. Their band gaps are 3.2 and 3.0 eV, respectively, which means they are primarily activated not by visible light but by ultraviolet (UV) light. Anatase exhibits a higher photocatalytic activity compared to rutile, because of the deeper sub-surface region that contributes charge carriers to photoreactions [147]. Despite the fact that only a small fraction of solar radiation can be used, titania has the advantage of being able to efficiently catalyze reactions due to suitable positions of valence and conduction bands, and, in addition, it is chemically and photocatalytically stable, relatively easy to produce and use, cheap and, due to the biological inertness, safe for the ecosystem.

The immobilization of  $\text{TiO}_2$  nanoparticles on various supports facilitates the handling of the titania photocatalyst and prevents its agglomeration. Moreover, textural and surface properties of supports may have direct impact on the course of photocatalytic reaction. Clay minerals, due to their abundance, ecofriendly nature, and physicochemical properties

enabling the formation of nanoarchitectures, have been widely explored in the capacity of TiO<sub>2</sub> carriers for photocatalytic purposes (see reviews [17,29–34,148,149]).

The first reports on the use of Ti-PILC materials as photocatalysts [58,150] appeared only a few years after syntheses of these porous solids had been described [44,45]. Tanguy et al. [150] investigated the use of various titania catalysts in the photocatalytic destruction of dichloromethane and found that the Ti-PILC obtained by the method of Sterte [44] from TiCl<sub>4</sub> precursor was more active than the un-pillared clay but less active than unsupported rutile or anatase. Around the same time Yoneyama et al. [58] reported that Ti-PILC, synthesized following the Yamanaka approach [45] from a titanium tetraisopropoxide precursor, was more active in the photocatalytic decomposition of 2-propanol and *n*-carboxylic acids ( $n \leq 8$ ) than powder TiO<sub>2</sub>. In the case of capric acid ( $n = 10$ ), the activity of Ti-PILC was lower than that of the TiO<sub>2</sub> reference. The effect was attributed to the difficulties regarding the accommodation of large organic molecules in the Ti-PILC pore network and suggested that classical Ti-PILC, characterized by a long-range stacking order and being predominantly microporous, may exert diffusional limitations when used as photocatalysts.

It took a decade before the next important contributions addressing aspects of key significance for the development of TiO<sub>2</sub>–clay composite photocatalysts appeared [61,151–153]. The paper by Ding et al. [151] drew attention to the fact that the efficiency of photocatalysis depended on the accessibility of TiO<sub>2</sub> pillars to both the organic reagents and the light. The former requires a well-developed network of pores large enough to enable the facile diffusion of reagents. Accessibility to light depends on the pillar location within the clay grain. Although clay is transparent to UV irradiation, the absorption of light by TiO<sub>2</sub> pillars buried deeply in the clay platelet is obstructed by pillars located closer to the surface. Therefore, a possibly high external surface area plays a crucial role in controlling the photocatalytic activity of titania–clay composites. The authors prepared Ti-PILC composites from montmorillonite and titanium tetraisopropoxide as a pillar precursor and demonstrated that the application of different drying methods such as air drying, air drying after ethanol extraction, and supercritical drying had a great impact on the size of the TiO<sub>2</sub> nanoparticles (6.6–12.3 nm) and the development of the pore network, affecting as a consequence the photocatalytic performance. In particular, the sample obtained by supercritical drying was characterized by the smallest anatase crystallites, the highest microporosity, and the highest external surface area, and it displayed the best photocatalytic activity in the degradation of phenol. It is noteworthy that the titania nanoparticles prepared in this study were of significantly larger dimensions than titania pillars in the classical Ti-PILC (usually not exceeding 2 nm), and the clay layers showed no long-range stacking order; therefore, the composites should be considered rather as nanocrystalline titania supported on a disordered clay. A different aspect of TiO<sub>2</sub>–clay composite design was addressed by Ooka et al. [61], who pointed out that small TiO<sub>2</sub> pillars present in conventionally synthesized Ti-PILC were generally amorphous or very poorly crystalline and hence unfavorable for photoactivity. To overcome this obstacle, they subjected Ti-pillared montmorillonite to the post-synthetic hydrothermal treatment which led, after calcination at 500 °C, to the crystallization of pillars in the form of anatase, while retaining the porosity of the pillared clay. The TiO<sub>2</sub> crystal size could be controlled in the range 4–9 nm by the appropriate choice of hydrothermal treatment temperature (200–250 °C) and/or time (1–24 h). A quantum size effect, consisting of blue shift of the UV absorption edge with respect to the bulk anatase, was observed with the decreasing size of TiO<sub>2</sub> props. Both the crystallization of pillars and the decrease in their size were found to be beneficial for the photocatalytic activity in the degradation of trichloroethylene in water. The same group [152] found that hydrothermally crystallized TiO<sub>2</sub> pillars had a higher photocatalytic activity for the degradation of dibutyl phthalate (DBP), which is a model endocrine disruptor, i.e., a substance that enters the body and mimics hormones, thus disrupting the functions of hormones naturally secreted by the organism. Another interesting observation has been made by Cheng [153], who reported that in the case of phenyl pollutants, the efficiency of photodegradation by Ti-PILC, as com-

pared to TiO<sub>2</sub> powder reference, varied and depended on the contaminant hydrophobicity. Thus, Ti-PILC showed superior photocatalytic activity when the phenyl contaminants were hydrophobic, such as, e.g., benzene, but it performed poorer in the case of the hydrophilic phenol. The phenomenon suggested that the hydrophobic/hydrophilic interactions at the internal surface of Ti-PILC pore network played an important role in directing the reactant toward the photoactive site.

The issues raised in these works, in particular the role of the composite architecture in relation to the accessibility of the photoactive sites, the importance of the TiO<sub>2</sub> nanoparticles distribution and crystallinity, as well as the role of the clay mineral surface hydrophobicity, identified the areas of interest in titania–clay photocatalysts design, which continued to be widely explored in the next few years, especially in the field of environmental remediation.

### 6.1. Photodegradation of Organic Pollutants in Water

The increasing pollution of the world's freshwater resources, caused by the discharge of agricultural, industrial, and municipal wastes into natural water bodies, constitutes a serious threat to human health and to the sustainability of ecosystems. According to recent estimates, by 2050, nearly six billion people will suffer from clean water scarcity, which makes the remediation of water pollution a topic of prime importance and universal awareness [154]. Accordingly, as indicated in a number of reviews [17,29–31,148,149,155], the majority of published research on the application of TiO<sub>2</sub>–clay mineral composites in photocatalysis are related to the purification of water from toxic organic contaminants. Most of the research has been carried out on the degradation of dyes and phenolic compounds, the refractory contaminants released from a wide spectrum of sources, including textile, leather, printing, paper, food, chemical, and paint industries. More recently, destruction of the so-called emerging pollutants (pharmaceuticals, pesticides, herbicides, etc.) became the target of investigation.

#### 6.1.1. Photodegradation of Dyes

It is estimated that up to 20% of the total world production of dyes may be lost during the dyeing processes and end up as water contaminants [156]. In view of the dyes' chemical stability and toxicity, this constitutes a serious health risk and is a source an increasing environmental concern.

The first works on the ability of TiO<sub>2</sub>/clay composites to photocatalyze the degradation of dye pollutants in aqueous medium appeared two decades ago [157–160], and the topic continues to attract an ever-growing scientific interest. From the very beginning, modifications of the synthetic procedures of titania–clay composites, aiming at improvement of their photocatalytic activity, belonged to the leading research trends. Thus, Awate and Suzuki [157] investigated the effect of hydrothermal post-synthesis treatment of Ti-pillared montmorillonite synthesized from Ti tetraisopropoxide on its photocatalytic activity in the degradation of two dyes: Methylene Blue and Victoria Pure Blue. In agreement with earlier results [61,152], the authors found that the post-synthesis hydrothermal treatment, enhancing the crystallization of anatase nanoparticles, was beneficial for the photocatalytic activity. Comparing to the untreated Ti-PILC, the efficiency of adsorption and photo-oxidation of Methylene Blue increased from 85 to 99%, and that of Victoria Pure Blue increased from 58 to 93%. Noteworthy, it has been recently demonstrated [55] that also hydrothermal treatment applied during the pillaring of montmorillonite increased the crystallinity of titania pillars and improved the photocatalytic properties of the composites in the degradation of Methyl Orange and Rhodamine B under UV. Sun et al. [158] reported that the TiO<sub>2</sub>–bentonite nanocomposite obtained using Ti tetrabutoxide as a precursor displayed higher photocatalytic activity in the degradation of an azo dye Cationic Red GTL than the commercial titania P25, manufactured by Degussa, which has an established high activity photocatalytic standard. In Figure 10, the morphology of P25 is compared with that of TiO<sub>2</sub> nanoparticles obtained by the sol–gel method and by an inverse micellar route. Sun et al. observed that the composite catalysts sedimented much faster than P25 nanoparticles and

could be easily recovered from the reaction medium. Various studies carried out over the next few years confirmed that facile settlement from aqueous suspension, much swifter than in the case of bare titania nanopowders, was a characteristic feature of titania–clay composites, irrespective of the details of the synthesis procedure.

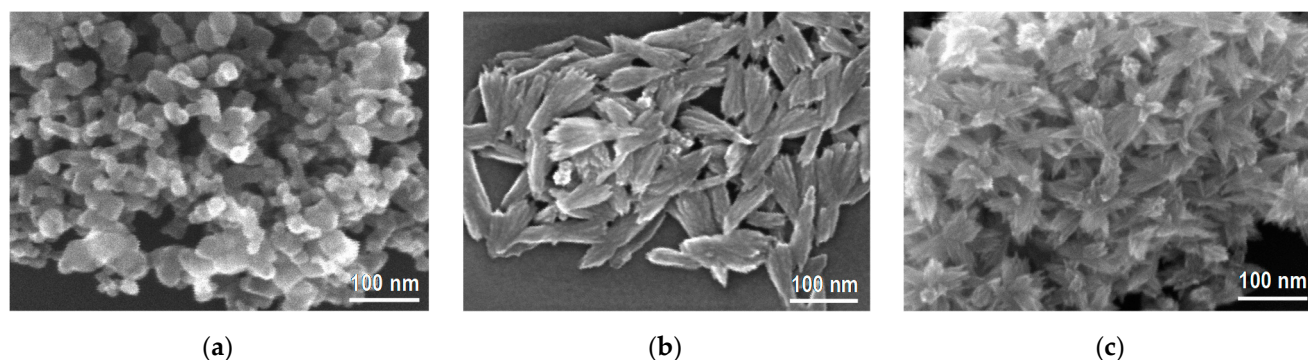


**Figure 10.** SEM images of (a) P25 standard; (b) TiO<sub>2</sub> obtained by sol–gel method; (c) TiO<sub>2</sub> obtained by inverse microemulsion method. Both (b,c) samples obtained from TiCl<sub>4</sub> precursor.

Interesting results were obtained when Laponite, a synthetic hectorite, which readily undergoes exfoliation when dispersed in water, was employed for the preparation of composites with titania [159,160]. Zhu et al. [159] synthesized the photocatalysts from the dispersion of Laponite containing polyethylene oxide surfactant (PEO). The authors pointed out that the addition of strongly acidic pillaring solution prepared from Ti tetraisopropoxide to Laponite clay of basic character, followed by hydrothermal treatment, led to the leaching of magnesium from the clay and simultaneously prompted the polymerization of the Ti sol particles. The presence of PEO increased the porosity and surface area of the solids. Moreover, the size of the TiO<sub>2</sub> particles could be tailored by manipulating the synthesis parameters. Nearly 100% removal of Rhodamine 6G could be achieved over such a composite within 1 h of UV irradiation, due to both adsorption and photocatalysis. When calculated per mass of titania, the photocatalytic performance of composite solids in the degradation of Rhodamine 6G was superior to that of P25 reference. Li et al. [160] investigated three titania–clay composites as photocatalysts for the degradation of sulforhodamine B, one based on Laponite and two based on bentonite, using the hydrolysis of titanium tetraisopropoxide for TiO<sub>2</sub> component synthesis. Of the bentonite composites, one was dried in air, while the other was dried in the supercritical conditions. The Laponite-based catalyst, which eliminated 77% dye within 40 min of UV irradiation, proved comparable to P25 (95% efficiency) despite the lower content of TiO<sub>2</sub> in the sample. In the case of bentonite-based catalysts, the material subjected to supercritical drying performed better (56% efficiency) than the air-dried one (2% efficiency) due to the higher crystallinity of the TiO<sub>2</sub> phase and better textural properties. However, the photo-effect overlapped with a very strong sorption of the cationic dye, which the authors considered as potentially detrimental to the photocatalytic application. In fact, the sorption of this and other cationic dyes is a common effect when clay minerals with prominent cation exchange properties are used for composite synthesis. Nevertheless, most authors consider the combination of sorptive and photocatalytic properties an advantage. The difference in the performance of titania/montmorillonite composite toward the photocatalytic destruction of cationic (Crystal Violet, Methylene Blue, Rhodamine B) and anionic (Methyl Orange, Congo Red) dyes was clearly illustrated in the work of Djellabi et al. [161] for materials obtained by the impregnation of clay with TiCl<sub>4</sub>, which was followed by calcination at 350 °C. The comparison demonstrated that in the case of cationic dyes, the TiO<sub>2</sub>/clay composite was more efficient in the elimination of pollutant than the P25 reference, which was due to the enhanced adsorption of dye on its surface. The authors argued that adsorption led to a higher concentration of dye molecules around the TiO<sub>2</sub> particles, resulting in an increase in

the degradation rate. The effect was absent in the case of anionic dyes, for which P25 was a better photocatalyst.

Research following the early works covered the photodegradation of a number of different dyes and various titania–clay composites, which were designed with the use of a range of synthetic procedures, different clay minerals, and variously generated titania components.

The majority of photocatalyst syntheses involved the use of montmorillonite/bentonite and addressed various aspects of the materials preparation. One of the frequently explored synthesis modifications was the use of microwave irradiation at various stages of composite formation [52,64,162]. The advantage of microwave heating over conventional heating consisted primarily of shorter reaction times, but the impact on the composite structure and texture was also observed. For instance, Sun et al. [64] obtained Ti-pillared montmorillonite using microwave irradiation at the stage of clay treatment with pillaring solution prepared from Ti tetrabutoxide precursor and compared its performance in the photocatalytic degradation of Methyl Orange with that of the reference Ti-PILC obtained without the use of microwave heating. The authors found that the composite treated by microwaves was nearly four times more active than the one obtained by the conventional method, and they attributed the effect to the enhanced crystallinity of titania pillars coupled with the preferred formation of anatase phase and improved porosity. Damardji et al. [52,162] obtained final Ti-PILC solids either by 3 h calcination at 400 °C or by 10 min heat treatment in a commercial microwave apparatus. The crystallinity of anatase after the microwave treatment was higher than after conventional heating but lower than that of P25. The materials were tested as photocatalysts in the degradation of Solophenyl Red 3BL, which is an anionic azo dye used in textile plants. Photodegradation was higher at acidic pH, which is in agreement with the optimum adsorption of the dye on the pillared montmorillonites. In the same irradiation time of 160 min, the microwave calcined Ti-PILC displayed higher photoreactivity (83%) than the catalyst obtained by conventional heating (55% efficiency) but lower than P25 (100% efficiency), which suggested that the photocatalytic effect was enhanced by the increasing crystallinity of TiO<sub>2</sub> nanoparticles. The authors identified hydroxyl radicals as the main species involved in photocatalysis.

Miao et al. [163] obtained the TiO<sub>2</sub>–montmorillonite composites by the intercalation of Ti tetrabutoxide into the interlayers of clay mineral in supercritical ethanol, which was followed by hydrolysis in water and calcination at 500 °C. The composite was shown to contain anatase particles with less than 5 nm size, which were deposited onto the partially exfoliated montmorillonite layers. It was demonstrated that the photocatalysts exhibited high efficiency to remove cationic dye Methylene Blue from aqueous solutions, eliminating 99% of dye within 1 h, due to the combined effect of the adsorptive capacity of clay component and the photocatalytic degradation ability of TiO<sub>2</sub> nanoparticles.

In an attempt to prepare the photocatalyst with enhanced porosity, Liu et al. [164] prepared montmorillonite intercalated with mixed SiO<sub>2</sub>–TiO<sub>2</sub> particles, which was characterized by an interlayer spacing of 4.65 nm and large SSA of 445 m<sup>2</sup>/g. The material proved efficient in the degradation of Methyl Orange (89% in 6 h), but the result was not referred to the unsupported titania.

Zhang et al. [165] synthesized TiO<sub>2</sub>/montmorillonite photocatalysts following the method of Sterte [44] by the intercalation of titania sol prepared from TiCl<sub>4</sub> precursor, varying the temperature of aging in the 30–70 °C range. The stage of calcination was eliminated, leaving drying at 80 °C as the final thermal treatment. The materials showed high photocatalytic activity for the degradation of Acid Red G, which could be completely destroyed within 60 min of UV light irradiation. XRD analysis pointed to the disordered character of the clay component structure, which was confirmed by TEM images showing exfoliated single-layered and multilayered sheets, as marked in Figure 11a,b. Moreover, TEM analysis identified TiO<sub>2</sub> (anatase) nanoparticles with the lattice fringe spacing of about 0.33 nm and size less than 5 nm, as indicated by arrows in Figure 11c. The selected area electron diffraction (SAED) confirmed that the nanoparticles possess the structure

of anatase (Figure 11d). Despite the size of nanoparticles estimated to be less than 5 nm, the UV absorption edge was red shifted with respect to that of bare TiO<sub>2</sub>, rather than blue shifted as expected for quantum size effect.

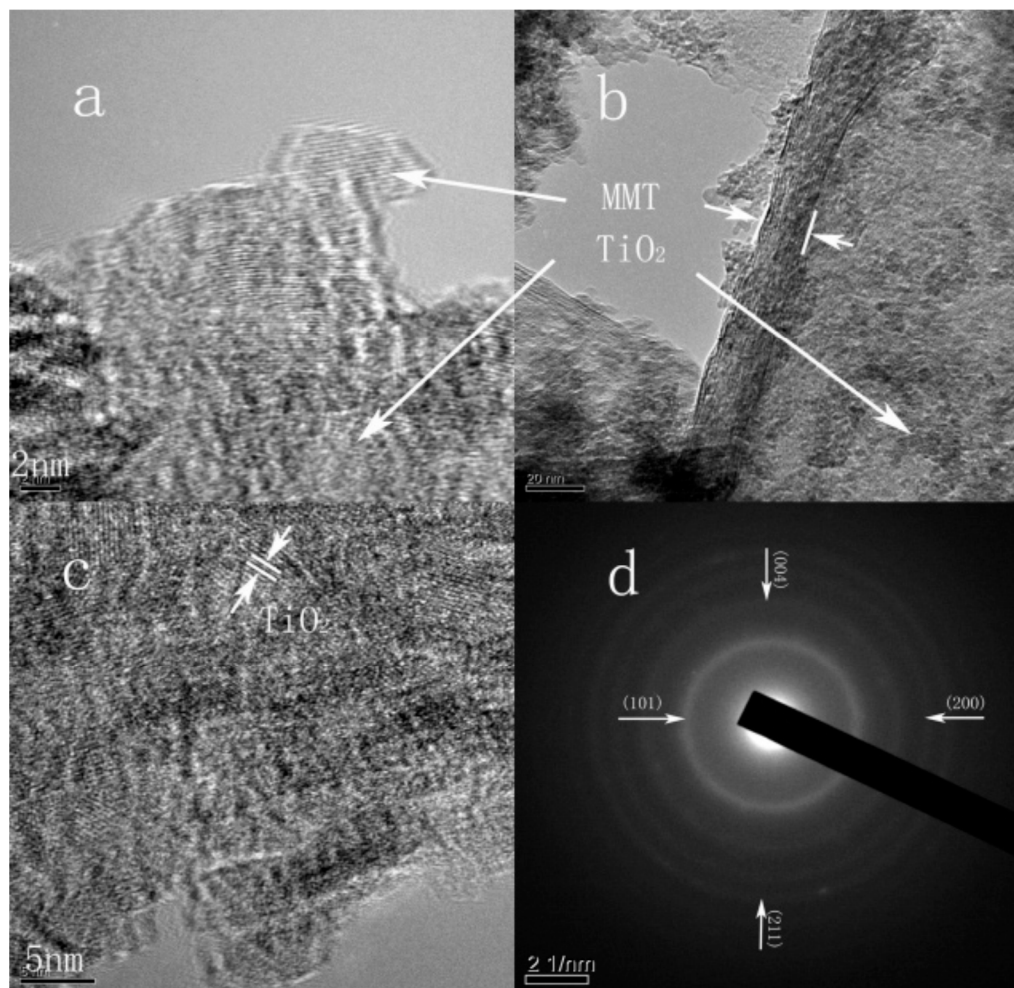


**Figure 11.** (a–c) TEM images of TiO<sub>2</sub> pillared montmorillonite, (d) SAED pattern of TiO<sub>2</sub> nanoparticle. Adapted with permission from ref. [165]. Copyright 2008 American Chemical Society.

No calcination was also required in the synthetic procedure developed by Liu et al. [166]. Ti-pillared montmorillonites were prepared by solvothermal reaction using water with ethanol as solvent, hexamethylene tetramine as precipitant, and various quantities of TiCl<sub>3</sub> as precursor. The best performance in the photodegradation of Methylene Blue (100% efficiency within 40 min) was achieved for the material with the optimum combination of TiO<sub>2</sub> content, high specific surface area, and suitable pore size distribution. The results were not referenced to unsupported TiO<sub>2</sub>.

Recognition that expansion of the interlayer space, or exfoliation of the clay support favored the accessibility of titania nanoparticles, prompted the widespread use of organoclays intercalated with long-chain organocations in the design of TiO<sub>2</sub>/clay composites. Moreover, the organic modification of clay minerals enabled tuning of the composite hydrophobic properties, favoring the adsorption of organic pollutants. Synthesis of the organic derivatives of clay minerals was usually achieved by treatment with various surfactants, both monomeric and polymeric.

Ding et al. [167] investigated the role of hydrophobicity of titania–montmorillonite hybrids in controlling the photocatalytic activity in the degradation of Methyl Orange, and they found that clay mineral pretreatment with hexadecyltrimethylammonium (also referred to as cetyltrimethylammonium) bromide surfactant prior to the introduction of

titania component rendered the composite more hydrophobic, which, in turn, significantly enhanced adsorption of the dye. The photocatalytic activity could be further increased by carrying out the hydrolysis of Ti tetrabutoxide in acetic rather than hydrochloric acid and by doping with platinum. The resulting catalyst was able to degrade 91% of Methyl Orange within 60 min UV irradiation. The importance of hydrophobic properties was also recognized by Meng et al. [168], who prepared  $\text{SiO}_2/\text{TiO}_2$ -organomontmorillonite hybrids with high adsorption capability and high photocatalytic activity toward the degradation of Methyl Orange. The addition of silica played a role in reducing  $\text{TiO}_2$  particle size and dispersing nanosized  $\text{TiO}_2$  on organoclay. The authors separated the adsorption in the dark process (3 h) from the photocatalytic one (15 h UV irradiation,) and the best catalyst achieved ca. 97% dye removal.

Pre-expansion of the montmorillonite interlayer with cetyltrimethylammonium cations prior to the insertion of Ti species obtained by alkoxide hydrolysis was also carried out by Dvininov et al. [169]. The calcined materials were used for the degradation of Congo Red dye under UV irradiation. It was found that the size of pillars increased with the interlayer expansion, and that larger pillars led to enhanced photoactivity. The best catalyst removed 100% of the dye within 30 min of UV irradiation. The authors stressed the combined effect of adsorption of the cationic dye and its photodestruction.

Following the reports on the exceptionally large expansion of the montmorillonite interlayer (up to 9.2 nm) by the intercalation of poly(oxyalkylene)diamine [170], Chen et al. [66] prepared titania pillared montmorillonite by intercalating colloidal  $\text{TiO}_2$  obtained by alkoxide hydrolysis into clay in the presence of high molecular weight polyoxypropylene-backed di-quaternary salt (POP) as an expanding agent. As a result, composites of anatase nanoparticles of ca. 5 nm crystal size dispersed in a highly porous delaminated clay were obtained. The Methylene Blue degradation experiments showed that the photocatalytic efficiency of the novel composites (up to 98% in 90 min) surpassed that of the P25 reference. Interestingly, in a later work [171], the same group prepared and investigated  $\text{TiO}_2$ /montmorillonite composites obtained in a similar manner but with a common cetyl trimethylammonium bromide surfactant. The synthesized composites had a mesoporous delaminated structure with anatase crystals of 5–10 nm dimensions, and their photocatalytic activity in Methylene Blue degradation (up to 99% in 60 min) was superior not only to P25 but also to the previously reported POP-templated materials.

The use of organoclays, beside ensuring hydrophobic environment and enabling expansion of the interlayer for the insertion of larger titania pillars, was also essential for a couple of novel synthetic procedures. Yang et al. [172] prepared titania pillared montmorillonite with an ordered interlayer mesoporous structure by an intra-gallery templating method, which consisted of the simultaneous intercalation of a cationic surfactant and titanium tetrabutoxide into the clay interlayers, which was followed by the hydrolysis of alkoxide upon interaction with adventitious water and calcination at 500 °C. The use of surfactants with carbon chains of increasing length ( $\text{C}_{12}$ ,  $\text{C}_{14}$ ,  $\text{C}_{16}$ , and  $\text{C}_{18}$ ) led to the formation of well-ordered composites with increasing interlayer spacing, pore volume, and pore size. In the photocatalytic experiments, a highly effective degradation of Methylene Blue was observed (98% in 25 min for the best catalyst). However, the results were not referred to a titania standard and neither was the adsorption effect of the cationic dye discussed.

The formation of alkylammonium-exchanged clays was also a key step of an ingenious sol-gel route to prepare porous clay nanostructures composed of delaminated smectites and oxide nanoparticles [33]. This approach, based on the organocolloidal route involving the heterocoagulation of an organic Ti precursor within the organoclay matrix, was originally developed by Letaief and Ruiz-Hitzky for the synthesis of silica-clay composites [173]. It has been adopted by Belver et al. [174] for the preparation of porous titania-clay heterostructures based on Cloisite<sup>®</sup>30B, a commercial organoclay. Titanium alkoxide hydrolysis and coagulation was induced in the presence of the organoclay dispersed in an organic solvent. The procedure led to the exfoliation of clay layers, which enabled the deposition of  $\text{TiO}_2$  nanoparticles on the exposed internal surface. The composites, with

various TiO<sub>2</sub>/clay ratios, contained anatase particles of crystal size around 9–15 nm assembled over the disordered clay layers, and they were characterized by surface area in the range of 100–233 m<sup>2</sup>/g, which was accompanied by a well-developed mesoporosity. Upon illumination with a simulated solar light, a complete discoloration of Rhodamine B could be achieved on all studied photocatalysts, but analysis of the total organic content in the solution showed that full mineralization was not achieved, and organic intermediates, not detectable by UV–vis, were produced.

An interesting variation on the composite design based on a clay organoderivative has been proposed by Huang et al. [175], who immobilized P25 nanoparticles on montmorillonite coated with dopamine, which is a natural amino acid abundantly present in mussel adhesive protein. Thermal treatment in nitrogen led to the carbonization of dopamine and formation of P25–C–clay composite. The material showed high photocatalytic activity in the degradation of Rhodamine B under simulated solar light, good reusability, and excellent ability of dye adsorption, which contributed greatly to the efficiency of its removal (100% in 30 min irradiation).

Huo et al. [176], in a recent paper, have shown that an ultrafine dispersion of montmorillonite and entrapment of TiO<sub>2</sub> species between exfoliated clay could be achieved without the use of a surfactant simply by careful manipulation of pH value during the hydrothermal synthesis of a TiO<sub>2</sub>/montmorillonite composite. The TiO<sub>2</sub> crystal size in the composite was around 15 nm, while in the TiO<sub>2</sub> reference synthesized without montmorillonite, it was ca. 40 nm, indicating the growth-restraining function of dispersed clay lamellae. Furthermore, the novel composite displayed much higher photocatalytic activity and recycling ability in the photodegradation of Methyl Orange (complete elimination within 50 min) than both the composite prepared without the pH-controlled hydrothermal treatment and the pure TiO<sub>2</sub> reference. The authors argued that the pH-controlled process resulted in a material with enhanced light and mass transfer efficiency.

Since UV light, which can excite TiO<sub>2</sub>, corresponds to less than ca. 3–5% of sunlight, an important area of research on TiO<sub>2</sub>–clay mineral composites was related to the attempts of shifting the photoresponse of the materials into the visible region. The doping of titania with foreign elements, a known way for obtaining visible light active photocatalyst [17], was a popular approach. The incorporation of a dopant into TiO<sub>2</sub> lattice results in the formation of donor and/or acceptor levels in the bandgap, which enables excitation by photons of lower energy and causes a red shift of the absorption edge. The dopant may also act as a trapping center for either electrons or holes, thereby reducing the recombination rate of photogenerated charge carriers and contributing to the higher quantum efficiency of photocatalysis.

Following the reports on the positive effect on the photocatalytic properties of titania brought about by loading with Ag, Liu et al. [177] synthesized a Ag–TiO<sub>2</sub>/montmorillonite composite by pillaring clay mineral with acid-hydrolyzed TiCl<sub>4</sub>, which was followed by calcination and the introduction of Ag by the reduction of silver nitrate, and they tested the material's ability to degrade Methylene Blue. Experiments carried out in the dark demonstrated that ca. 80% of the cationic dye disappeared due to the adsorption on the composite. In the photocatalytic experiments, the Ag-doped TiO<sub>2</sub>–clay composite performed better than its Ag-free counterpart (100% degradation reached within 30 and 15 min, respectively), and both clay-based composites were more efficient than the P25 reference (complete MB destruction in 40 min). The effect was attributed to the increased surface area of pillared clays, and, in the case of Ag-containing composite, to the improved light absorption, as evidenced by the appearance of an additional absorption band in the visible region. A similar method of doping with Ag was employed by Sahel et al. [67] for Ti-PILC material obtained from Ti ethoxide precursor. Cationic Methylene Blue and anionic Remazol Black dyes were chosen as model water pollutants. The cationic dye was totally removed from the solution in the dark by cation exchange with the composite catalysts, which made the photocatalysis experiment impossible. Anionic Remazol Black was less adsorbed, and the tests of dye photodegradation showed that both clay-based composites performed significantly poorer

than the P25 reference. Moreover, the doping with Ag actually decreased the photoactivity, from 55% degradation efficiency within 10 h for Ti-PILC to 15% for Ag-doped catalyst; the effect was assigned to the much weaker adsorption capacity of the Ag-containing sample. Deterioration of the TiO<sub>2</sub>-clay composite photoactivity upon doping with noble metal was also reported by Li et al. [178]. The authors prepared Au-loaded TiO<sub>2</sub>/bentonite samples by the deposition-precipitation of Au on the surface of the composite obtained by the conventional sol-gel method with Ti(OC<sub>4</sub>H<sub>9</sub>)<sub>4</sub> as a precursor, and they tested the materials in the photodegradation of Sulforhodamine B. The presence of gold nanoparticles resulted in the appearance of an absorption in the visible region. Despite this fact, Au-containing catalyst was less efficient under visible light illumination than the undoped composite. The rate of dye decomposition over both clay-based composites was lower than on the P25 reference, but in the case of Au-TiO<sub>2</sub>/bentonite nanocomposites, the actual mineralization, measured by the loss of chemical oxygen demand (COD), was more efficient than on P25 (8.9 vs. 7.0%, after 136 h visible light irradiation).

Zhang et al. [179] synthesized N,S-co-doped titania-pillared montmorillonite skipping the calcination step, as described in their earlier work [165], and they studied the photocatalytic degradation of 4BS dye under visible light irradiation. The doping was found to cause a red shift in the absorption edge of UV-Vis spectra. A considerable improvement of the photocatalytic activity was observed for all the doped samples. The best catalyst decomposed 96% of the dye within 60 min, while in the same time, only 55 and 80% degradation was achieved on the undoped TiO<sub>2</sub> pillared clay and P25 standard, respectively. Titania-rich (ca. 90 wt %) TiO<sub>2</sub>-montmorillonite composites doped with vanadium and/or carbon were prepared by Chen et al. [180]. The doped materials exhibited a red shift of the UV-Vis absorption edge. When irradiated with UV light, the doped samples performed poorer in the degradation of Sulforhodamine B than the undoped composite, but under visible light, their dye degradation ability was better than that of the undoped TiO<sub>2</sub>-montmorillonite composite.

In the continuation of research on porous titania-clay heterostructures [174], Belver et al. [181] synthesized Ce-doped composites of this type by organocolloidal route, employing the sequential addition of Ti(OC<sub>3</sub>H<sub>7</sub>)<sub>4</sub> isopropanol solution, followed by Ce nitrate aqueous solution, to the isopropanol suspension of Cloisite®30B (Figure 12). Calcined materials were used as photocatalysts of Rhodamine B degradation under simulated solar irradiation. The composites were highly porous, with well-developed SSA. The titania component appeared as anatase, and the Ce dopant was incorporated into the TiO<sub>2</sub> lattice, which caused a red shift of the absorption band edge. At low Ce doping levels, a remarkable enhancement of Rhodamine B photodegradation was observed in comparison to the undoped composite, but a further increase in the Ce content caused a deterioration of the photocatalytic efficiency, because Ce ions acted as recombination centers for the photogenerated electron-hole pairs. The TOC reduction was almost negligible, indicating that, similarly as in the case of the photocatalysts without cerium [174], no significant mineralization occurred.

Another strategy of enhancing the photocatalytic properties of titania is coupling with narrow gap semiconductors to extend the visible light response [182]. In addition, such heterojunctions can lead to the improvement of the charge carrier separation. This approach has been recently employed by Mishra et al. [183], who coupled TiO<sub>2</sub>/bentonite composites with graphitic carbon nitride (g-C<sub>3</sub>N<sub>4</sub>), a semiconductor with a visible light-driven band gap and high stability, which was frequently used in recent years as a component of heterostructures with TiO<sub>2</sub>. The synthesis involved the preparation of a TiO<sub>2</sub>/bentonite hybrid by the sol-gel procedure, using Ti(OC<sub>4</sub>H<sub>9</sub>)<sub>4</sub> as a precursor. The calcined material was added to the slurry of g-C<sub>3</sub>N<sub>4</sub> in water, and the mixture was subjected to sonication and drying. The g-C<sub>3</sub>N<sub>4</sub>/TiO<sub>2</sub>-bentonite nanocomposites proved very efficient in the photocatalytic degradation of Reactive Brilliant Red dye under visible light irradiation, showing activity higher than reference g-C<sub>3</sub>N<sub>4</sub>/bentonite, g-C<sub>3</sub>N<sub>4</sub>, TiO<sub>2</sub>-bentonite, TiO<sub>2</sub>, or bentonite. The

high activity was attributed to the suppression of electron–hole recombination and to the shift of the photoresponse to the visible region of the solar spectrum.

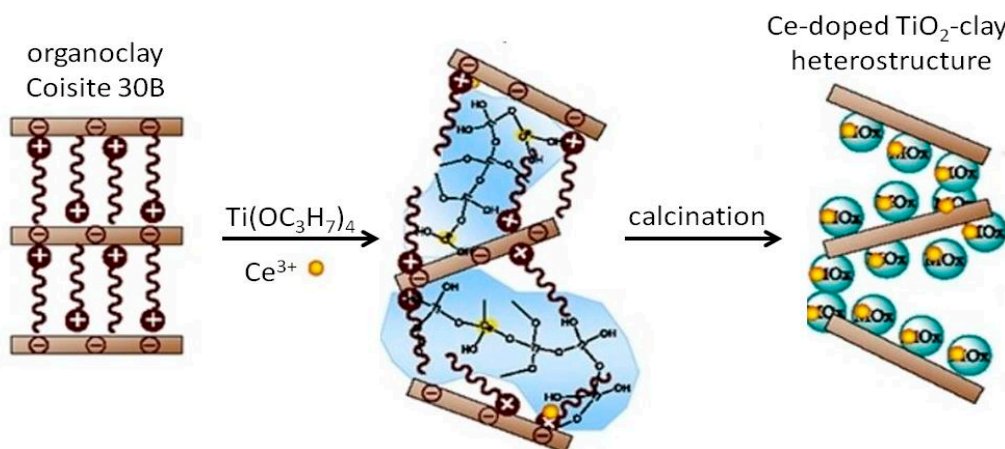


**Figure 12.** Synthesis of Ce-doped TiO<sub>2</sub>–clay photoactive heterostructure by the organoclay colloidal route. Sequential treatment of the starting organoclay with Ti precursor and Ce<sup>3+</sup> aqueous solution yields an intermediate which after calcination forms the desired nanoarchitecture. Adapted with permission from ref. [181]. Copyright 2015 Elsevier.

Table 4 gathers the most relevant information on the synthesis and photocatalytic performance in dyes decomposition of selected TiO<sub>2</sub>–montmorillonite composites.

**Table 4.** Main synthesis and photocatalysis data for selected examples of TiO<sub>2</sub>–montmorillonite composites used as photocatalysts for the degradation of dyes (ARG—Acid Red G, CR—Congo Red, CR GTL—Cationic Red GTL, CV—Crystal Violet, MB—Methylene Blue, MO—Methyl Orange, RB—Remazol Black, RBR-X3BS—Reactive Brilliant Red-X3BS, RhB—Rhodamine B, SR3BL—Solophenyl Red 3BL, SRB—Sulforhodamine B, VPB—Victoria Pure Blue, Bent—bentonite, Mt—montmorillonite, CTA—cetyltrimethylammonium cation, CA—catalyst amount).

TiO <sub>2</sub> –Clay Mineral Composite	Synthesis	Experimental Conditions	Dye	Degradation Rate	Ref.
Ti-pillared Mt	Ti(OC <sub>3</sub> H <sub>7</sub> ) <sub>4</sub> precursor + Mt, calcination 500 °C, SSA = 140 m <sup>2</sup> g <sup>−1</sup>	UV irradiation CA: 1 mg mL <sup>−1</sup> dye 10 ppm	MB	85%—70 min	[157]
Ti-pillared Mt	Ti(OC <sub>3</sub> H <sub>7</sub> ) <sub>4</sub> precursor + Mt, post-intercalation hydrothermal treatment 250 °C, calcination 500 °C, SSA = 216 m <sup>2</sup> g <sup>−1</sup>	UV irradiation CA: 1 mg mL <sup>−1</sup> Dye: 10 ppm	MB	99%—70 min	[157]
Ti-pillared Mt	Ti(OC <sub>4</sub> H <sub>9</sub> ) <sub>4</sub> precursor + Mt, calcination 400 °C, SSA = 368 m <sup>2</sup> g <sup>−1</sup>	UV irradiation CA: 1 mg mL <sup>−1</sup> Dye: 3 × 10 <sup>−5</sup> mmol mL <sup>−1</sup>	MB	58%—50 min	[64]
Ti-pillared Mt	Ti(OC <sub>4</sub> H <sub>9</sub> ) <sub>4</sub> precursor + Mt, clay/TiO <sub>2</sub> sol microwave treated, calcination 400 °C, SSA = 405 m <sup>2</sup> g <sup>−1</sup>	UV irradiation CA: 1 mg mL <sup>−1</sup> Dye: 3 × 10 <sup>−5</sup> mmol mL <sup>−1</sup>	MB	93%—50 min	[64]

Table 4. Cont.

TiO <sub>2</sub> -Clay Mineral Composite	Synthesis	Experimental Conditions	Dye	Degradation Rate	Ref.
Ti-pillared Mt	Ti(OC <sub>3</sub> H <sub>7</sub> ) <sub>4</sub> precursor + POP surfactant + Mt, calcination 400 °C, SSA = 244 m <sup>2</sup> g <sup>-1</sup>	UV irradiation CA: 0.2 mg mL <sup>-1</sup> dye: 0.03 mg mL <sup>-1</sup>	MB	98%—90 min	[170]
Ti-pillared Mt	Ti(OC <sub>3</sub> H <sub>7</sub> ) <sub>4</sub> precursor + CTA-Mt, calcination 500 °C, SSA = 194 m <sup>2</sup> g <sup>-1</sup>	UV irradiation CA: 0.2 mg mL <sup>-1</sup> dye: 0.03 mg mL <sup>-1</sup>	MB	99%—60 min	[171]
Ti-pillared Mt	Ti(OC <sub>4</sub> H <sub>9</sub> ) <sub>4</sub> precursor + ODMBAC in ethanol + Mt, calcination 500 °C, SSA = 352 m <sup>2</sup> g <sup>-1</sup>	UV irradiation CA: 0.5 mg mL <sup>-1</sup> dye: 10 <sup>-4</sup> mmol/ mL <sup>-1</sup>	MB	98%—25 min	[172]
Ag/Ti-pillared Mt	TiCl <sub>4</sub> precursor + Mt, calcination 500 °C, Ti-PILC SSA = 323 m <sup>2</sup> g <sup>-1</sup> , Ag doping: AgNO <sub>3</sub> solution reduced with ascorbic acid, SSA = 323 m <sup>2</sup> g <sup>-1</sup>	UV irradiation CA: 0.2 mg mL <sup>-1</sup> dye: 10 <sup>-4</sup> mmol mL <sup>-1</sup>	MB	100%—15 min	[177]
TiO <sub>2</sub> /Mt	Mt impregnated with TiCl <sub>4</sub> precursor, calcination at 350 °C, SSA = 52 m <sup>2</sup> g <sup>-1</sup>	UV irradiation CA: 0.16 mg mL <sup>-1</sup> dye: 10 <sup>-4</sup> mmol mL <sup>-1</sup>	MB	93%—360 min	[161]
TiO <sub>2</sub> /Mt	TiCl <sub>3</sub> precursor + Mt, solvothermal treatment in H <sub>2</sub> O and C <sub>2</sub> H <sub>5</sub> OH, hexamethylene tetramine precipitant, hydrothermal treatment at 90/190 °C, no calcination, SSA = 102 m <sup>2</sup> g <sup>-1</sup>	UV irradiation CA: 0.5 mg mL <sup>-1</sup> dye: 1.2 × 10 <sup>-4</sup> mmol mL <sup>-1</sup>	MB	100%—40 min	[166]
Ti-pillared Mt	TiCl <sub>4</sub> precursor + Mt, hydrothermal treatment 115 °C during intercalation, calcination 500 °C, SSA = 135 m <sup>2</sup> g <sup>-1</sup>	UV irradiation CA: 1 mg mL <sup>-1</sup> dye: 0.04 mg mL <sup>-1</sup>	RhB	98%—100 min	[55]
Ce,TiO <sub>2</sub> /Mt	Ti(OC <sub>3</sub> H <sub>7</sub> ) <sub>4</sub> precursor + Cloisite <sup>®</sup> 30B + Ce(NO <sub>3</sub> ) <sub>3</sub> solution induced hydrolysis, calcination 500 °C; 0.25 wt % Ce, SSA = 211 m <sup>2</sup> g <sup>-1</sup>	Solar irradiation CA: 0.5 mg mL <sup>-1</sup> dye: 0.025 mg mL <sup>-1</sup> (after saturation with adsorbed RhB in dark)	RhB	100%—400 min	[181]
TiO <sub>2</sub> /Mt	Mt impregnated with TiCl <sub>4</sub> precursor, calcination at 350 °C, SSA = 52 m <sup>2</sup> g <sup>-1</sup>	UV irradiation CA: 0.16 mg mL <sup>-1</sup> dye: 10 <sup>-4</sup> mmol mL <sup>-1</sup>	RhB	80%—360 min	[161]
TiO <sub>2</sub> /Mt	Ti(OC <sub>3</sub> H <sub>7</sub> ) <sub>4</sub> precursor + Cloisite <sup>®</sup> 30B, induced hydrolysis, calcination 550 °C, SSA = 143 m <sup>2</sup> g <sup>-1</sup>	Solar irradiation CA: 0.5 mg mL <sup>-1</sup> dye: 0.025 mg mL <sup>-1</sup> (after saturation with adsorbed RhB in dark)	RhB	100%—6 h	[174]
TiO <sub>2</sub> /C-Mt	Polydopamine modified exfoliated Mt coated with P25, carbonized at 600 °C	Solar irradiation CA: 0.5 mg mL <sup>-1</sup> dye: 12 ppm	RhB	100% -30 min	[175]
Ti-pillared Mt	Ti(OC <sub>3</sub> H <sub>7</sub> ) <sub>4</sub> precursor + Mt, calcination 500 °C, SSA = 140 m <sup>2</sup> g <sup>-1</sup>	UV irradiation CA: 1 mg mL <sup>-1</sup> dye 10 ppm	VPB	58%—70 min	[161]

Table 4. Cont.

TiO <sub>2</sub> -Clay Mineral Composite	Synthesis	Experimental Conditions	Dye	Degradation Rate	Ref.
Ti-pillared Mt	Ti(OC <sub>3</sub> H <sub>7</sub> ) <sub>4</sub> precursor + Mt, post-intercalation hydrothermal treatment 250 °C, calcination 500 °C, SSA = 216 m <sup>2</sup> g <sup>-1</sup>	UV irradiation CA: 1 mg mL <sup>-1</sup> Dye: 10 ppm	VPB	93%—70 min	[157]
Ti-pillared Mt	Ti(OC <sub>4</sub> H <sub>9</sub> ) <sub>4</sub> precursor + Mt, calcination 500 °C	UV irradiation CA: 3 mg mL <sup>-1</sup> Dye: 0.14 mg mL <sup>-1</sup>	CR GTL	90%—240 min	[158]
Ti-pillared Mt	TiCl <sub>4</sub> precursor + Mt, hydrothermal treatment 115 °C during intercalation, calcination 500 °C, SSA = 135 m <sup>2</sup> g <sup>-1</sup>	UV irradiation CA: 1 mg mL <sup>-1</sup> dye: 0.04 mg mL <sup>-1</sup>	MO	100%—100 min	[55]
TiO <sub>2</sub> /Mt	Mt impregnated with TiCl <sub>4</sub> precursor, calcination at 350 °C, SSA = 52 m <sup>2</sup> g <sup>-1</sup>	UV irradiation CA: 0.16 mg mL <sup>-1</sup> dye: 10 <sup>-4</sup> mmol mL <sup>-1</sup>	MO	36%—360 min	[161]
TiO <sub>2</sub> /Mt	Mt (pH controlled delamination) + TiOSO <sub>4</sub> precursor (pH controlled hydrolysis), pH controlled coagulation, hydrothermal treatment, no calcination	UV irradiation CA: 0.4 mg mL <sup>-1</sup> dye: 0.02 mg mL <sup>-1</sup>	MO	100%—50 min	[176]
TiO <sub>2</sub> -SiO <sub>2</sub> /Mt	Sol from Ti(OC <sub>4</sub> H <sub>9</sub> ) <sub>4</sub> precursor mixed with sol from Si(OC <sub>2</sub> H <sub>5</sub> ) <sub>4</sub> precursor, added to CTA-Mt. Solid product not calcined.	UV irradiation CA: 0.2 mg mL <sup>-1</sup> dye: 0.015 mg mL <sup>-1</sup>	MO	97%—18 h	[168]
Au/Ti-pillared Mt	Ti(OC <sub>4</sub> H <sub>9</sub> ) <sub>4</sub> precursor + Mt, calcination 400 °C, Ti-PILC SSA = 238 m <sup>2</sup> g <sup>-1</sup> , Au doping: treatment with HAuCl <sub>4</sub> solution + NaOH precipitant, SSA = 178 m <sup>2</sup> g <sup>-1</sup>	UV irradiation CA: 0.5 mg mL <sup>-1</sup> dye: 2 × 10 <sup>-5</sup> mmol mL <sup>-1</sup>	SRB	100%—120 min	[178]
Au/Ti-pillared Mt	Ti(OC <sub>4</sub> H <sub>9</sub> ) <sub>4</sub> precursor + Mt, calcination 400 °C, Ti-PILC SSA = 238 m <sup>2</sup> g <sup>-1</sup> , Au doping: treatment with HAuCl <sub>4</sub> solution + NaOH precipitant, SSA = 178 m <sup>2</sup> g <sup>-1</sup>	Visible light irradiation CA: 0.5 mg mL <sup>-1</sup> dye: 2 × 10 <sup>-5</sup> mmol mL <sup>-1</sup>	SRB	75%—21 h	[178]
V,C-TiO <sub>2</sub> /Mt	Ti(OC <sub>3</sub> H <sub>7</sub> ) <sub>4</sub> precursor + urea + vanadyl acetylacetonate + Mt, (120 mmol Ti/g Mt), calcination 500 °C, 0.09 wt % V, SSA = 86 m <sup>2</sup> g <sup>-1</sup>	Visible light irradiation CA: 0.5 mg mL <sup>-1</sup> dye: 2 × 10 <sup>-5</sup> mmol mL <sup>-1</sup>	SRB	67%—18 h	[180]
Ti-pillared Mt	Ti(OC <sub>3</sub> H <sub>7</sub> ) <sub>4</sub> precursor + CTA-Mt, calcination 500 °C	UV irradiation CA: 0.4 mg mL <sup>-1</sup> dye: 0.02 mg mL <sup>-1</sup>	CR	100%—30 min	[169]
TiO <sub>2</sub> /Mt	Mt impregnated with TiCl <sub>4</sub> precursor, calcination at 350 °C, SSA = 52 m <sup>2</sup> g <sup>-1</sup>	UV irradiation CA: 0.16 mg mL <sup>-1</sup> dye: 10 <sup>-4</sup> mmol mL <sup>-1</sup>	CR	23%—360 min	[161]

Table 4. Cont.

TiO <sub>2</sub> -Clay Mineral Composite	Synthesis	Experimental Conditions	Dye	Degradation Rate	Ref.
Ti-pillared Mt	Ti(OC <sub>3</sub> H <sub>7</sub> ) <sub>4</sub> precursor + Mt, post-synthesis microwave treatment, calcination 400 °C, SSA = 151 m <sup>2</sup> g <sup>-1</sup>	UV irradiation CA: 2.5 mg mL <sup>-1</sup> dye: 0.1 mg mL <sup>-1</sup>	SR3BL	95%—220 min	[162]
Ti-pillared Mt	TiCl <sub>4</sub> precursor + Mt, hydrothermal treatment 70 °C during intercalation, no calcination, SSA = 277 m <sup>2</sup> g <sup>-1</sup>	UV irradiation CA: 1 mg mL <sup>-1</sup> dye: 0.03 mg mL <sup>-1</sup>	ARG	100%—60 min	[165]
TiO <sub>2</sub> /Mt	Mt impregnated with TiCl <sub>4</sub> precursor, calcination at 350 °C, SSA = 52 m <sup>2</sup> g <sup>-1</sup>	UV irradiation CA: 0.16 mg mL <sup>-1</sup> dye: 10 <sup>-4</sup> mmol mL <sup>-1</sup>	CV	97%—360 min	[161]
Ag/Ti-pillared Mt	Ti(OC <sub>2</sub> H <sub>5</sub> ) <sub>4</sub> precursor + Mt, calcination 500 °C, Ti-PILC SSA = 208 m <sup>2</sup> g <sup>-1</sup> , Ag doping: treatment with AgNO <sub>3</sub> solution reduced with ascorbic acid, SSA = 195 m <sup>2</sup> g <sup>-1</sup>	UV irradiation CA: 0.5 mg mL <sup>-1</sup> dye: 2.1 × 10 <sup>-5</sup> mmol mL <sup>-1</sup>	RB	15%—600 min	[67]
N,S,Ti-pillared Mt	TiCl <sub>4</sub> precursor + CS(NH <sub>2</sub> ) <sub>2</sub> + Mt, Ti:S = 1:4, calcination 350 °C, SSA = 277 m <sup>2</sup> g <sup>-1</sup>	Visible light irradiation CA: 2 mg mL <sup>-1</sup> dye: 0.03 mg mL <sup>-1</sup>	4BS	96%—60 min	[179]
g-C <sub>3</sub> N <sub>4</sub> /TiO <sub>2</sub> -Bent	Ti(OC <sub>4</sub> H <sub>9</sub> ) <sub>4</sub> precursor + Bent at pH = 3, calcination 550 °C, addition of g-C <sub>3</sub> N <sub>4</sub> slurry under sonication, drying 60 °C; 40 wt % g-C <sub>3</sub> N <sub>4</sub> , SSA = 70 m <sup>2</sup> g <sup>-1</sup>	Visible light irradiation CA: 1 mg mL <sup>-1</sup> dye: 40 ppm	RBR-X3BS	90%—100 min	[183]

In addition to montmorillonite, also other clay minerals were investigated as matrices for the synthesis of composites with titania nanoparticles. As described earlier, already among the first reports on the photocatalytic degradation of dyes over TiO<sub>2</sub>-clay composites, a couple of works [159,160] dealt with materials based on the synthetic hectorite, Laponite, which is particularly attractive for composite synthesis due to its readiness for delamination in aqueous suspensions. Later, Laponite was also used by Daniel et al. [184], who prepared composite catalyst in a manner similar to that of Zhu et al. [159], except that TiO<sub>2</sub> nanocrystals were synthesized prior to the addition to the clay dispersion by microwave hydrothermal treatment of hydrolyzed Ti(OC<sub>3</sub>H<sub>7</sub>)<sub>4</sub>. The role of PEO was to inhibit the aggregation of clay platelets and enlarge in such a way the surface available for TiO<sub>2</sub> immobilization. The photocatalytic activity of the samples in the degradation of Sulphorhodamine B increased with the Ti/clay ratio and with the temperature of the microwave treatment up to over 90%, indicating the importance of the anatase availability and crystallinity. Synthetic hectorite-based composites with low titania loadings (1–12.5 wt %) prepared by Ma et al. [185] using the conventional sol-gel procedure with TiCl<sub>4</sub> as a source of TiO<sub>2</sub> particles were capable of over 90% decolorization of Methylene Blue within 15 min of UV irradiation. However, no information was provided on the behavior of neat hectorite support; hence, it was not clear to what extent the formation of composites was beneficial for the dye degradation. Deeppracha et al. [186] demonstrated that the aqueous dispersion of anatase nanopowder and synthetic hectorite could form stable films on a borosilicate glass and showed photocatalytic activity in the decolorization of Methylene Blue and Methyl Orange. In an acidic environment, a synergy effect in the decomposition of Methylene Blue over mixed titania-hectorite film was observed, the reaction being much faster than on the pure anatase film. Recently, You et al. [187] added a g-C<sub>3</sub>N<sub>4</sub> component to TiO<sub>2</sub>-synthetic fluorinated hectorite hybrids obtained by the sol-gel procedure with

Ti tetrabutoxide as a precursor. The ternary composite was prepared by the mechanical mixing of graphitic carbon nitride with the TiO<sub>2</sub>-clay system, which was followed by calcination. The g-C<sub>3</sub>N<sub>4</sub>-TiO<sub>2</sub>-hectorite composite reached 94% degradation of Rhodamine B after 2 h irradiation with visible light, thus surpassing significantly the activity of the binary TiO<sub>2</sub>-hectorite catalyst and the P25 standard. The enhancement of the photocatalytic efficiency of the composites was attributed to the improved light-harvesting ability, high specific surface area, and effective charge separation. Fluorine dopant, stemming from hectorite, generated oxygen vacancy and Ti<sup>3+</sup> defects in TiO<sub>2</sub>, shifting its photoresponse to the visible light. The composites showed good reusability, as 84% of Rhodamine B could still be degraded after five cycles. Fatimah et al. [69] prepared Ti-PILC composite from another magnesium silicate mineral, saponite, using hydrolyzed TiCl<sub>4</sub> as a pillaring agent. The authors investigated the photosensitization of the material with tris(2,2'-bipyridyl) dichlororuthenium complex and observed a shift in the absorption spectrum toward the visible region. Accordingly, in the test reaction of Bromophenol Blue degradation, the photosensitized sample performed better than the parent Ti-PILC. Under UV irradiation, the dye degradation efficiencies were 97 and 65%, respectively, while upon illumination with the visible light, the corresponding figures were 90 and 39%.

Machado et al. [188] synthesized composite photocatalysts by the impregnation of exfoliated vermiculite with Ti tetraisopropoxide, which was followed by hydrolysis with HCl/H<sub>2</sub>O vapor and calcination. The materials, which were capable of floating at the water surface, were tested in the photodegradation of textile dye Drimaren Red in a special reactor with no stirring and a preferential surface irradiation to simulate a stagnant water environment. Under such conditions, the TiO<sub>2</sub>-vermiculite photocatalysts stayed at the surface and proved active in dye discoloration. The best catalyst displayed ca. 20% degradation efficiency upon 4 h UV irradiation, while the P25 reference sank to the bottom of the reactor and remained almost inactive. The experiment showed the potential of the floating photocatalyst for the purification of stagnant waters.

Several groups used kaolinite as a component of photoactive composites with titania. Chong et al. [189] prepared dehydrated and dehydroxylated kaolinite by outgassing of the raw caly at 750 °C, and they used it as a support for the deposition of titania generated by the heterocoagulation of acid-hydrolyzed Ti tetrabutoxide. The size of TiO<sub>2</sub> particles increased from 6 nm for material calcined at 500 °C to 18 nm for sample calcined at 700 °C, with respective SSA values changing from 39 to 24 m<sup>2</sup>/g. Photocatalytic experiments aiming at the degradation of Congo Red showed that both the adsorption of dye and its photodegradation over the composite material were enhanced with respect to pure titania component, and a complete dye degradation could be achieved within 6 h of UV irradiation. The same group reported later that the photocatalytic performance of composites could be improved by an additional acid and alkaline pretreatment of kaolinite. The photocatalyst obtained in such a way could destroy 95% of Congo Red upon 3 h UV irradiation, while it took over 4 h for P25 standard to achieve a similar result [190]. Zhang et al. [191] prepared the composite photocatalysts by the addition of Ti sol obtained from TiCl<sub>4</sub> precursor to the aqueous suspension of the acid-treated kaolinite, which was followed by drying or calcination. The best photoactivity in the degradation of Acid Red G dye, corresponding to complete dye removal within 60 min of UV irradiation, was observed for the sample with the highest SSA (114 m<sup>2</sup>/g), dried at 70 °C, in which the mixed phases of anatase and brookite existed. In a study by Kutlakova et al. [192], the preparation of nanocomposite photocatalysts was carried out by the thermal hydrolysis of TiSO<sub>4</sub>, which is a cheap and easy to handle titania precursor, in the presence of an untreated kaolinite, followed by drying at 105 °C or calcination at 600 °C. In the latter case, kaolinite transformed to metakaolinite. In the photocatalytic tests of Acid Orange 7 discoloration, the activity of calcined nanocomposites surpassed that of dried samples and of the unsupported TiO<sub>2</sub> reference. The best performance was observed for the catalyst with 40 wt % titania, which after 60 min of UV irradiation degraded ca. 70% of the dye. Both the experimental (SEM) and the theoretical studies indicated that TiO<sub>2</sub> particles grew preferably on the edges

of kaolinite particles. Barbosa et al. [193] obtained  $\text{TiO}_2$ /clay mineral photocatalysts by the treatment of kaolinite with Ti tetraisopropoxide via the hydrolytic sol–gel route and calcination between 100 and 1000 °C. Titania was initially present as an amorphous phase and transformed to anatase at 400 °C. The composite obtained at this temperature was most active in the photodegradation of Methyl Orange II (93% efficiency) and Methylene Blue (99% efficiency), reaching maximum degradation capacity within a few minutes. The effect pointed to the strong adsorption component in the dye removal process. Comparative studies with P25 proved the composites more active than the reference.

A couple of recent papers compared the photocatalytic performance of kaolinite-derived composites with that of materials prepared with the use of other clay minerals. Thus, Mishra et al. [194] obtained  $\text{TiO}_2$ /clay hybrids by the sol–gel procedure from Ti tetrabutoxide precursor added to an ethanol suspension of clay under microwave irradiation. The final products were calcined at 500 °C. Montmorillonite, bentonite, and kaolinite were used in the capacity of clay component, and the synthesized photocatalysts were tested in the degradation of Methylene Blue. Both adsorption and photocatalytic degradation contributed to the dye removal. The order of the composite decolorization efficiencies was  $\text{TiO}_2$ –bentonite (99%) >  $\text{TiO}_2$ –montmorillonite (80%) >  $\text{TiO}_2$ –kaolinite (54%) > P25 reference (50%), and it was in part related to the SSA and porosity, which fell in the same sequence. Kaolinite was found to be highly reflective throughout the UV spectrum, which lowered its photoactivity. In another work, Wu et al. [195] synthesized composites of titania and three clays (kaolinite, halloysite, and palygorskite) with different morphologies (plates, tubes, and rods with micropore tunnels) and different SSA (18, 60, and 130  $\text{m}^2/\text{g}$ ), using Ti tetrabutoxide as a precursor of  $\text{TiO}_2$ . Comparison of the photocatalytic performance of obtained materials in the degradation of Methyl Orange showed that the order of photocatalytic efficiencies was  $\text{TiO}_2$ –kaolinite (99%) >  $\text{TiO}_2$ –halloysite (65%) >  $\text{TiO}_2$ –palygorskite (45%), i.e., opposite to that of clays SSA. It was argued that the poor activity of palygorskite-based photocatalyst was due to the agglomeration of  $\text{TiO}_2$  particles at the surface, which is coupled with a weak adsorption of the dye and inaccessibility of the structural tunnels. In the case of halloysite and kaolinite, the  $\text{TiO}_2$  nanoparticles were distributed more evenly, but the hydroxyl-terminated interior of the halloysite nanotubes was covered to a much lesser extent than the external surface. In view of this, the adsorption of dye, occurring preferentially at the surface hydroxyls, did not play an important role in photocatalysis by halloysite-based composite, but it contributed to the efficiency of the photocatalytic process over kaolinite-supported  $\text{TiO}_2$ .

The enhancement of titania component photoactivity by coupling with ZnO was described by Bel Hadjtaief et al. [196], who used a natural Tunisian clay of mixed mineral composition for the preparation of the photocatalyst. First, the  $\text{TiO}_2$ –clay system was prepared by exposing the clay support to  $\text{Ti}(\text{OC}_3\text{H}_7)_4$  vapor at 600 °C. Subsequently, ZnO insertion was achieved by the sol–gel procedure, using anhydrous Zn acetate as a precursor. The ZnO– $\text{TiO}_2$ –clay composite was used as a photocatalyst for the degradation of Methyl Green and yielded 100% decolorization and almost 90% mineralization of the dye upon 30 min of UV irradiation. Its photocatalytic activity was higher than that of the ZnO-free  $\text{TiO}_2$ –clay sample. The synthesis of similar composites, based on a series of raw Ecuadorian clays of various mineral compositions, supporting  $\text{ZnTiO}_3$ – $\text{TiO}_2$  photoactive phase deposited by the sol–gel procedure, was reported recently by Jaramillo-Fierro et al. [197]. The clay-supported heterojunction system proved active in the degradation of Methylene Blue, reaching, on average, over 80% decolorization in 150 min of simulated solar light irradiation.

Halloysite, the mineral differing from kaolinite by the presence of variable water content in the interlayer, and tending therefore to display tubular morphology, was also used in the design of  $\text{TiO}_2$ –clay photocatalysts for dyes destruction. Li et al. [198] synthesized  $\text{TiO}_2$ –halloysite composites by mixing sol prepared from  $\text{Ti}(\text{OC}_3\text{H}_7)_4$  precursor with halloysite nanotubes. The adsorption of sol species at the clay surface induced the in situ growth of  $\text{TiO}_2$  nanocrystals on the support. An appropriate choice of sol concentration and

pH, combined with hydrothermal treatment at 65 °C, enabled the formation of crystalline phases of anatase or anatase/rutile. No calcination was required, which preserved the halloysite nanotube structure and prevented the further growth of TiO<sub>2</sub> crystallites. Under visible light irradiation, the as-prepared TiO<sub>2</sub>-halloysite nanotubes demonstrated higher photocatalytic degradation efficiency of Rhodamine B (69%) and Gentian Violet (51%) than the P25 standard (35%) and parent halloysite nanotubes (40%). In order to extend the composite photoresponse to the visible region, the same group used the developed synthetic procedure to obtain TiO<sub>2</sub>-halloysite composites photosensitized with polyaniline (PANI), absorbing light both in the UV and the visible region [199]. The photocatalytic activities of PANI-TiO<sub>2</sub>-halloysite materials under visible-light irradiation were tested in the degradation of Rhodamine B. The composites showed enhanced efficiency in the dye removal due to the charge transfer from the photoexcited PANI sensitizer to TiO<sub>2</sub>. Their photocatalytic activity depended on the synthesis pH and the aniline to Ti(OC<sub>3</sub>H<sub>7</sub>)<sub>4</sub> ratio. The best performance, corresponding to 77% dye degradation efficiency, was achieved with the composite containing PANI and mixed phase anatase/rutile nanoparticles.

The effect of calcination temperature on the structure and photocatalytic properties of TiO<sub>2</sub>-halloysite composites was evaluated by Du and Zheng [200]. A titania component was obtained by the hydrolysis of Ti tetrabutoxide, and the hydrothermally synthesized composite was subjected to heat treatment at different temperatures in the 100–500 °C range. Increasing calcination temperature improved the anatase particles' crystallinity but destroyed the structure of halloysite. The materials showed high efficiency in the photodegradation of Methylene Blue with optimum properties displayed by the composite calcined at an intermediate temperature of 300 °C. The result was attributed to the combined effect of dye adsorption and photocatalysis by TiO<sub>2</sub> particles (82% degradation). In the subsequent work [201], the authors used amylose-covered halloysite for the composite synthesis. The polysaccharide coating, formed by the dry milling of both components, acted as a template for the growth of TiO<sub>2</sub> nanoparticles at the halloysite surface during sol-gel synthesis from a Ti tetrabutoxide precursor. The composite exhibited better dispersion and a larger specific surface area than the reference prepared without amylose. It was also more effective in the photodegradation of Methylene Blue (91% vs. 81% for the amylose-free sample).

TiO<sub>2</sub>-clay photocatalysts have also been designed with the use of sepiolite and palygorskite (attapulgit) fibrous clay minerals. The unique tunnel structure endows these minerals with properties different from the rest of the phyllosilicates, such as high SSA, and an elevated population of surface silanols [202]. Both factors favor interaction with deposited nanoparticles and facilitate the assembling of composite structures.

Bouna et al. [203] prepared TiO<sub>2</sub>-palygorskite nanocomposites following the colloidal route originally proposed by Aranda et al. [202], involving the controlled hydrolysis of titanium tetraisopropoxide in the presence of palygorskite pretreated with cationic surfactant, which provided an organophilic environment for the formation of TiO<sub>2</sub> nanoparticles. Anatase grains with the size of ca. 8 nm, which formed upon calcination above 450 °C, were remarkably stable up to 900 °C, in contrast to pure TiO<sub>2</sub> xerogel, which readily transformed into rutile beyond 600 °C. The materials were tested in the photocatalytic degradation of Orange G, and the best TiO<sub>2</sub>-palygorskite photocatalyst, calcined at 600 °C, accomplished complete removal of dye within 90 min of UV irradiation. Its activity was superior to P25 standard, when normalized to Ti content. Stathatos et al. [204] showed that the TiO<sub>2</sub>-palygorskite composites could be prepared as thin films on a borosilicate glass substrate via the sol-gel method employing titanium tetraisopropoxide, palygorskite nanofibers, and nonionic surfactant (X100) as a template. The films proved highly effective in the photodiscoloration of Basic Blue 41 dye with the best one achieving complete discoloration within 90 min of exposure to UV light. The composite photoactivity surpassed that of single components, pointing to the occurrence of a synergistic effect between titania and palygorskite.

The TiO<sub>2</sub>–sepiolite composites were obtained by Zhang et al. [205] by the conventional sol–gel method using TiCl<sub>4</sub> as the TiO<sub>2</sub> precursor and different temperatures for final heat treatment. TiO<sub>2</sub> crystallized as anatase with nanoparticles approximately 5–10 nm in size. Under UV light irradiation, the composite treated thermally at 70 °C was capable of 100% destruction of Acid Red G anionic dye within 120 min, significantly exceeding the performance of unsupported titania. Zhou et al. [206,207] compared the effects of different thermal treatments on the properties of TiO<sub>2</sub>–sepiolite composites. The materials were obtained by the sol–gel procedure with the use of titanium tetraisopropoxide as a precursor, and they were subjected either to conventional calcination or to microwave hydrothermal treatment. The latter method proved advantageous for the materials synthesis, as it preserved the structure of sepiolite, resulted in a higher surface area, ensured the homogeneous dispersion of TiO<sub>2</sub> nanocrystals on the sepiolite surface, and, as a consequence, led to better photocatalytic performance in the degradation of Orange G. The recycling experiments confirmed the stability of the catalyst.

Several works addressed modification of the TiO<sub>2</sub>–fibrous clay composites by the introduction of a dopant and/or coupling of titania with another semiconductor. Zhao et al. [208] prepared a composite of TiO<sub>2</sub> with palygorskite exchanged with copper ions using the sol–gel method. It was expected that Cu dopant would boost the rate of the photocatalytic degradation of Methylene Blue. In fact, the mineralization of Methylene Blue over the composite was significantly higher than over the P25 reference, but no experiments were reported for a composite without Cu dopant; hence, it is impossible to conclude whether the exchange with Cu ions was a right move. Another study by the same authors [209], on the photocatalytic activity of Ag-exchanged TiO<sub>2</sub>–palygorskite composite, suffered a similar drawback, as no data on the Ag-free composite were provided. The photocatalytic removal of Methyl Orange under UV radiation has been studied by Zhang et al. [210] who investigated attapulgite (palygorskite) composites with SnO<sub>2</sub>–TiO<sub>2</sub> hybrid oxides prepared by a sequential deposition of Sn and Ti components. The photoactivity of the composites decreased in the sequence: SnO<sub>2</sub>–TiO<sub>2</sub>–attapulgite > SnO<sub>2</sub>–attapulgite > TiO<sub>2</sub>–attapulgite > attapulgite. The photocatalyst with the optimized proportion of SnO<sub>2</sub> and TiO<sub>2</sub> reached 99% Methyl Orange degradation within 30 min. Later, the same group reported a similar procedure for the synthesis of BiOBr–TiO<sub>2</sub>–attapulgite hybrid system and tested the materials in the photocatalytic degradation of Methyl Orange upon visible light illumination [211]. The catalysts' activity decreased in the order BiOBr–TiO<sub>2</sub>–attapulgite > BiOBr–attapulgite > TiO<sub>2</sub>–attapulgite > attapulgite. The superior performance of the ternary system (97% within 120 min illumination) was attributed to the synergistic effect, leading to the efficient separation of photogenerated electrons and holes in the heterojunction structure and to the enhancement of the SSA. Chen et al. [212] investigated another type of palygorskite–heterojunction system, obtained by the colloidal route of Aranda et al. [202]. The authors combined titania component with cadmium sulfide, widely used to sensitize TiO<sub>2</sub> for visible light driven applications. Coupling with CdS extended the photoresponse of the TiO<sub>2</sub> component to the visible-light region. In the test reaction of Methylene Blue degradation under visible light irradiation, the TiO<sub>2</sub>–CdS–palygorskite nanocomposite exhibited much higher degradation efficiency (37%) than TiO<sub>2</sub>–palygorskite (10%) and CdS–palygorskite (22%), thus confirming the rationale behind the composite catalyst design. Liu et al. [213] prepared Ag-decorated TiO<sub>2</sub>–sepiolite composites by solvothermal reaction in an acetic acid–water solvent, using Ti tetrabutoxide pillaring solution containing Ag dopant. Physicochemical characterization showed that Ag-decorated TiO<sub>2</sub> nanoparticles with a diameter of 10–20 nm were highly dispersed on the sepiolite nanofibers. Doping with Ag caused a red shift of the absorption edge in the UV-Vis spectra. Compared with TiO<sub>2</sub>, sepiolite, and TiO<sub>2</sub>–sepiolite, the Ag-doped composites exhibited significantly enhanced photocatalytic activity in the degradation of Methyl Orange. With the best catalyst, 100% degradation of the dye could be achieved after 50 min of UV-vis irradiation (similarly as with the P25 reference) or 86% within 220 min of visible light irradiation (i.e., in the conditions when P25 showed only weak activity). The excellent photocatalytic performance was attributed

to the enhanced visible light absorption, the effective charge separation, and the sepiolite carrier effect (large specific surface area, good distribution of the photoactive phase, and enhanced adsorption ability). In the subsequent work from this laboratory [214], the same synthetic procedure was adopted for the manufacturing of ternary Ag–TiO<sub>2</sub>–palygorskite composites. In the photodegradation of Methylene Blue, the materials performed in a manner comparable to the sepiolite-based systems. Both types of photocatalysts were characterized by good reusability.

Recently, Li et al. [215,216] reported the results of their study on the photocatalytic activity of TiO<sub>2</sub> and N-doped TiO<sub>2</sub> deposited on muscovite, which is the most common mica-type clay mineral. The nanocomposites were prepared by precipitation and/or the precipitation-grinding method, using muscovite as the matrix, TiOSO<sub>4</sub> as the titania precursor, and urea as the nitrogen source. The undoped materials proved active in the degradation of Rhodamine B under UV irradiation, with optimized photocatalyst achieving 98% destruction within 120 min. The destruction of Rhodamine B was caused by both the photocatalytic reaction on TiO<sub>2</sub> and the adsorption on muscovite. After doping with N, a red shift of the photoresponse was observed, and a similar level of Rhodamine B photodegradation (96%) could be achieved already under visible light illumination. It was found that the muscovite matrix had a retarding effect on the growth and phase transformation of TiO<sub>2</sub>. Further inhibition of the growth of TiO<sub>2</sub> nanoparticles resulted from N-doping.

The most relevant synthesis and photocatalysis data for selected examples of TiO<sub>2</sub> composites with clays other than montmorillonite, used for the degradation of dyes, are summarized in Table 5.

**Table 5.** Main synthesis and photocatalysis data for examples of TiO<sub>2</sub> composites with clay minerals other than montmorillonite, which were used as photocatalysts for the degradation of dyes (AO7—Acid Orange 7, Acid Red G—ARG, CR—Congo Red, GV—Gentian Violet, MB—Methylene Blue, MG—Methyl Green, MO—Methyl Orange, MOII—Methyl Orange II, OG—Orange G, BPB—bromophenol blue, RhB—Rhodamine B, RhG—Rhodamine G, SRB—sulforhodamine B, Att—attapulgite, Hal—halloysite, Hec—hectorite, Kao—kaolinite, Lap—Laponite, Mus—muscovite, Pal—palygorskite, Sap—saponite, Sep—sepiolite, CTA—cetyltrimethylammonium cation, CA—catalyst amount, MOCVD—metal-organic chemical vapor deposition).

TiO <sub>2</sub> –Clay Mineral Composite	Synthesis	Experimental Conditions	Dye	Degradation Efficiency	Ref.
g-C <sub>3</sub> N <sub>4</sub> /TiO <sub>2</sub> -Hec	Ti(OC <sub>3</sub> H <sub>7</sub> ) <sub>4</sub> precursor + fluorinated Hect, calcination 500 °C, SSA = 229 m <sup>2</sup> g <sup>-1</sup> ; TiO <sub>2</sub> -Hect mixed with g-C <sub>3</sub> N <sub>4</sub> by grinding, SSA = 219 m <sup>2</sup> g <sup>-1</sup>	visible light irradiation CA: 0.03 mg mL <sup>-1</sup> dye: 10 ppm	RhB	94%—120 min	[187]
TiO <sub>2</sub> /Hal	Ti(OC <sub>3</sub> H <sub>7</sub> ) <sub>4</sub> precursor + Hal, hydrothermal treatment at 65 °C, no calcination, SSA = 112 m <sup>2</sup> g <sup>-1</sup>	solar irradiation CA: 0.5 mg mL <sup>-1</sup> dye: 0.01 mg mL <sup>-1</sup>	RhB	89%—6 h	[198]
TiO <sub>2</sub> /Hal	Ti(OC <sub>3</sub> H <sub>7</sub> ) <sub>4</sub> precursor + Hal, hydrothermal treatment at 65 °C, no calcination, SSA = 112 m <sup>2</sup> g <sup>-1</sup>	visible light irradiation CA: 0.5 mg mL <sup>-1</sup> dye: 0.01 mg mL <sup>-1</sup>	RhB	69%—6 h	[198]

Table 5. Cont.

TiO <sub>2</sub> -Clay Mineral Composite	Synthesis	Experimental Conditions	Dye	Degradation Efficiency	Ref.
PANI-TiO <sub>2</sub> /Hal	Ti(OC <sub>3</sub> H <sub>7</sub> ) <sub>4</sub> precursor + aniline + FeCl <sub>3</sub> + Hal, hydrothermal treatment at 65 °C	visible light irradiation CA: 0.5 mg mL <sup>-1</sup> dye: 0.01 mg mL <sup>-1</sup>	RhB	77%—6 h	[199]
TiO <sub>2</sub> /Mus	Mus + TiOSO <sub>4</sub> precursor, calcination 400 °C	UV irradiation CA: 0.5 mg mL <sup>-1</sup> dye: 0.02 mg mL <sup>-1</sup>	RhB	98%—120 mn	[215]
N-TiO <sub>2</sub> /Mus	Mus + TiOSO <sub>4</sub> precursor, calcination 400 °C, grinding with urea, calcination 400 °C	visible light irradiation CA: 0.5 mg mL <sup>-1</sup> dye: 0.02 mg mL <sup>-1</sup>	RhB	96%—120 mn	[216]
TiO <sub>2</sub> /Lap	Ti(OC <sub>3</sub> H <sub>7</sub> ) <sub>4</sub> precursor + Lap + PEO, hydrothermal treatment 100 °C, calcination 500 °C, SSA = 379 m <sup>2</sup> g <sup>-1</sup>	UV irradiation CA: 1 mg mL <sup>-1</sup> dye: 0.01 mg mL <sup>-1</sup>	RhG	97%—60 min	[159]
TiO <sub>2</sub> /Kao	Ti(OC <sub>3</sub> H <sub>7</sub> ) <sub>4</sub> precursor + Kao, calcination 400 °C, SSA = 16 m <sup>2</sup> g <sup>-1</sup>	UV irradiation CA: 10 mg mL <sup>-1</sup> dye: 0.025 mg mL <sup>-1</sup>	MB	99%—5 min	[193]
TiO <sub>2</sub> /Kao	Ti(OC <sub>4</sub> H <sub>9</sub> ) <sub>4</sub> precursor + Kao microwave treated at 180 °C, mixture microwave treated at 180 °C; calcination 550 °C, SSA = 36 m <sup>2</sup> g <sup>-1</sup>	UV irradiation CA: 0.2 mg mL <sup>-1</sup> dye: 1.9 × 10 <sup>-5</sup> mmol mL <sup>-1</sup>	MB	54%—60 min	[194]
TiO <sub>2</sub> /Hal	Ti(OC <sub>3</sub> H <sub>7</sub> ) <sub>4</sub> precursor + Hal, calcination 300 °C	UV irradiation CA: 0.5 mg mL <sup>-1</sup> dye: 10 <sup>-4</sup> mmol mL <sup>-1</sup>	MB	82%—4 h	[200]
TiO <sub>2</sub> /amylose/Hal	Hal + amylose ground together, dispersed in DMSO/H <sub>2</sub> O, amylose/Hal extracted from the supernatant; Ti(OC <sub>3</sub> H <sub>7</sub> ) <sub>4</sub> precursor + amylose/Hal, drying 110 °C	UV irradiation CA: 1 mg/mL dye: 0.032 mg/mL	MB	91%—10 h	[201]
Ag-TiO <sub>2</sub> /Pal	Pal calcined at 500 °C + AgNO <sub>3</sub> , heated at 200 °C in N <sub>2</sub> + Ti(OC <sub>4</sub> H <sub>9</sub> ) <sub>4</sub> precursor, calcination 400 °C	UV irradiation CA: 0.25 mg dye: 1.6 × 10 <sup>-3</sup> mmol mL <sup>-1</sup>	MB	87%—120 min	[206]
CdS-TiO <sub>2</sub> /Pal	CTA-Pal + Ti(OC <sub>4</sub> H <sub>9</sub> ) <sub>4</sub> precursor, calcination 500 °C + CdSO <sub>4</sub> , calcination 500 °C + Na <sub>2</sub> S	visible light irradiation dye: 0.02 mg mL <sup>-1</sup>	MB	37%—150 min	[212]
TiO <sub>2</sub> /Kao	Ti(OC <sub>4</sub> H <sub>9</sub> ) <sub>4</sub> precursor + K outgassed at 750 °C, calcination 600 °C, SSA = 35 m <sup>2</sup> g <sup>-1</sup>	UV irradiation CA: 10 mg mL <sup>-1</sup> dye: 0.04 mg mL <sup>-1</sup>	CR	100%—6 h	[189]
TiO <sub>2</sub> /Kao	Ti(OC <sub>4</sub> H <sub>9</sub> ) <sub>4</sub> precursor + acid and base treated Kao outgassed at 750 °C, calcination 600 °C, SSA = 58 m <sup>2</sup> g <sup>-1</sup>	UV irradiation CA: 10 mg mL <sup>-1</sup> dye: 5.7 × 10 <sup>-5</sup> mmol mL <sup>-1</sup>	CR	95%—3 h	[190]
TiO <sub>2</sub> /Hal	Ti(OC <sub>3</sub> H <sub>7</sub> ) <sub>4</sub> precursor + Hal, hydrothermal treatment at 65 °C, no calcination, SSA = 112 m <sup>2</sup> g <sup>-1</sup>	solar irradiation CA: 0.5 mg mL <sup>-1</sup> dye: 0.02 mg mL <sup>-1</sup>	GV	60%—6 h	[198]

Table 5. Cont.

TiO <sub>2</sub> -Clay Mineral Composite	Synthesis	Experimental Conditions	Dye	Degradation Efficiency	Ref.
TiO <sub>2</sub> /Hal	Ti(OC <sub>3</sub> H <sub>7</sub> ) <sub>4</sub> precursor + Hal, hydrothermal treatment at 65 °C, no calcination, SSA = 112 m <sup>2</sup> g <sup>-1</sup>	visible light irradiation CA: 0.5 mg mL <sup>-1</sup> dye: 0.02 mg mL <sup>-1</sup>	GV	51%—6 h	[198]
ZnO-TiO <sub>2</sub> /clay	TiO <sub>2</sub> deposited on clay dehydrated at 400 °C by MOCVD of Ti(OC <sub>3</sub> H <sub>7</sub> ) <sub>4</sub> at 600 °C; ZnO deposited by sol-gel from Zn acetate precursor, calcination 300 °C, SSA = 105 m <sup>2</sup> g <sup>-1</sup>	UV irradiation CA: 4 mg mL <sup>-1</sup> dye: 0.075 mg mL <sup>-1</sup>	MG	100%—30 min	[196]
TiO <sub>2</sub> /Kao	Ti(OC <sub>4</sub> H <sub>9</sub> ) <sub>4</sub> precursor + Kao, drying 80 °C, no calcination, SSA = 63 m <sup>2</sup> g <sup>-1</sup>	solar irradiation CA: 1 mg mL <sup>-1</sup> dye: 0.01 mg mL <sup>-1</sup>	MO	83%—150 min	[195]
TiO <sub>2</sub> /Hal	Ti(OC <sub>4</sub> H <sub>9</sub> ) <sub>4</sub> precursor + Kao, drying 80 °C, no calcination, SSA = 124 m <sup>2</sup> g <sup>-1</sup>	solar irradiation CA: 1 mg mL <sup>-1</sup> dye: 0.01 mg mL <sup>-1</sup>	MO	65%—150 min	[195]
TiO <sub>2</sub> /Pal	Ti(OC <sub>4</sub> H <sub>9</sub> ) <sub>4</sub> precursor + Kao, drying 80 °C, no calcination, SSA = 194 m <sup>2</sup> g <sup>-1</sup>	solar irradiation CA: 1 mg mL <sup>-1</sup> dye: 0.01 mg mL <sup>-1</sup>	MO	45%—150 min	[196]
BiOBr-TiO <sub>2</sub> /Att	Att + Bi(NO <sub>3</sub> ) <sub>3</sub> + NH <sub>4</sub> Br precursor, calcination 320 °C + Ti(OC <sub>4</sub> H <sub>9</sub> ) <sub>4</sub> precursor, calcination 320 °C	visible light irradiation CA: 1 mg mL <sup>-1</sup> dye: 0.02 mg mL <sup>-1</sup>	MO	97%—120 min	[211]
Ag-TiO <sub>2</sub> /Sep	Ti(OC <sub>4</sub> H <sub>9</sub> ) <sub>4</sub> precursor + AgNO <sub>3</sub> , reduced with ascorbic acid + Sep, hydrothermal treatment at 150 °C; 5 wt % Ag	UV/visible light irradiation CA: 1 mg mL <sup>-1</sup> dye: 0.02 mg mL <sup>-1</sup>	MO	100%—50 min	[213]
Ag-TiO <sub>2</sub> /Sep	Ti(OC <sub>4</sub> H <sub>9</sub> ) <sub>4</sub> precursor + AgNO <sub>3</sub> , reduced with ascorbic acid + Sep, hydrothermal treatment at 150 °C; 5 wt % Ag	visible light irradiation CA: 1 mg mL <sup>-1</sup> dye: 0.02 mg mL <sup>-1</sup>	MO	86%—220 min	[213]
SnO <sub>2</sub> -TiO <sub>2</sub> /Att	Att + SnCl <sub>2</sub> precursor, calcination 300 °C + Ti(OC <sub>4</sub> H <sub>9</sub> ) <sub>4</sub> precursor, calcination 300 °C, SSA = 147 m <sup>2</sup> g <sup>-1</sup>	UV irradiation CA: 1 mg mL <sup>-1</sup> dye: 0.02 mg mL <sup>-1</sup>	MO	99%—30 min	[210]
TiO <sub>2</sub> /Kao	Ti(OC <sub>3</sub> H <sub>7</sub> ) <sub>4</sub> precursor + Kao, calcination 400 °C, SSA = 16 m <sup>2</sup> g <sup>-1</sup>	UV irradiation CA: 10 mg mL <sup>-1</sup> dye: 0.025 mg mL <sup>-1</sup>	MOII	93%—5 min	[193]
TiO <sub>2</sub> /Kao	TiCl <sub>4</sub> precursor + acid treated Kao, drying at 70 °C, calcination 400 °C, SSA = 114 m <sup>2</sup> g <sup>-1</sup>	UV irradiation CA: 1.5 mg mL <sup>-1</sup> dye: 0.03–0.05 mg mL <sup>-1</sup>	ARG	100%—60 min	[191]
TiO <sub>2</sub> /Sep	Sep + Ti(OC <sub>3</sub> H <sub>7</sub> ) <sub>4</sub> precursor, heated at 70 °C, SSA = 247 m <sup>2</sup> g <sup>-1</sup>	UV irradiation CA: 1.5 mg/mL dye: 0.03 mg/mL	ARG	100%—120 min	[205]
TiO <sub>2</sub> /Pal	CTA-Pal + Ti(OC <sub>3</sub> H <sub>7</sub> ) <sub>4</sub> precursor, calcination 600 °C	UV irradiation CA: 1 mg mL <sup>-1</sup> dye: 10 <sup>-5</sup> mmol mL <sup>-1</sup>	OG	100%—90 min	[203]

Table 5. Cont.

TiO <sub>2</sub> -Clay Mineral Composite	Synthesis	Experimental Conditions	Dye	Degradation Efficiency	Ref.
TiO <sub>2</sub> /Sep	Sep + Ti(OC <sub>3</sub> H <sub>7</sub> ) <sub>4</sub> precursor, microwave hydrothermal treatment, SSA = 161 m <sup>2</sup> g <sup>-1</sup>	UV irradiation CA: 0.3 mg mL <sup>-1</sup> dye: 0.01 mg mL <sup>-1</sup>	OG	90%—120 min	[206]
Ru(Bpy) <sub>3</sub> /Ti-pillared Sap	Ti(OC <sub>3</sub> H <sub>7</sub> ) <sub>4</sub> precursor, calcination 400 °C, SSA = 154 m <sup>2</sup> g <sup>-1</sup> ; + Ru(BPy) <sub>3</sub> , SSA = 150 m <sup>2</sup> g <sup>-1</sup>	UV irradiation CA: 0.4 mg mL <sup>-1</sup> dye: 0.02 mg mL <sup>-1</sup>	BPB	97%—120 min	[69]
Ru(Bpy) <sub>3</sub> /Ti-pillared Sap	Ti(OC <sub>3</sub> H <sub>7</sub> ) <sub>4</sub> precursor, calcination 400 °C, SSA = 154 m <sup>2</sup> g <sup>-1</sup> ; + Ru(BPy) <sub>3</sub> , SSA = 150 m <sup>2</sup> g <sup>-1</sup>	visible light irradiation CA: 0.4 mg mL <sup>-1</sup> dye: 0.02 mg mL <sup>-1</sup>	BPB	90%—120 min	[69]
TiO <sub>2</sub> /Lap	TiO <sub>2</sub> colloid from Ti(OC <sub>3</sub> H <sub>7</sub> ) <sub>4</sub> precursor-treated hydrothermally + Lap + PEO, 40 mmol Ti/g Lap, hydrothermal treatment 180 °C, calcination 500 °C,	UV irradiation CA: 1 mg mL <sup>-1</sup> dye: 1.8 × 10 <sup>-5</sup> mmol mL <sup>-1</sup>	SRB	92%—90 min	[184]
TiO <sub>2</sub> /Kao	TiOSO <sub>4</sub> precursor + raw Kao, calcination 600 °C, SSA = 32 m <sup>2</sup> g <sup>-1</sup>	UV irradiation CA: 1.5 mg mL <sup>-1</sup> dye: 0.03—0.05 mg mL <sup>-1</sup>	AO7	70%—60 min	[192]

### 6.1.2. Photodegradation of Phenolic Compounds

The pollution of aquatic systems with phenolic compounds constitutes a major concern because the contaminants are resistant to biodegradation, tend to accumulate, and persist for a long time in the environment, having toxic effects on humans and animals [217]. For this reason, phenolic compounds are considered pollutants of priority concern. A vast range of wastewater streams, stemming mainly from petrochemical, paper, paint, fabric, and chemical industries, are contaminated by phenol and its derivatives. To minimize their devastating impact on the environment, the purification of wastewaters prior to their disposal into water bodies is necessary.

As described previously, the photodegradation of phenol was addressed already in 1999, at the onset of the rapidly spreading interest in the photocatalytic properties of titania-clay composites. Ding et al. [151] investigated TiO<sub>2</sub>-montmorillonite systems and found that the factors critical for the photocatalysis, such as the size of anatase crystallites, or the development of the external surface, essential for ensuring good accessibility of the deposited titania, could be controlled by the manner of the composite drying. In the test reaction of photocatalytic degradation of phenol, the highest reaction rate was observed for the Ti-pillared montmorillonite, which in the final stage of synthesis was subjected to the supercritical drying.

A few years later, Ilisz et al. [218], in the study of the combined effect of pollutants adsorption and destruction, prepared three types of titania/clay photocatalytic systems: a conventional Ti-pillared montmorillonite, TiO<sub>2</sub> deposited on organomontmorillonite, and a mixture of organomontmorillonite with P25. The organomontmorillonite component was expected to act as a hydrophobic adsorbent. Tests of the photocatalytic destruction of 2-chlorophenol revealed that the best degradation efficiency was observed for the mixture with P25 (100% in 400 min), which was followed by Ti-PILC (75% in 600 min) and the organoclay-supported TiO<sub>2</sub> (45% in 600 min). Poor result of the latter was attributed to the continuous destruction of the adsorbent during photocatalytic reaction. Pichat et al. [219], who studied the photocatalytic removal of 4-chlorophenol over Ti-pillared montmorillonite, also found that the clay-based catalyst was less active than P25.

About the same time, Zhu et al. [220] investigated the photocatalytic degradation of phenol and dichlorophenol by composites of titania with two smectite clays, Laponite and montmorillonite, which were prepared according to the previously described procedure [159] by the sol-gel method from Ti tetraisopropoxide, with or without the presence of PEO surfactant. In the destruction of dichlorophenol, the Laponite-based photocatalyst showed 88% efficiency, while the montmorillonite-based one was almost inactive. In the case of phenol degradation, both types of  $\text{TiO}_2$ -Laponite composites, synthesized with and without PEO, showed high activity, removing 82 and 94% pollutant, respectively. Moreover, per mass of titania, the photocatalytic performance of composite solids was superior to that of the P25 reference.

Kun et al. [221] studied the degradation of phenol over a series of  $\text{TiO}_2$ -montmorillonite nanocomposites prepared under highly acidic ( $\text{pH} \approx 1$ ) and weakly acidic ( $\text{pH} \approx 4$ ) conditions by the heterocoagulation method, consisting of the addition of well-defined titania sol derived from  $\text{Ti}(\text{OC}_3\text{H}_7)_4$  to the aqueous suspension of clay mineral. The resulting composites contained anatase particles of few nanometers incorporated into the interlamellar spaces of montmorillonite. The samples synthesized at  $\text{pH} = 1$  had larger SSA and were more active photocatalytically than those obtained at  $\text{pH} = 4$ . For instance, of two catalysts containing 50 wt %  $\text{TiO}_2$ , the one obtained at  $\text{pH} = 1$  converted 52% phenol, while that synthesized at  $\text{pH} = 4$  converted only 45%. Per mass of  $\text{TiO}_2$ , both types of  $\text{TiO}_2$ /montmorillonite samples performed better than the reference pure titania catalyst, thus proving the advantage of composite formation.

An interesting approach to the formation of  $\text{TiO}_2$ -clay composite photocatalysts was proposed by Ménesi et al. [222], who employed grinding in an agate ball mill as means to mix and bind by electrostatic interactions the positively charged P25 titania nanopowder with the negatively charged surface of Ca-montmorillonite. The mixture with 25 wt %  $\text{TiO}_2$  loading degraded 70% of the phenol in 60 min, while the one with 80 wt %  $\text{TiO}_2$  and pure P25 removed 95% and 98% phenol in 40 min, respectively. The authors established that when normalized to the unit weight of  $\text{TiO}_2$ , aqueous phenol solution was degraded at a significantly higher rate on  $\text{TiO}_2$ -Ca-montmorillonite composites than on pure P25 titania.

Aranda et al. [202] prepared titania composites with sepiolite and tested the materials in the photocatalytic degradation of phenol. The photocatalysts were prepared from cetyltrimethylammonium-exchanged sepiolite by means of the colloidal route developed by the authors and described in the previous section (Figure 13).

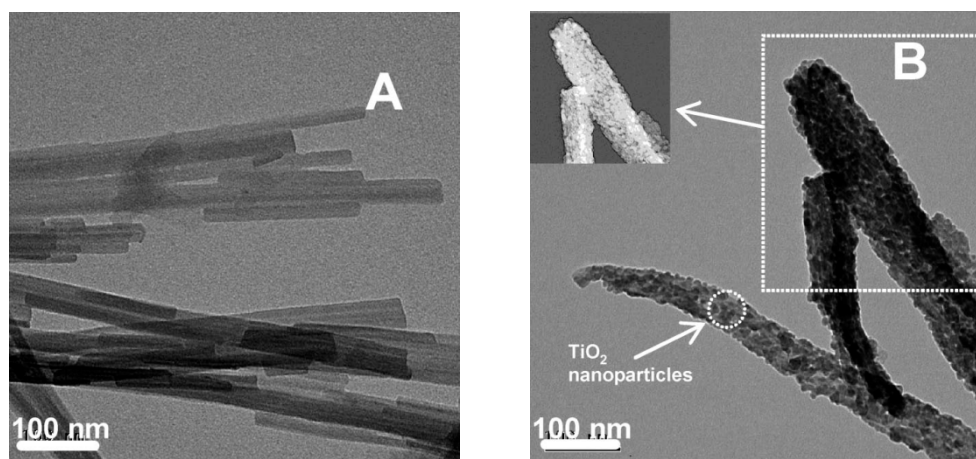


**Figure 13.** TEM images of: (A) cetyltrimethylammonium-exchanged sepiolite; (B) S-doped  $\text{TiO}_2$ /sepiolite nanocomposite. Adapted with permission from ref. [202]. Copyright 2008 American Chemical Society.

The photocatalytic activity of composites was further enhanced by adding thiourea to the initial colloidal system, which enabled the incorporation of sulfur atoms into the

titania component and stabilized the anatase phase. The degradation of phenol over the best S-doped TiO<sub>2</sub>/sepiolite photocatalyst upon UV irradiation reached over 90%. The authors prepared also mixed TiO<sub>2</sub>-SiO<sub>2</sub>-sepiolite composites, but the materials showed lower photoactivity than the composites containing pure titania. Similarly, Chen et al. [223] found that TiO<sub>2</sub>-SiO<sub>2</sub> co-pillared montmorillonite was substantially less active in the UV light photodegradation of 2,4,6-trichlorophenol than Ti-pillared clay (40 and 100% efficiency, respectively). The colloidal route was applied by Manova et al. [224], who used Fe-rich smectite and vermiculite for the synthesis of TiO<sub>2</sub>-clay and TiO<sub>2</sub>-SiO<sub>2</sub>-clay composites. Anatase nanoparticles were formed in the former, and noncrystalline TiO<sub>2</sub>-SiO<sub>2</sub> mixed oxides were formed in the latter case. The materials were tested in the photocatalytic degradation of 2,4-dichlorophenol, and their efficiency per mass of TiO<sub>2</sub> was higher than that of the P25 standard. It appeared that mixed TiO<sub>2</sub>-SiO<sub>2</sub>-clays were slightly more active than the TiO<sub>2</sub>-clays counterparts (e.g., 97 vs. 85% of pollutant removal for TiO<sub>2</sub>-SiO<sub>2</sub>/vermiculite and TiO<sub>2</sub>/vermiculite, respectively), which is at variance with the results obtained for sepiolite and montmorillonite-based materials [202,223]. In the already discussed work by Belver et al. [174], the composites prepared by the colloidal route from Cloisite<sup>®</sup>30B were tested in phenol photodegradation. The authors pointed out that some intermediates in the degradation of phenol were highly toxic species; hence, a very high degree of mineralization was required in order to decrease the initial ecotoxicity of phenol-contaminated water. On most catalysts, upon 10 h of UV irradiation, nearly 80% of phenol was removed. The satisfactory level of phenol degradation over TiO<sub>2</sub>-Cloisite<sup>®</sup>30B composites could be achieved for irradiation times of 24 h.

Several works suggested that the use of titanil sulfate as a precursor of titania component was beneficial for the photocatalytic activity [225–227]. The synthesis involved the reaction of clay suspensions with TiOSO<sub>4</sub> under hydrothermal conditions. Yang et al. [225] used beidellite as the clay component and found that the anatase nanoparticles' crystal size, the pore size, and the specific surface area of the catalysts could be tailored by manipulating the acidity, the ratio of Ti/clay, and the hydrothermal temperature of the synthesis systems. The materials proved more efficient in the photodegradation of phenol compared to the conventional titania-pillared beidellite with the best catalyst removing ca. 50% of pollutant in 300 min. Xuzhuang et al. [226] applied this strategy to prepare TiO<sub>2</sub>-Laponite composite photocatalysts for the removal of phenol and also found the TiOSO<sub>4</sub>-derived solids superior to the conventionally Ti-pillared Laponite. The materials performed better than the previously studied beidellite-based samples, as the complete degradation of phenol could be achieved within 120 min. A recent study by Décsiné Gombos et al. [227] confirmed the previous findings and shed more light on the nature of TiO<sub>2</sub>-Laponite hybrids prepared with the use of TiOSO<sub>4</sub> as compared to the reference Ti-pillared Laponite. Pillaring resulted in a mesoporous composite in which the clay component retained the parent Laponite morphology, and anatase formed particles of 5–6 nm. In contrast, by hydrothermal treatment with titanium oxysulfate, the Laponite structure was destroyed, and a more opened nanoporous silica/titania material was formed with bigger, ca. 14 nm anatase grains. Tests of the photooxidation of phenol and 2,4,6-trichlorophenol showed that the TiO<sub>2</sub>-Laponite sample prepared hydrothermally from TiOSO<sub>4</sub> showed much better performance than the one prepared by conventional TiCl<sub>4</sub> pillaring. The composite samples performed poorer than the P25 standard, but, as usually found with TiO<sub>2</sub>-clay hybrids, they were much easier to separate from the reaction medium than the commercial titania.

The photocatalytic removal of 4-nitrophenol was studied by Zhang et al. using TiO<sub>2</sub>-kaolinite [191] and TiO<sub>2</sub>-sepiolite [205] composites described in the previous section. Titania nanoparticles in the former were a mixture of anatase and brookite, while in the latter, pure anatase phase was present. Both TiO<sub>2</sub>-kaolinite and TiO<sub>2</sub>-sepiolite were active in the degradation of 4-nitrophenol, removing within 240 min 85 and 79% of the pollutant, respectively.

Several works reported the attempts to achieve enhanced photocatalytic activity in the degradation of the phenolic compounds by doping of the titania component with

foreign elements, or by the formation of a heterojunction with another semiconductor. Thus, Carriazo et al. [228] investigated the doping of Ti-pillared bentonite with Fe and its effect on the photocatalytic activity of the composite in the destruction of phenol. The authors found that the method of Fe incorporation was of key importance for determining the photocatalytic performance. Post-synthesis Fe insertion by means of cation exchange or impregnation worsened the activity of Ti-PILC. On the other hand, the use of pillaring solution containing both  $\text{Fe}^{3+}$  and  $\text{Ti}^{4+}$  resulted in a photocatalyst with improved efficiency of phenol degradation (90% efficiency). The effect was assigned to the formation of anatase nanoparticles substitutionally doped with iron and the possible shift of the band-gap of this structure to the visible range of the spectrum. In the already discussed paper by Belver et al. [181], the  $\text{TiO}_2$  component in the titania–montmorillonite composite was modified by doping with cerium, which resulted in a red shift of the absorption band edge. As a consequence, the photocatalyst with the optimized Ce content showed improved photoactivity in the degradation of phenol (80%) with respect to the Ce-free composite (75%). A heterojunction system was designed by Zhang et al. [229], who used palygorskite as a matrix for the immobilization of mixed  $\text{SnO}_2$ – $\text{TiO}_2$  oxides by the in situ hydrolysis of  $\text{SnCl}_2$  and  $\text{Ti}(\text{OC}_4\text{H}_9)_4$ , following their own previously developed procedure [210]. In the photocatalytic degradation of phenol, the  $\text{SnO}_2$ – $\text{TiO}_2$ –palygorskite sample showed much higher activity than composites with single oxides and P25 standard, reaching 100% phenol decomposition within 100 min. COD analysis confirmed the nearly complete mineralization of the pollutant.

In Table 6, the most relevant synthesis and photocatalysis data for selected examples of  $\text{TiO}_2$ –clay mineral composites used as photocatalysts for the degradation of phenolic compounds are summarized.

**Table 6.** Main synthesis and photocatalysis data for examples of  $\text{TiO}_2$  composites with clay minerals used as photocatalysts for the degradation of phenolic compounds (CP—chlorophenol, DCP—dichlorophenol, TCP—trichlorophenol, NP—nitrophenol, Ph—phenol, Bei—beidellite, Kao—kaolinite, Lap—Laponite, Pal—palygorskite, Sep—sepiolite, Ver—vermiculite, CTA—cetyltrimethylammonium cation, HDPM—hexadecylpyridinium cation, P—pollutant, CA—catalyst amount).

TiO <sub>2</sub> –Clay Mineral Composite	Synthesis	Experimental Conditions	Pollutant	Degradation Efficiency	Ref.
TiO <sub>2</sub> /Mt	Ti(OC <sub>3</sub> H <sub>7</sub> ) <sub>4</sub> precursor + Mt, acidified to pH = 1, + Mt, drying at 50 °C, SSA = 251 m <sup>2</sup> g <sup>−1</sup>	UV irradiation CA: 1 mg mL <sup>−1</sup> P: 5 × 10 <sup>−4</sup> mmol mL <sup>−1</sup>	Ph	52%—120 min	[221]
TiO <sub>2</sub> /Mt	Ti(OC <sub>3</sub> H <sub>7</sub> ) <sub>4</sub> precursor + Cloisite <sup>®</sup> 30B, induced hydrolysis, calcination 550 °C, SSA = 143 m <sup>2</sup> g <sup>−1</sup>	solar irradiation CA: 0.5 mg mL <sup>−1</sup> P: 0.025 mg mL <sup>−1</sup> (after saturation with adsorbed Ph in dark)	Ph	ca. 80%—10 h	[174]
Fe,Ti-pillared Mt	TiCl <sub>4</sub> precursor + Fe(NO <sub>3</sub> ) <sub>3</sub> + Mt, calcination 400 °C, SSA = 129 m <sup>2</sup> g <sup>−1</sup>	UV irradiation CA: 5 mg mL <sup>−1</sup> P: 5 × 10 <sup>−4</sup> mmol mL <sup>−1</sup>	Ph	90%—240 min	[228]
Ce,TiO <sub>2</sub> /Mt	Ti(OC <sub>3</sub> H <sub>7</sub> ) <sub>4</sub> precursor + Cloisite <sup>®</sup> 30B + Ce(NO <sub>3</sub> ) <sub>3</sub> solution induced hydrolysis, calcination 500 °C; 0.25 wt % Ce, SSA = 211 m <sup>2</sup> g <sup>−1</sup>	solar irradiation CA: 0.5 mg mL <sup>−1</sup> dye: 0.025 mg mL <sup>−1</sup> (after saturation with adsorbed RhB in dark)	Ph	80%—600 min	[181]

Table 6. Cont.

TiO <sub>2</sub> -Clay Mineral Composite	Synthesis	Experimental Conditions	Pollutant	Degradation Efficiency	Ref.
TiO <sub>2</sub> /Lap	TiOSO <sub>4</sub> precursor + Lap, hydrothermal treatment at 150 °C, calcination 500 °C, SSA = 323 m <sup>2</sup> g <sup>-1</sup>	UV irradiation CA: 0.6 mg mL <sup>-1</sup> P: 5 × 10 <sup>-5</sup> mmol mL <sup>-1</sup>	Ph	100%—80 min	[227]
TiO <sub>2</sub> /Lap	Ti(OC <sub>3</sub> H <sub>7</sub> ) <sub>4</sub> precursor + Lap, hydrothermal treatment 100 °C, calcination 500 °C, SSA = 435 m <sup>2</sup> g <sup>-1</sup>	UV irradiation CA: 1 mg mL <sup>-1</sup> P: 10 ppm	Ph	94%—240 min	[220]
SnO <sub>2</sub> -TiO <sub>2</sub> /Pal	Pal + SnCl <sub>2</sub> precursor, calcination 300 °C + Ti(OC <sub>4</sub> H <sub>9</sub> ) <sub>4</sub> precursor, calcination 300 °C, SSA = 147 m <sup>2</sup> g <sup>-1</sup>	UV irradiation CA: 1 mg mL <sup>-1</sup> dye: 0.08 mg mL <sup>-1</sup>	Ph	100%—100 min	[229]
Ti-pillared Mt	Ti(OC <sub>3</sub> H <sub>7</sub> ) <sub>4</sub> precursor + Mt, drying at 50 °C, no calcination	UV irradiation CA: 6 mg mL <sup>-1</sup> P: 2.5 × 10 <sup>-3</sup> mmol mL <sup>-1</sup>	CP	75%—600 min	[218]
TiO <sub>2</sub> /HDPM-Mt	Sonicated HDPM-Mt + Ti(OC <sub>3</sub> H <sub>7</sub> ) <sub>4</sub> precursor, hydrothermal treatment at 150 °C	UV irradiation CA: 6 mg mL <sup>-1</sup> P: 2.5 × 10 <sup>-3</sup> mmol mL <sup>-1</sup>	CP	45%—600 min	[218]
Ti-pillared Mt	Ti(OC <sub>4</sub> H <sub>9</sub> ) <sub>4</sub> precursor + Mt, calcination 450 °C, SSA = 133 m <sup>2</sup> g <sup>-1</sup>	UV irradiation CA: 2 mg mL <sup>-1</sup> P: 0.02 mg mL <sup>-1</sup>	TCP	100%—120 min	[223]
Ti,Si-pillared Mt	Ti(OC <sub>4</sub> H <sub>9</sub> ) <sub>4</sub> precursor + Si(OC <sub>2</sub> H <sub>5</sub> ) <sub>4</sub> precursor + Mt, calcination 450 °C, SSA = 259 m <sup>2</sup> g <sup>-1</sup>	UV irradiation CA: 2 mg mL <sup>-1</sup> P: 0.02 mg mL <sup>-1</sup>	TCP	40%—120 min	[223]
TiO <sub>2</sub> /Lap	TiOSO <sub>4</sub> precursor + Lap, hydrothermal treatment at 150 °C, calcination 500 °C, SSA = 323 m <sup>2</sup> g <sup>-1</sup>	UV irradiation CA: 0.6 mg mL <sup>-1</sup> P: 5 × 10 <sup>-5</sup> mmol/ mL <sup>-1</sup>	TCP	100%—80 min	[227]
TiO <sub>2</sub> /Kao	TiCl <sub>4</sub> precursor + acid treated Kao, drying at 70 °C, calcination 400 °C, SSA = 114 m <sup>2</sup> g <sup>-1</sup>	UV irradiation CA: 1 mg mL <sup>-1</sup> P: 0.01 mg mL <sup>-1</sup>	NP	85%—240 min	[191]
TiO <sub>2</sub> /Sep	Sep + Ti(OC <sub>3</sub> H <sub>7</sub> ) <sub>4</sub> precursor, heated at 70 °C, SSA = 247 m <sup>2</sup> g <sup>-1</sup>	UV irradiation CA: 1.5 mg mL <sup>-1</sup> P: 0.01 mg mL <sup>-1</sup>	NP	79%—240 min	[205]

### 6.1.3. Photodegradation of Emerging Pollutants

Emerging pollutants are a diverse group of organic chemicals, natural or synthetic, usually not monitored, but identified as potentially dangerous [230]. Such contaminants may stem from domestic, municipal, industrial, or agricultural sources, and they pervade the environment in an uncontrolled manner, causing adverse ecological or health effects. The examples of emerging pollutants encompass pharmaceuticals, endocrine disruptors (environmental hormones), cosmetics, pesticides, herbicides, etc. Their widespread presence in the aquatic systems and wastewater effluents is well documented [230]. In general, the conventional water treatment technologies are not suitable for the removal of such compounds; therefore, an innovative approach based on the photocatalytic degradation is currently considered a promising option.

The already mentioned work by Yoshida et al. [152] was the first to report on the ability of TiO<sub>2</sub>-clay mineral composites to catalyze the photodegradation of compounds classified currently as emerging pollutants [230]. The authors chose dibutyl phthalate as a model endocrine disruptor and studied its destruction over Ti-pillared montmorillonite photocatalyst prepared by the sol-gel procedure from Ti tetraisopropoxide precursor with or without hydrothermal treatment. They concluded that the improved crystallinity of the pillars in the hydrothermally-treated sample boosted the photocatalytic activity in comparison with the untreated catalyst (ca. 90% efficiency vs. ca. 70%, respectively) and that the adsorptive properties of Ti-PILC enhanced the overall process. In the continuation of this work, Ooka et al. [231] focused on the purification of water from endocrine disruptors of different hydrophobicities (dibutyl phthalate, diethyl phthalate, dimethyl phthalate, and bisphenol-A). The authors found that the efficiency of photodegradation increased with the increasing hydrophobicity of the pollutant, and they attributed the effect to the facilitated adsorption at the hydrophobic interlayer surface of the Ti-PILC photocatalyst. The authors pursued the issue further in their next paper [63] and used four clay minerals of different surface hydrophobicities (saponite, fluorine hectorite, montmorillonite, fluorine mica) as components of Ti-PILC photocatalysts for the degradation of dibutyl and dimethyl phthalates. They found that the surface hydrophobicity of the synthesized composites increased with the growing hydrophobicity of the host clay, and so did their photoactivity in the degradation of phthalates, which is an important guideline for the design of photocatalysts for the destruction of hydrophobic organic contaminants. Bisphenol-A was used as a model compound in the study of Sasai et al. [232], who aimed at extension of the photoresponse of the TiO<sub>2</sub>-clay composite obtained by treatment of an organomontmorillonite with titania sol from Ti(OC<sub>3</sub>H<sub>7</sub>)<sub>4</sub> without calcination. Cationic Cu-phthalocyanine was added as a photosensitizer to the composite in order to develop a visible light-driven photoactivity. Indeed, a significant red shift of the absorption edge was observed for the sensitized material. It was found that the prepared hybrid solid readily adsorbed bisphenol-A by hydrophobic interaction with the interlayer organocations and could photocatalytically decompose the endocrine disruptor even under visible light, as monitored by the quantitative analysis of the evolved CO<sub>2</sub>.

A series of recent papers addressed the use of TiO<sub>2</sub>-clay mineral composites, which were modified by the addition of various components enhancing their photoresponse, for the photodegradation of pharmaceuticals. Basing on the report indicating that the doping of titania with Zr decreased the recombination of holes and electrons, Belver et al. [233] prepared composites made of Zr-containing TiO<sub>2</sub> nanoparticles and exfoliated commercial organoclay Cloisite<sup>®</sup>30B, using the sol-gel method, with Ti isopropoxide and Zr butoxide as precursors. The resulting materials contained Zr-doped anatase nanoparticles of 15–20 nm dispersed over a delaminated clay. The incorporation of Zr improved the photocatalytic activity with respect to the undoped TiO<sub>2</sub>-clay system, which was attributed to the band-gap reduction and charge trapping caused by the Zr dopant. The materials were tested in the solar photodegradation of an analgesic drug, antipyrine (phenazone). High degradation rates were obtained, which were enhanced by the presence of the Zr dopant. However, despite the high conversion of antipyrine (up to ca. 90%), only moderate mineralization was observed. In another work from this group, Tobajas et al. [234] prepared TiO<sub>2</sub>-ZnO/montmorillonite composites by a sol-gel method, using Cloisite<sup>®</sup>30B as the parent clay, and they obtained mixed TiO<sub>2</sub>-ZnO nanoparticles supported on the surface of a delaminated clay. As indicated earlier, the presence of such a heterojunction can reduce the probability of electron-hole recombination and promote the migration of photogenerated carriers [182]. The photocatalysts were tested in the degradation under the solar light irradiation of acetaminophen (paracetamol) and antipyrine. Both pharmaceuticals could be removed almost completely within 10 h of irradiation. The remaining intermediates corresponded to short-chain carboxylic acids and unidentified by-products with very low ecotoxicity. In the pursuance of further improvement of the catalysts, Belver et al. [235] added Ag component to the TiO<sub>2</sub>-ZnO-clay system to combine the semiconductor proper-

ties of TiO<sub>2</sub>–ZnO heterojunctions with the light absorption properties of Ag and the porous texture of the delaminated clay. The incorporation of silver was carried out by the photoreduction of Ag<sup>+</sup> ions adsorbed at the composite surface during treatment with AgNO<sub>3</sub> solution. The presence of silver nanoparticles extended the light absorption of the solids to the visible region. The nearly complete degradation of antipyrine and 100% destruction of acetaminophen could be reached within 6 h of solar light irradiation in the presence of the optimized Ag–ZnO–TiO<sub>2</sub>–clay composite. Vaizoğullar [236] combined a TiO<sub>2</sub>–ZnO photoactive phase with sepiolite, using the sol–gel method with Ti tetrabutoxide and Zn acetate as precursors, and they used the materials for the photocatalytic degradation of flumequine antibiotic. The results showed that TiO<sub>2</sub>–ZnO–sepiolite, which degraded 85% flumequine in 240 min, was more photoactive than TiO<sub>2</sub>–ZnO (67%), TiO<sub>2</sub> (23%), and ZnO (11%) catalysts, owing to the increased adsorption ability of the supported system and inhibition of the charge recombination by the TiO<sub>2</sub>–ZnO heterojunction.

Another type of heterojunction system, based on kaolinite, titania, and graphitic carbon nitride, was designed by Li et al. [237] and tested in the photodegradation of ciprofloxacin, which is an antibiotic used to treat a broad spectrum of bacterial infections. The composite was synthesized from a TiO<sub>2</sub>–kaolinite hybrid, which was prepared by a conventional sol–gel method using Ti tetrabutoxide as a precursor. The calcined material was acid activated and mixed, in the acid medium, with g-C<sub>3</sub>N<sub>4</sub> powder. Compared to the parent composite, the ternary g-C<sub>3</sub>N<sub>4</sub>/TiO<sub>2</sub>/kaolinite system showed a red shift of the absorption band edge (Figure 14) and superior performance in the photocatalytic degradation of ciprofloxacin under visible light illumination (92% vs. 65% for the former). Moreover, the composite retained high activity in the recycling experiments. The enhancement of photocatalytic properties was attributed to the improvement of light harvesting as well as the better charge separation and transfer efficiency.

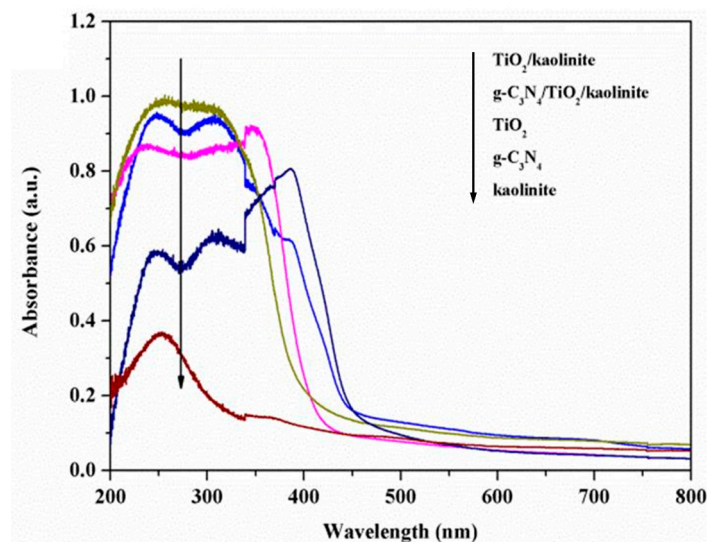


**Figure 14.** UV-Vis DRS of TiO<sub>2</sub>/kaolinite and g-C<sub>3</sub>N<sub>4</sub>/TiO<sub>2</sub>/kaolinite composite systems, and of the single components TiO<sub>2</sub>, g-C<sub>3</sub>N<sub>4</sub>, and kaolinite. Ordering of the spectra as indicated by black vertical arrow and the adjacent legend. Adapted with permission from ref. [237]. Copyright 2017 Elsevier.

Recently, Gonzalez et al. [56] prepared titanium-pillared montmorillonites according to the procedure proposed by Lin et al. [47], introducing Cr<sup>3+</sup> or Fe<sup>3+</sup> dopant at the stage of preparation of the pillaring solution. The solids were used as catalysts for the photodegradation of the antibiotic trimethoprim. The Cr-Ti-PILC sample showed better activity, reaching 76% photodegradation of the pollutant after 180 min of reaction, while in the same period, only about 30% of trimethoprim was converted over Fe-Ti-PILC photocatalyst. Unfortunately, the work provided no data on the behavior of undoped Ti-PILC, so it was impossible to judge whether doping itself was beneficial for the abatement

of trimethoprim. Hu et al. [238] synthesized a ternary BiOCl–TiO<sub>2</sub>–sepiolite composite by a successive deposition of TiO<sub>2</sub> and BiOCl, from TiSO<sub>4</sub> and Bi(NO<sub>3</sub>)<sub>3</sub> precursors, which was followed by calcination, and they tested the material in the photodegradation of antibiotic tetracycline under visible light illumination. The formation of a ternary heterojunction structure resulted in the enhanced visible light response with respect to the BiOCl-free composite (>90 and 65% efficiency, respectively). In addition, the superior adsorption capacity and good reusability of the novel composite offered a promising prospect of application in antibiotic wastewater treatment.

There are also examples of the use of titania–clay mineral composites for the photocatalytic purification of water from various pesticides. Belessi et al. [239] synthesized composites of TiO<sub>2</sub> with montmorillonite and Laponite using the standard sol–gel procedure with Ti isopropoxide as precursor, and they investigated their photocatalytic properties in the degradation of chloroacetanilide herbicide (dimethachlor). Both types of composites exhibited good photodegradation efficiency, reaching, for maximum TiO<sub>2</sub> loadings, ca. 90% pollutant conversion in 180 min. Their performance per mass of TiO<sub>2</sub> was better than that of unsupported TiO<sub>2</sub> but poorer than that of the P25 standard. Paul et al. [240] subjected a series of herbicides (bromacil, alachlor, chlorotoluron, sulfosulfuron, and imazaquin) to photocatalytic degradation over TiO<sub>2</sub>–Laponite composites prepared according to the previously described procedure [226]. The order of degradation efficiency was as follows: alachlor (66%) < chlorotoluron (77%) < sulfosulfuron (80%) < bromacil (84%) < imazaquin (100%). Based on the TiO<sub>2</sub> mass, the composites were displaying a higher degradation rate than commercial P25. The photodegradation of another herbicide, atrazine, was studied by Belver et al., who used titania–organoclay composites modified by doping [241] or by heterojunction formation [235]. In the first study, the W-doped TiO<sub>2</sub>–clay photocatalysts were obtained by the modified colloidal route, using the commercial organomontmorillonite Cloisite as the clay component, Ti isopropoxide as the precursor, and ammonium metatungstate as the source of W dopant. The calcined products contained W–TiO<sub>2</sub> nanoparticles (13–16 nm) anchored on the surface of an exfoliated clay. The incorporation of W resulted in a moderate narrowing of the TiO<sub>2</sub> band gap. The photocatalyst with the highest level of W doping (W/Ti = 0.05) presented the best photoactivity in atrazine removal under solar light, achieving nearly complete degradation in 4 h, in contrast to only ca. 35% destruction observed for the undoped composite. The doped catalysts showed also weaker but appreciable photoactivity under visible light (the highest conversion of 42% in 7 h), while the TiO<sub>2</sub>–clay composite was in these circumstances inactive. The same group demonstrated that in the presence of the heterojunction Ag–ZnO–TiO<sub>2</sub>–clay composite, which was described in detail in the former paragraph, atrazine could be destroyed almost totally within 6 h of irradiation [235].

Table 7 gathers the most relevant information on the synthesis of selected examples of TiO<sub>2</sub>–clay mineral composites and their photocatalytic performance in the degradation of emerging pollutants.

**Table 7.** Main synthesis and photocatalysis data for selected examples of TiO<sub>2</sub> composites with clay minerals used for the degradation of emerging pollutants (ALA—alachlor, ACE—acetaminophen, ANT—antipyrine, ATR—atrazine, BRO—bromacil, DBP—dibutyl phthalate, CHT—chlorotoluron, CIP—ciprofloxacin, DIM—dimethachlor, IMA—imazaquin, SUS—sulfosulfuron, TCY—tetracycline, TRI—trimethoprim, Kao—kaolinite, Lap—Laponite, Mt—montmorillonite, Sep—sepiolite, P—pollutant, CA—catalyst amount).

TiO <sub>2</sub> –Clay Mineral Composite	Synthesis	Experimental Conditions	Pollutant	Degradation Efficiency	Ref.
Ti-pillared Mt	Ti(OC <sub>3</sub> H <sub>7</sub> ) <sub>4</sub> precursor + Mt, hydrothermal treatment 200 °C, calcination 500 °C, SSA = 233 m <sup>2</sup> g <sup>−1</sup>	UV irradiation CA: 1 mg mL <sup>−1</sup> P: 17 ppm	DBP	90%—180 min	[152]
Zr–TiO <sub>2</sub> /Mt	Ti(OC <sub>3</sub> H <sub>7</sub> ) <sub>4</sub> + Zr(OC <sub>4</sub> H <sub>9</sub> ) <sub>4</sub> precursor + Cloisite <sup>®</sup> 30B-induced hydrolysis, calcination 500 °C, SSA = 168 m <sup>2</sup> g <sup>−1</sup>	Solar irradiation CA: 0.25 mg mL <sup>−1</sup> P: 0.01 mg mL <sup>−1</sup>	ANT	ca. 90%—360 min	[233]
ZnO–TiO <sub>2</sub> /Mt	Ti(OC <sub>3</sub> H <sub>7</sub> ) <sub>4</sub> precursor + Cloisite <sup>®</sup> 30B + Zn(CH <sub>3</sub> COO) <sub>2</sub> precursor-induced hydrolysis, calcination 500 °C, SSA = 165 m <sup>2</sup> g <sup>−1</sup>	Solar irradiation CA: 0.25 mg mL <sup>−1</sup> P: 0.01 mg mL <sup>−1</sup>	ANT	100%—600 min	[234]
Ag–ZnO–TiO <sub>2</sub> /Mt	Ti(OC <sub>3</sub> H <sub>7</sub> ) <sub>4</sub> precursor + Cloisite <sup>®</sup> 30B, + Zn(CH <sub>3</sub> COO) <sub>2</sub> precursor-induced hydrolysis, calcination 500 °C, + AgNO <sub>3</sub> , photoreduction, 0.91 wt % Ag, SSA = 144 m <sup>2</sup> g <sup>−1</sup>	Solar irradiation CA: 0.25 mg mL <sup>−1</sup> P: 0.005 mg mL <sup>−1</sup>	ANT	95%—360 min	[235]
ZnO–TiO <sub>2</sub> /Mt	Ti(OC <sub>3</sub> H <sub>7</sub> ) <sub>4</sub> precursor + Cloisite <sup>®</sup> 30B, + Zn(CH <sub>3</sub> COO) <sub>2</sub> precursor-induced hydrolysis, calcination 500 °C, SSA = 165 m <sup>2</sup> g <sup>−1</sup>	Solar irradiation CA: 0.25 mg mL <sup>−1</sup> P: 0.01 mg mL <sup>−1</sup>	ACE	100%—600 min	[234]
Ag–ZnO–TiO <sub>2</sub> /Mt	Ti(OC <sub>3</sub> H <sub>7</sub> ) <sub>4</sub> precursor + Cloisite <sup>®</sup> 30B + Zn(CH <sub>3</sub> COO) <sub>2</sub> precursor-induced hydrolysis, calcination 500 °C, + AgNO <sub>3</sub> under UV irradiation, 0.91 wt % Ag, SSA = 144 m <sup>2</sup> g <sup>−1</sup>	Solar irradiation CA: 0.25 mg mL <sup>−1</sup> P: 0.005 mg mL <sup>−1</sup>	ACE	100%—360 min	[235]
g-C <sub>3</sub> N <sub>4</sub> –TiO <sub>2</sub> /Kao	Ti(OC <sub>3</sub> H <sub>7</sub> ) <sub>4</sub> precursor + Kao, calcination 500 °C + H <sub>2</sub> SO <sub>4</sub> + g-C <sub>3</sub> N <sub>4</sub> , SSA = 52 m <sup>2</sup> g <sup>−1</sup>	Solar irradiation 2 mg mL <sup>−1</sup> P: 10 ppm	CIP	92%—240 min	[237]
Cr,Ti-pillared Mt	TiCl <sub>4</sub> precursor + Cr <sup>3+</sup> + Mt, calcination 500 °C, SSA = 272 m <sup>2</sup> g <sup>−1</sup>	UV irradiation CA: 1 mg mL <sup>−1</sup> P: 0.025 mg/mL	TRI	76%—180 min	[56]
BiOCl–TiO <sub>2</sub> /Sep	Sequential precipitation of TiO <sub>2</sub> and BiOCl onto Sep from TiSO <sub>4</sub> and Bi(NO <sub>3</sub> ) <sub>3</sub> precursors, calcination 500 °C, SSA = 97 m <sup>2</sup> g <sup>−1</sup>	Visible light irradiation CA: 0.6 mg mL <sup>−1</sup> P: 0.05 mg mL <sup>−1</sup>	TCY	>90%—180 min	[238]

Table 7. Cont.

TiO <sub>2</sub> -Clay Mineral Composite	Synthesis	Experimental Conditions	Pollutant	Degradation Efficiency	Ref.
Ag-ZnO-TiO <sub>2</sub> /Mt	Ti(OC <sub>3</sub> H <sub>7</sub> ) <sub>4</sub> precursor + Cloisite <sup>®</sup> 30B + Zn(CH <sub>3</sub> COO) <sub>2</sub> precursor-induced hydrolysis, calcination 500 °C + AgNO <sub>3</sub> , photoreduction, 0.91 wt % Ag, SSA = 144 m <sup>2</sup> g <sup>-1</sup>	Solar irradiation CA: 0.25 mg mL <sup>-1</sup> P: 0.005 mg mL <sup>-1</sup>	ATR	96%—360 min	[235]
W,TiO <sub>2</sub> /Mt	Ti(OC <sub>3</sub> H <sub>7</sub> ) <sub>4</sub> precursor + Cloisite <sup>®</sup> 30B + (NH <sub>4</sub> ) <sub>6</sub> H <sub>2</sub> W <sub>12</sub> O <sub>40</sub> · xH <sub>2</sub> O precursor-induced hydrolysis, calcination 500 °C, 5 M% W, SSA = 148 m <sup>2</sup> g <sup>-1</sup>	Solar irradiation CA: 0.25 mg mL <sup>-1</sup> P: 0.0025 mg mL <sup>-1</sup>	ATR	100%—240 min	[241]
W,TiO <sub>2</sub> /Mt	Ti(OC <sub>3</sub> H <sub>7</sub> ) <sub>4</sub> precursor + Cloisite <sup>®</sup> 30B + (NH <sub>4</sub> ) <sub>6</sub> H <sub>2</sub> W <sub>12</sub> O <sub>40</sub> · xH <sub>2</sub> O precursor-induced hydrolysis, calcination 500 °C, 5 M% W, SSA = 148 m <sup>2</sup> g <sup>-1</sup>	Visible light irradiation CA: 0.25 mg mL <sup>-1</sup> P: 0.0025 mg mL <sup>-1</sup>	ATR	100%—240 min	[241]
TiO <sub>2</sub> /Lap	Ti(OC <sub>3</sub> H <sub>7</sub> ) <sub>4</sub> precursor + Lap, hydrothermal treatment at 60 °C, calcination 500 °C, SSA = 320 m <sup>2</sup> g <sup>-1</sup>	UV irradiation CA: 0.2 mg TiO <sub>2</sub> mL <sup>-1</sup> P: 0.002 mg mL <sup>-1</sup>	DIM	90%—180 min	[239]
TiO <sub>2</sub> /Mt	Ti(OC <sub>3</sub> H <sub>7</sub> ) <sub>4</sub> precursor + Mt, hydrothermal treatment at 60 °C, calcination 500 °C, SSA = 183 m <sup>2</sup> g <sup>-1</sup>	UV irradiation CA: 0.2 mg TiO <sub>2</sub> mL <sup>-1</sup> P: 0.002 mg mL <sup>-1</sup>	DIM	86%—180 min	[239]
TiO <sub>2</sub> /Lap	TiOSO <sub>4</sub> precursor + Lap, hydrothermal treatment at 200 °C, calcination 500 °C, SSA = 232 m <sup>2</sup> g <sup>-1</sup>	UV irradiation CA: 1 mg mL <sup>-1</sup> P: 10 ppm	ALA	66%—60 min	[240]
TiO <sub>2</sub> /Lap	TiOSO <sub>4</sub> precursor + Lap, hydrothermal treatment at 200 °C, calcination 500 °C, SSA = 232 m <sup>2</sup> g <sup>-1</sup>	UV irradiation CA: 1 mg mL <sup>-1</sup> P: 10 ppm	BRO	84%—60 min	[240]
TiO <sub>2</sub> /Lap	TiOSO <sub>4</sub> precursor + Lap, hydrothermal treatment at 200 °C, calcination 500 °C, SSA = 232 m <sup>2</sup> g <sup>-1</sup>	UV irradiation CA: 1 mg mL <sup>-1</sup> P: 5 ppm	CHT	77%—60 min	[240]
TiO <sub>2</sub> /Lap	TiOSO <sub>4</sub> precursor + Lap, hydrothermal treatment at 200 °C, calcination 500 °C, SSA = 232 m <sup>2</sup> g <sup>-1</sup>	UV irradiation CA: 1 mg mL <sup>-1</sup> P: 5 ppm	IMA	100%—45 min	[240]
TiO <sub>2</sub> /Lap	TiOSO <sub>4</sub> precursor + Lap, hydrothermal treatment at 200 °C, calcination 500 °C, SSA = 232 m <sup>2</sup> g <sup>-1</sup>	UV irradiation CA: 1 mg mL <sup>-1</sup> P: 5 ppm	SUS	80%—60 min	[240]

## 6.2. Photodegradation of Air Pollutants

Air purification by means of photocatalytic processes has been widely studied since the 1970s. Volatile organic compounds and nitrogen oxides represent air pollutants of main

environmental concern, and considerable research has been devoted to their removal by means of photocatalytic processes [242].

#### 6.2.1. Photodegradation of Volatile Organic Compounds

One of the most important aspects of TiO<sub>2</sub> photocatalysis is its potential for the removal of air pollutants under indoor conditions [13]. The main concern of indoor air pollution relates to volatile organic compounds, which are mostly released from the products and materials containing trapped VOCs [16]. The benign nature of titania–clay mineral composites, combined with a well-developed porous structure and high adsorption capacity, render the materials particularly suitable as photocatalysts for indoor air purification. The report by Ooka [243] on the adsorption–photocatalytic degradation of gaseous toluene, trichloroethylene, ethylene, and ethanol over Ti-PILC catalysts was among the first works addressing this issue. Saponite, montmorillonite, and fluorine mica were used for Ti-PILC synthesis with Ti tetraisopropoxide precursor, yielding materials of increasing hydrophobicity. In the case of highly hydrophobic reactants, such as toluene and trichloroethylene, the rate constants of adsorption and photocatalytic degradation increased with the increase in the photocatalyst hydrophobicity, showing that this property was an important factor to be considered in the design of a photocatalyst for the degradation of hydrophobic pollutants. For instance, the toluene degradation rate constant over TiO<sub>2</sub>/mica was 7.5 times higher than that over TiO<sub>2</sub>/saponite. No significant difference was observed in the case of less hydrophobic substances such as ethylene and ethanol. Ti-PILC prepared in a similar manner was used by Pichat et al. [219] in the photodegradation of methanol vapor, and it proved more active than the P25 reference. In the already discussed work, Ménesi et al. [222], who prepared the TiO<sub>2</sub>–montmorillonite composites by grinding the clay mineral with P25 in a ball mill, found that upon UV–VIS irradiation, the titania–clay photocatalysts containing up to 50% TiO<sub>2</sub> degraded ethanol at a rate 1.3–1.4 times higher than P25, when calculated per unit mass of titania. The rate of toluene degradation surpassed 1.5–2.4 times that on P25 on all tested composites. The result pointed to the existence of a synergistic effect associated with composite formation. A slowdown of the photocatalytic reaction was observed upon the accumulation of water vapor in the reaction mixture.

A series of works on the photocatalytic destruction of VOCs was published by Kibanova et al. [244–246]. The authors studied the photodegradation of toluene over kaolinite and hectorite-based composites with TiO<sub>2</sub>, which were prepared by the sol–gel method from acid-hydrolyzed Ti isopropoxide followed by hydrothermal treatment [244,245]. The toluene removal efficiency calculated on the TiO<sub>2</sub> mass basis was either comparable to that of P25 (TiO<sub>2</sub>–hectorite) or better (TiO<sub>2</sub>–kaolinite). Under UVA irradiation, the maximum toluene removal of 26% was reported for the TiO<sub>2</sub>–hectorite sample. The value increased upon UVC illumination to 58%. The photocatalytic performance was strongly dependent on the presence of water vapor. A net inhibition was observed for higher relative humidity values, indicating that water molecules competed effectively with toluene for reactive surface sites and limited the overall photocatalytic conversion. In another work by this group [246], the TiO<sub>2</sub>–hectorite catalyst was used for the photodegradation of formaldehyde. The removal efficiency of the pollutant was ca. 55% for UVA and 62% for UVC irradiation. Overall, when normalized by the mass content of TiO<sub>2</sub>, the composite showed efficiency comparable to that of P25.

The photodegradation of another widely encountered aromatic pollutant, styrene, was tested over highly thermostable titania-pillared clay photocatalysts prepared by Lim et al. [247]. The materials were synthesized by mixing Laponite dispersion containing PEO surfactant with pillaring solution prepared from Ti tetraisopropoxide, which was followed by hydrothermal treatment, i.e., similarly to previously reported procedures known to enhance the textural parameters of the composite [159,184]. Under UV irradiation and dry conditions, the catalysts proved very efficient in destroying gaseous styrene, the most active sample showing 87% efficiency, but at 20% relative humidity, the catalyst's activity fell to 5%.

Papoulis et al. [248–250] used clay minerals of tubular and fibrous morphologies, i.e., halloysite, palygorskite, and a mixture of both clays, to prepare composites loaded with anatase, aiming at the photodegradation of toluene vapor. Ti isopropoxide precursor and the sol–gel method combined with hydrothermal treatment were employed in the synthesis. Both TiO<sub>2</sub>–halloysite and TiO<sub>2</sub>–palygorskite showed higher catalytic activity, per mass of the catalyst, in decomposing toluene under sunlight and UV irradiation than the P25 standard. For instance, under UV illumination, the reaction rate constant over the TiO<sub>2</sub>–halloysite composite was 1.8 times higher than that over P25, and in the case of TiO<sub>2</sub>–palygorskite with a similar TiO<sub>2</sub> loading, the enhancement factor was 1.6. The authors attributed the increase in photocatalytic activity to the good dispersion of TiO<sub>2</sub> nanocrystals on the surface of clay minerals. Moreover, the three-phase TiO<sub>2</sub>–halloysite–palygorskite nanocomposites showed significantly higher photocatalytic activity in decomposing toluene than single-clay-based materials, the reaction rate under UV irradiation being two times higher than over the P25 reference. It was proposed that the use of two clays with different grain morphologies led to the disaggregation of the clay support particles, thus exposing more surface for the anatase deposition than was available in single-clay-based nanocomposites (Figure 15).

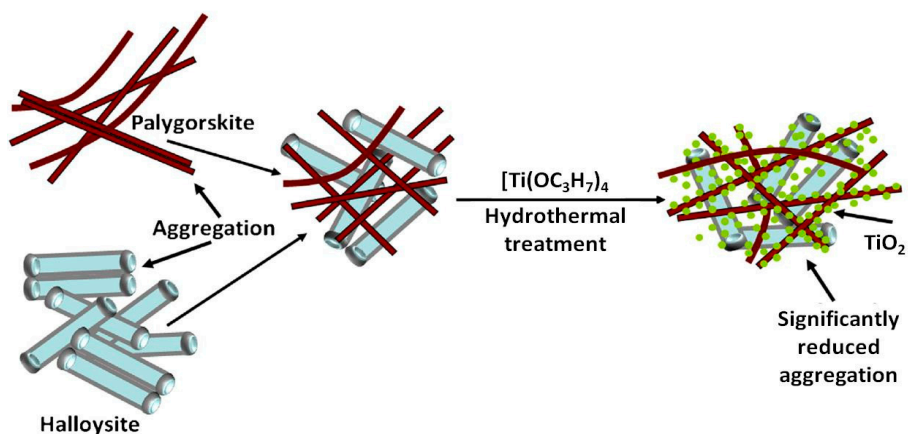


**Figure 15.** Schematic representation of the hydrothermal synthesis of three-phase nanocomposites with two nanoclays, showing the reduced aggregation of clay mineral particles in the three-phase system. Adapted with permission from ref. [250]. Copyright 2014 Elsevier.

Another fibrous clay, sepiolite, was used by Liu et al. [251] in the design of efficient photocatalysts for formaldehyde removal. The materials were prepared by a hydrolysis–precipitation method using the TiCl<sub>4</sub>/(NH<sub>4</sub>)<sub>2</sub>SO<sub>4</sub> system as titania precursor and acid-activated sepiolite pretreated with sodium hexametaphosphate dispersant. The composite catalysts showed high efficiency in the removal of formaldehyde. Upon UV illumination, the best catalyst degraded 88% of HCHO, i.e., twice as much as unsupported titania, which was assigned to the synergistic effect between the catalytic ability of highly dispersed TiO<sub>2</sub> nanoparticles and the adsorption capacity of sepiolite. The degradation of formaldehyde was also studied by Portela et al. [252], who aimed at developing a simple, low-cost method of photocatalyst synthesis with potential for industrial application. The investigated materials were prepared as extrudates of 1:1 mechanical mixture of commercial nananatase powder with four natural silicates, of which three were clay minerals: bentonite, kaolinite, and sepiolite. Calcination at 500 °C ensured an optimum combination of mechanical, textural, and HCHO adsorption properties. The degradation rate of formaldehyde, normalized per gram of TiO<sub>2</sub>, decreased in the order TiO<sub>2</sub>–kaolinite > TiO<sub>2</sub>–sepiolite > TiO<sub>2</sub>–bentonite > TiO<sub>2</sub>. The authors found that the exposed fraction of titania particles and the size of the TiO<sub>2</sub> anatase crystalline domains were the dominant factors determining the photocatalytic efficiency.

Composites of titania with fibrous clays were also used as photocatalysts for the removal of acetone and trichloroethylene [253,254]. Zhang et al. [253] prepared a series of Cu-TiO<sub>2</sub>-organoattapulgitic nanocomposites by the sol-gel method using a Cu-containing Ti sol obtained from titania TiCl<sub>4</sub> precursor. Synthesis variables included the Cu content and the temperature of calcination. The materials tested in the photocatalytic degradation of acetone in air under UV light irradiation showed very good activity, higher than the reference TiO<sub>2</sub>-attapulgitic sample and the pure TiO<sub>2</sub> component. The best catalyst prepared at the Cu/TiO<sub>2</sub> molar ratio of 0.003, calcined at 400 °C, removed 90% of acetone in 6 h. The good performance of composites was attributed to the synergy between the hydrophobicity of organoclay, its micro-mesopore structure, and the presence of Cu-TiO<sub>2</sub> heterojunctions, which slowed down the electron-hole recombination.

The ability of TiO<sub>2</sub>-sepiolite composites to degrade chlorinated volatile organics was investigated in a series of papers by Suárez et al. [254–256]. The photocatalysts were prepared as extruded plates, and commercial TiO<sub>2</sub> nanopowder was used as the photoactive component. The authors compared materials obtained by the addition of TiO<sub>2</sub> at the stage of the ceramic dough preparation with those prepared by post-synthesis coating of clay extrudates with titania. Tests of trichloroethylene degradation revealed that the former approach ensured a better performance. The authors argued that an intimate contact between sepiolite and TiO<sub>2</sub> was essential for the migration of the undesired intermediate species (e.g., highly toxic COCl<sub>2</sub>) to the clay adsorbent. There, the reaction with the surface OH groups could take place and enhance the trichloroethylene mineralization. Combination of the adsorptive and the photocatalytic functions in the composite widened the operating conditions window of the system, with the former function dominating under low solar irradiation and the latter dominating under high irradiation conditions. Under optimized conditions, the hybrid catalyst containing TiO<sub>2</sub> and sepiolite in a 1:1 ratio, calcined at 500 °C, converted nearly 100% TCE, although COCl<sub>2</sub> emission remained an issue [256].

In the works reviewed above, the studies of TiO<sub>2</sub>-clay minerals' ability to photodegrade VOCs concentrated on single pollutants, while realistic indoor conditions usually involve the presence of several different organic contaminants. This aspect has been addressed by Chen et al. [257], who chose toluene, ethyl acetate, and ethanethiol as model pollutants and tested their photocatalytic degradation both as single pollutants and as a mixture, using titania-montmorillonite-silica composites as catalysts. The materials were prepared by mixing Ti-pillared montmorillonite, obtained via the sol-gel method from Ti(OC<sub>4</sub>H<sub>9</sub>)<sub>4</sub> precursor, with the silica gel, which was followed by drying and calcination. The composites exhibited excellent photocatalytic activity, degrading almost 100% of each pollutant within 120 min of UV irradiation, with the degradation rate constants following the order toluene < ethyl acetate < ethanethiol, which paralleled the adsorption capacities of the catalysts versus particular pollutants. In the case of binary and ternary VOCs mixtures, the degradation rate constants were lower than those for single systems due to the competitive adsorption of reagents and related decrease in the adsorption capacities. Ma et al. [258], who employed the heterojunction system composed of palygorskite, titania, and goethite with a mass ratio of 10:5:5 as a photocatalyst for the removal of benzene vapors, studied the effect of the ethanol addition to the reaction mixture. The composites, prepared by the sol-gel method in which palygorskite and goethite were added to the solution of Ti(OC<sub>4</sub>H<sub>9</sub>)<sub>4</sub> precursor, showed a strong red shift of the absorption edge with respect to the pure titania. The good catalytic performance of the materials in benzene degradation (70% efficiency) was assigned to the presence of the heterojunction lowering the electron-hole recombination rate. In mixture with ethanol, the efficiency of benzene degradation decreased to 60%. In view of the known OH radical quenching properties of ethanol, the result suggested that the scavenging of hydroxyl radicals might be responsible, at least in part, for the observed poorer activity.

### 6.2.2. Photodegradation of Nitrogen Oxides

Apart from the abatement of VOCs, photocatalysis has gained growing importance in the purification of outdoor air from nitrogen oxides [242,259], and several studies appeared on the NO<sub>x</sub> photooxidation over titania–clay mineral composites [248–250,260–263]. Basically, the aim of NO photo-oxidation at the surface of a TiO<sub>2</sub> photocatalyst is its transformation to nitric acid, which involves three steps: NO → HNO<sub>2</sub> → NO<sub>2</sub> → HNO<sub>3</sub>. Water treatment of the photocatalyst surface enables removal of the accumulated HNO<sub>3</sub>. Each step may occur by the direct reaction with valence band holes or indirectly via reaction with a photogenerated surface superoxide anion, H<sub>2</sub>O<sub>2</sub>, or hydroxyl radical. In many works, the efficiency of the process is evaluated only by the disappearance of NO without considering the whole spectrum of products. However, it may happen that the NO<sub>2</sub> intermediate, which is more toxic than the primary NO reactant, escapes to the atmosphere before it is converted to HNO<sub>3</sub>; hence, it is desirable to assess the NO photooxidation not only on the basis of NO removal but also NO<sub>2</sub> or total NO<sub>x</sub> removal [264].

The major input into the assessment of TiO<sub>2</sub>–clay mineral composites as photocatalysts for NO<sub>x</sub> abatement stems from the works of Papoulis et al. [248–250,260–262]. Clay components used for the composite synthesis encompassed saponite [260], halloysite [248,250,261], palygorskite [249,250,261], and sepiolite [262]. The TiO<sub>2</sub>–saponite composites [260] were prepared according to the procedure developed by Liu et al. [166]. Samples with 9.2 and 17 wt % TiO<sub>2</sub> were obtained. Other composites were synthesized using Ti isopropoxide precursor and the sol–gel method combined with hydrothermal treatment. In [248,250,261,262], the loading of titania corresponded to 70 wt %; in [249], it varied from 50 to 90 wt %. The TiO<sub>2</sub>–saponite nanocomposites performed poorer in NO removal than the P25 reference. Under UV irradiation, the NO decomposition rate constant was ca. 20% lower than that observed for P25. However, comparison on a TiO<sub>2</sub> content basis showed the superiority of the photocatalytically active phase supported on clay mineral, in which the effect was attributed to the better dispersion of titania on saponite surfaces [260]. In the photooxidation of NO, the TiO<sub>2</sub>–halloysite [248,261] and TiO<sub>2</sub>–palygorskite [249,261] samples showed significantly higher activity per mass of the catalyst than the commercial P25 titania, under both the visible and the UV light irradiation. For instance, under UV illumination, NO removal was 66% over TiO<sub>2</sub>–halloysite, 60% over TiO<sub>2</sub>–palygorskite, and 40% over P25. Again, the better dispersion of anatase was considered the main factor behind the improved performance. The photocatalytic activity could be further enhanced by the use of three-phase TiO<sub>2</sub>–halloysite–palygorskite nanocomposites, which with 69% deNO<sub>x</sub> ability performed better than single-clay-based materials. The effect was attributed to the deaggregation of support particles into smaller grains, facilitating the dispersion of titania nanocrystals [250]. It should be noted that in works [248–250,260,261], the effectiveness of the photocatalytic process was evaluated only by monitoring the NO conversion. Todorova et al. [263] were the first who assessed the efficiency of the photocatalytic deNO<sub>x</sub> over titania–clay composites by measuring the concentration of NO, NO<sub>2</sub>, and total NO<sub>x</sub>. The authors prepared composites using montmorillonite (parent Na form, as well as Al- and Ca-exchanged forms) or talc, mixed in a 1:1 weight ratio with P25 TiO<sub>2</sub> or urea-modified P25. The mixing of composite ingredients was carried out in sonicated aqueous suspensions, and the resulting slurries were dried at 70 °C. The photocatalytic behavior of the materials in NO<sub>x</sub> removal was investigated under UV and visible light irradiation. Importantly, the concentration of NO, NO<sub>2</sub>, and total NO<sub>x</sub> was assessed. The composite materials, except for the one based on parent Na–montmorillonite, exhibited appreciable photocatalytic activity under both types of irradiation. Both under UV and under visible illumination, the composite with talc was the most active one, showing 35 and 23% deNO<sub>x</sub> ability, respectively. The corresponding figures for the P25 reference were 31% and 14%. The result was related to the improved dispersion of TiO<sub>2</sub> and the NO<sub>x</sub> adsorption ability by the clay component. In the recent paper, Papoulis et al. [262] studied NO<sub>x</sub> abatement over sepiolite-based composites and also monitored the variation of NO, NO<sub>2</sub>, and total NO<sub>x</sub> content. The clay component was used as received and in the Cu- or Zn-exchanged forms.

The TiO<sub>2</sub>–Cu–sepiolite sample showed extremely low activity, which was possibly due to the enhanced recombination of the photogenerated charge carriers, but the photocatalytic activities in NO<sub>x</sub> removal of TiO<sub>2</sub>–sepiolite, and especially TiO<sub>2</sub>–Zn–sepiolite, under UV light irradiation were much higher compared to that of the P25 reference. The result was related to the synergetic effect of the porous sepiolite structure and the formation of a ZnO–TiO<sub>2</sub> heterojunction that enhanced the photoactivity of titania.

The most relevant information on the synthesis of selected examples of TiO<sub>2</sub>–clay mineral composites and their photocatalytic performance in the degradation of gaseous pollutants is summarized in Table 8.

**Table 8.** Main synthesis and photocatalysis data for selected examples of TiO<sub>2</sub> composites with clay minerals used for the degradation of gaseous pollutants in air (Hal—halloysite, Hec—hectorite, Kao—kaolinite, Lap—Laponite, Mt—montmorillonite, Pal—palygorskite, Sep—sepiolite, CTA—cetyltrimethylammonium cation, P—pollutant, CA—catalyst amount, R—reaction rate).

TiO <sub>2</sub> –Clay Mineral Composite	Synthesis	Experimental Conditions	Pollutant	Degradation Efficiency	Ref.
TiO <sub>2</sub> /Hec	Ti(OC <sub>3</sub> H <sub>7</sub> ) <sub>4</sub> precursor + Hec, hydrothermal treatment at 180 °C, SSA = 140 m <sup>2</sup> g <sup>−1</sup>	UVA irradiation P: 185 ppbv RH = 10% Circulating flow reactor	Toluene	26% removal	[244]
TiO <sub>2</sub> /Hec	Ti(OC <sub>3</sub> H <sub>7</sub> ) <sub>4</sub> precursor + Hec, hydrothermal treatment at 180 °C, SSA = 140 m <sup>2</sup> g <sup>−1</sup>	UVC irradiation P: 165 ppbv RH = 10% Circulating flow reactor	Toluene	58% removal	[244]
TiO <sub>2</sub> /Kao	Ti(OC <sub>3</sub> H <sub>7</sub> ) <sub>4</sub> precursor + Hec, hydrothermal treatment at 180 °C, SSA = 16 m <sup>2</sup> g <sup>−1</sup>	UVA irradiation P: 170 ppbv RH = 10% Circulating flow reactor	Toluene	4% removal	[244]
TiO <sub>2</sub> /Kao	Ti(OC <sub>3</sub> H <sub>7</sub> ) <sub>4</sub> precursor + Hec, hydrothermal treatment at 180 °C, SSA = 16 m <sup>2</sup> g <sup>−1</sup>	UVC irradiation P: 162 ppbv RH = 10% Circulating flow reactor	Toluene	50% removal	[244]
Ti-pillared Mt/SiO <sub>2</sub>	Ti(OC <sub>4</sub> H <sub>9</sub> ) <sub>4</sub> precursor + Mt, + acid-treated silica gel, calcination 450 °C, SSA = 306 m <sup>2</sup> g <sup>−1</sup>	UV irradiation CA: 5 g P: 500 ppb Fluidized bed reactor	Toluene	100%—120 min	[257]
TiO <sub>2</sub> /Hal	Ti(OC <sub>3</sub> H <sub>7</sub> ) <sub>4</sub> precursor + Hal, hydrothermal treatment 180 °C, SSA = 183 m <sup>2</sup> g <sup>−1</sup>	UV irradiation CA: 0.04 g P: 800 ppmv RH = 75% Flow reactor	Toluene	$R = 4.2 \times 10^{-8}$ mol s <sup>−1</sup> g <sup>−1</sup>	[248]
TiO <sub>2</sub> /Hal	Ti(OC <sub>3</sub> H <sub>7</sub> ) <sub>4</sub> precursor + Hal, hydrothermal treatment 180 °C, SSA = 183 m <sup>2</sup> g <sup>−1</sup>	Solar irradiation CA: 0.04 g P: 800 ppmv RH = 75% Flow reactor	Toluene	$R = 2.6 \times 10^{-8}$ mol s <sup>−1</sup> g <sup>−1</sup>	[248]

Table 8. Cont.

TiO <sub>2</sub> -Clay Mineral Composite	Synthesis	Experimental Conditions	Pollutant	Degradation Efficiency	Ref.
TiO <sub>2</sub> /Pal	Ti(OC <sub>3</sub> H <sub>7</sub> ) <sub>4</sub> precursor + Pal, hydrothermal treatment 180 °C, SSA = 240 m <sup>2</sup> g <sup>-1</sup>	UV irradiation CA: 0.04 g P: 800 ppmv RH = 75% Flow reactor	Toluene	R = 3.6 × 10 <sup>-8</sup> mol s <sup>-1</sup> g <sup>-1</sup>	[249]
TiO <sub>2</sub> /Pal	Ti(OC <sub>3</sub> H <sub>7</sub> ) <sub>4</sub> precursor + Pal, hydrothermal treatment 180 °C, SSA = 240 m <sup>2</sup> g <sup>-1</sup>	Solar irradiation CA: 0.04 g P: 800 ppmv RH = 75% Flow reactor	Toluene	R = 2.4 × 10 <sup>-8</sup> mol s <sup>-1</sup> g <sup>-1</sup>	[249]
TiO <sub>2</sub> /Hal/Pal	Ti(OC <sub>3</sub> H <sub>7</sub> ) <sub>4</sub> precursor + Hal + Pal, hydrothermal treatment 180 °C, SSA = 207 m <sup>2</sup> g <sup>-1</sup>	UV irradiation CA: 0.04 g P: 800 ppmv RH = 75% Flow reactor	Toluene	R = 4.5 × 10 <sup>-8</sup> mol s <sup>-1</sup> g <sup>-1</sup>	[250]
TiO <sub>2</sub> /Hal/Pal	Ti(OC <sub>3</sub> H <sub>7</sub> ) <sub>4</sub> precursor + Hal + Pal, hydrothermal treatment 180 °C, SSA = 207 m <sup>2</sup> g <sup>-1</sup>	Solar irradiation CA: 0.04 g P: 800 ppmv RH = 75% Continuous flow reactor	Toluene	R = 3.9 × 10 <sup>-8</sup> mol s <sup>-1</sup> g <sup>-1</sup>	[250]
TiO <sub>2</sub> /Lap	Ti(OC <sub>3</sub> H <sub>7</sub> ) <sub>4</sub> precursor + Lap + PEO, hydrothermal treatment 100 °C, calcination 1000 °C, SSA = 1040 m <sup>2</sup> g <sup>-1</sup>	UVC irradiation CA: 4 g P: 300 ppmv RH = 0% Fluidized bed reactor	Styrene	87%	[247]
TiO <sub>2</sub> /Lap	Ti(OC <sub>3</sub> H <sub>7</sub> ) <sub>4</sub> precursor + Lap + PEO, hydrothermal treatment 100 °C, calcination 1000 °C, SSA = 1040 m <sup>2</sup> g <sup>-1</sup>	UVC irradiation CA: 4 g P: 300 ppmv RH = 20% Fluidized bed reactor	Styrene	5%	[247]
TiO <sub>2</sub> /Fe <sub>2</sub> O <sub>3</sub> /Pal	Pal + goethite + Ti(OC <sub>4</sub> H <sub>9</sub> ) <sub>4</sub> precursor, calcination 350 °C, SSA = 97 m <sup>2</sup> g <sup>-1</sup>	UV irradiation P: 30 mg/m <sup>3</sup>	Benzene	70%—180 min	[258]
TiO <sub>2</sub> /Hec	Ti(OC <sub>3</sub> H <sub>7</sub> ) <sub>4</sub> precursor + Hec, hydrothermal treatment at 180 °C, SSA = 140 m <sup>2</sup> g <sup>-1</sup>	UVA irradiation P: 110–130 ppbv RH = 10% Circulating flow reactor	Formaldehyde	55% removal	[246]
TiO <sub>2</sub> /Hec	Ti(OC <sub>3</sub> H <sub>7</sub> ) <sub>4</sub> precursor + Hec, hydrothermal treatment at 180 °C, SSA = 140 m <sup>2</sup> g <sup>-1</sup>	UVC irradiation P: 110–130 ppbv RH = 10% Circulating flow reactor	Formaldehyde	62% removal	[246]
TiO <sub>2</sub> /Sep	Acid treated Sep + (NaPO <sub>3</sub> ) <sub>6</sub> dispersant, + TiCl <sub>4</sub> precursor + (NH <sub>4</sub> ) <sub>2</sub> SO <sub>4</sub> , + NH <sub>3</sub> (aq), hydrolysis/precipitation, calcination 550 °C, SSA = 135 m <sup>2</sup> g <sup>-1</sup>	UV irradiation CA: 10 g P: 6.56 mg (m <sup>3</sup> ) <sup>-1</sup> Batch reactor	Formaldehyde	90%—12 h	[251]

Table 8. Cont.

TiO <sub>2</sub> -Clay Mineral Composite	Synthesis	Experimental Conditions	Pollutant	Degradation Efficiency	Ref.
Ti-pillared Mt	Ti(OC <sub>3</sub> H <sub>7</sub> ) <sub>4</sub> precursor + Mt, Microwave calcination, 500 °C, SSA = 165 m <sup>2</sup> g <sup>-1</sup>	UV irradiation CA: 50 mg P: 1.34 × 10 <sup>-5</sup> mmol mL <sup>-1</sup> Continuous flow reactor	Methanol	ca. 50% removal	[219]
Ti-pillared Mt/SiO <sub>2</sub>	Ti(OC <sub>4</sub> H <sub>9</sub> ) <sub>4</sub> precursor + Mt, + acid-treated silica gel, calcination 450 °C, SSA = 306 m <sup>2</sup> g <sup>-1</sup>	UV irradiation CA: 5 g P: 500 ppb Fluidized bed reactor	Ethyl acetate	100%—120 min	[257]
Ti-pillared Mt/SiO <sub>2</sub>	Ti(OC <sub>4</sub> H <sub>9</sub> ) <sub>4</sub> precursor + Mt, + acid treated silica gel, calcination 450 °C, SSA = 306 m <sup>2</sup> g <sup>-1</sup>	UV irradiation CA: 5 g P: 500 ppb Fluidized bed reactor	Ethanthiol	100%—120 min	[257]
TiO <sub>2</sub> /Sep	Ceramic dough made of Sep + commercial TiO <sub>2</sub> + H <sub>2</sub> O, formation of extrudates, calcination 500 °C, SSA = 153 m <sup>2</sup> g <sup>-1</sup>	Solar irradiation CA: 35 mL P: 150 ppm Flow reactor	Trichloroethylene	100% removal	[256]
TiO <sub>2</sub> /Hal	Ti(OC <sub>3</sub> H <sub>7</sub> ) <sub>4</sub> precursor + Hal, hydrothermal treatment 180 °C, SSA = 167 m <sup>2</sup> g <sup>-1</sup>	UV irradiation CA: 0.04 g P: 1 ppm Flow reactor	NO	66% removal	[250]
TiO <sub>2</sub> /Pal	Ti(OC <sub>3</sub> H <sub>7</sub> ) <sub>4</sub> precursor + Pal, hydrothermal treatment 180 °C, SSA = 242 m <sup>2</sup> g <sup>-1</sup>	UV irradiation CA: 0.04 g P: 1 ppm Flow reactor	NO	60% removal	[250]
TiO <sub>2</sub> /Hal/Pal	Ti(OC <sub>3</sub> H <sub>7</sub> ) <sub>4</sub> precursor + Hal + Pal, hydrothermal treatment 180 °C, SSA = 206 m <sup>2</sup> g <sup>-1</sup>	UV irradiation CA: 0.04 g P: 1 ppm Flow reactor	NO	69% removal	[250]
TiO <sub>2</sub> /Hal	Ti(OC <sub>3</sub> H <sub>7</sub> ) <sub>4</sub> precursor + Hal, hydrothermal treatment 180 °C, SSA = 167 m <sup>2</sup> g <sup>-1</sup>	Visible light irradiation CA: 0.04 g P: 1 ppm Flow reactor	NO	21% removal	[250]
TiO <sub>2</sub> /Pal	Ti(OC <sub>3</sub> H <sub>7</sub> ) <sub>4</sub> precursor + Pal, hydrothermal treatment 180 °C, SSA = 242 m <sup>2</sup> g <sup>-1</sup>	Visible light irradiation CA: 0.04 g P: 1 ppm flow reactor	NO	20% removal	[250]
TiO <sub>2</sub> /Hal/Pal	Ti(OC <sub>3</sub> H <sub>7</sub> ) <sub>4</sub> precursor + Hal + Pal, hydrothermal treatment 180 °C, SSA = 228 m <sup>2</sup> g <sup>-1</sup>	Visible light irradiation CA: 0.04 g P: 1 ppm Flow reactor	NO	26% removal	[250]
TiO <sub>2</sub> /Talc	Sonicated Talc suspension + P25	UV irradiation P: 1 ppm RH = 50% Flow reactor	NO	35% removal	[263]

Table 8. Cont.

TiO <sub>2</sub> -Clay Mineral Composite	Synthesis	Experimental Conditions	Pollutant	Degradation Efficiency	Ref.
TiO <sub>2</sub> /Talc	Sonicated Talc suspension + P25	Visible light irradiation P: 1 ppm RH = 50% Flow reactor	NO	23% removal	[263]
TiO <sub>2</sub> /Sep	Ti(OC <sub>3</sub> H <sub>7</sub> ) <sub>4</sub> precursor + Sep, hydrothermal treatment 180 °C, SSA = 189 m <sup>2</sup> g <sup>-1</sup>	UV irradiation CA: 1 g P: 1 ppm RH = 50% Flow reactor	NO	35% removal	[262]
TiO <sub>2</sub> /Zn-Sep	Zn-exchanged Sep + Ti(OC <sub>3</sub> H <sub>7</sub> ) <sub>4</sub> precursor, hydrothermal treatment 180 °C, SSA = 179 m <sup>2</sup> g <sup>-1</sup>	UV irradiation CA: 1 g P: 1 ppm RH = 50% Flow reactor	NO	38% removal	[262]

## 7. Concluding Remarks

Protecting the environment while simultaneously ensuring economic growth and profit remains the fundamental scientific challenge of today. Maintaining the balance between these apparently competing issues depends greatly on our ability to neutralize the unwanted by-products of the economic activity, such as pollution and waste. Catalytic and photocatalytic processes aiming at the abatement of major pollutants in air and water have a leading role in the realization of this goal, and research into the design of novel catalytic materials represents a particularly important avenue. The advantage of using clay minerals in the engineering of catalytic materials is, on one hand, related to their abundance, low cost, and benign character, and, on the other, to their unique structural features and physicochemical properties enabling the development of functional nanoarchitectures with textural, acido-basic, redox, and hydrophilic–hydrophobic characteristics tuned to the requirement of a particular reaction. All these aspects are illustrated in the present review, which shows the potential of titania–clay mineral composites for environmental catalysis and photocatalysis. Despite the reported achievements, there are still issues to be addressed. Thus, in the fundamental research, it is essential to maximize the efforts directed at understanding the structure–property relationship. To this end, the use of a possibly wide range of characterization techniques is required in addition to the standard chemical analysis, X-ray diffraction, textural analysis, or mid-infrared spectroscopy, as it may reveal the yet-unknown characteristics of the catalysts/photocatalysts, and pave the way for an intelligent materials design. As to the methodology of the catalytic and photocatalytic studies, apart from monitoring the conversion of primary contaminants, the full control of the reaction selectivity should be standard in order to trace the possible toxic intermediates. This requirement is essential for the development of practical applications, and the improvement is particularly needed in the area of photocatalytic purification of water. Prospects of commercial use of titania–clay composites are also hampered by the sometimes laborious and costly synthetic procedures. Therefore, possible simplification of the composite preparation, favoring methods based on the simple mixing of components, for instance by mechanochemical treatment, and using cheap modifiers, such as, e.g., common biopolymers, is likely to increase the potential for large-scale applications.

This review focused on the application of titania–clay mineral composites in environmental catalysis related to the purification of water and air, because this is currently the most intensely explored research area, likely to attract the worldwide interest for many decades to come. However, the growing appreciation and acceptance of Green Chemistry concepts broadens opportunities and challenges regarding the use of clay-based catalysts

and photocatalysts. The development of environmentally-friendly heterogeneous catalysts based on TiO<sub>2</sub>-clay mineral systems for the manufacturing of fine chemicals, be it by the catalytic or the photoassisted route, represents an attractive possibility. Another field of great potential is the research on biocatalytic and biosensing applications, where the performance of a biological material is shaped by the nature, surface architecture, and surface chemistry of the support, and by the immobilization strategy. These aspects render the clay-based composite systems, providing a variety of parent structures and enabling diverse preparative approaches, ideally suited for biocatalyst or biosensor design. However, it should be remembered that rational engineering of clay-based composites for the above applications requires a profound interdisciplinary knowledge spanning mineralogy, materials engineering, colloid and interface chemistry, catalysis, electrochemistry, etc. Assembling a team fulfilling this condition is obviously a difficult task, and analysis of the literature reports shows that in some cases, research has been based on the less effective trial and error tactic. Thus, perfecting the interdisciplinary approach, enabling the exchange of ideas between specialists in different disciplines, represents the main challenge in achieving meaningful discoveries in the engineering of advanced clay-based materials.

**Funding:** This research was funded by the Polish National Science Center (NCN), grant OPUS, UMO-2018/31/B/ST5/03292.

**Conflicts of Interest:** The author declares no conflict of interest. The funders had no role in the design of the study; in the collection, analyses, or interpretation of data; in the writing of the manuscript, or in the decision to publish the results.

## References

1. Friedrichsen, W.; Goehre, O. Oxidation Catalyst Containing Vanadium and Titanium. GB Patent 1140264, 2 September 1969.
2. Grzybowska-Swierkosz, B. Vanadia-titania catalysts for oxidation of o-xylene and other hydrocarbons. *Appl. Catal. A Gen.* **1997**, *157*, 263–310. [[CrossRef](#)]
3. Matsuda, S.; Takeuchi, M.; Hishinuma, T.; Nakajima, F.; Narita, T.; Watanabe, Y.; Imanari, M. Selective reduction of nitrogen oxides in combustion flue gases. *J. Air Pollut. Control Assoc.* **1978**, *28*, 350–353. [[CrossRef](#)]
4. Nakajima, F.; Takeuchi, M.; Matsuda, S.; Uno, S.; Mori, T.; Watanabe, Y.; Imanari, M. Catalytic Process for Reducing Nitrogen oxides to Nitrogen. U.S. Patent 4085193, 18 April 1978.
5. Matsuda, S.; Kato, A. Titanium oxide based catalysts—A review. *Appl. Catal.* **1983**, *8*, 149–165. [[CrossRef](#)]
6. Coudurier, G.; Vedrine, J.C. EUROCAT oxide: An European V<sub>2</sub>O<sub>5</sub>–WO<sub>3</sub>/TiO<sub>2</sub> SCR standard catalyst study. Characterisation by electron microscopies (SEM, HRTEM, EDX) and by atomic force microscopy. *Catal. Today* **2000**, *56*, 415–430. [[CrossRef](#)]
7. Jung, H.; Park, E.; Kim, M.; Jurng, J. Pilot-scale evaluation of a novel TiO<sub>2</sub>-supported V<sub>2</sub>O<sub>5</sub> catalyst for DeNO<sub>x</sub> at low temperatures at a waste incinerator. *Waste Manag.* **2017**, *61*, 283–287. [[CrossRef](#)] [[PubMed](#)]
8. Damma, D.; Ettireddy, P.R.; Reddy, B.M.; Smirniotis, P.G. A Review of low temperature NH<sub>3</sub>-SCR for removal of NO<sub>x</sub>. *Catalysts* **2019**, *9*, 349. [[CrossRef](#)]
9. Haruta, M.; Tsubota, S.; Kobayashi, T.; Kageyama, H.; Genet, M.J.; Delmon, B. Low-temperature oxidation of CO over gold supported on TiO<sub>2</sub>, α-Fe<sub>2</sub>O<sub>3</sub>, and Co<sub>3</sub>O<sub>4</sub>. *J. Catal.* **1993**, *144*, 175–192. [[CrossRef](#)]
10. Haruta, M. Size- and support-dependency in the catalysis of gold. *Catal. Today* **1997**, *36*, 153–166. [[CrossRef](#)]
11. Chen, S.; Zhang, B.; Su, D.; Huang, W. Titania Morphology-Dependent Gold-Titania Interaction, Structure, and Catalytic Performance of Gold/Titania Catalysts. *ChemCatChem* **2015**, *7*, 3290–3298. [[CrossRef](#)]
12. Fujishima, A.; Honda, K. Electrochemical photolysis of water at a semiconductor electrode. *Nature* **1972**, *238*, 37–38. [[CrossRef](#)]
13. Nakata, K.; Fujishima, A. TiO<sub>2</sub> photocatalysis: Design and applications. *J. Photochem. Photobiol. C* **2012**, *13*, 169–189. [[CrossRef](#)]
14. Singh, R.; Dutta, S. A review on H<sub>2</sub> production through photocatalytic reactions using TiO<sub>2</sub>/TiO<sub>2</sub>-assisted catalysts. *Fuel* **2018**, *220*, 607–620. [[CrossRef](#)]
15. Shehzada, N.; Tahirc, M.; Joharia, K.; Murugesana, T.; Hussain, M.; Shehzad, N.; Tahir, M.; Johari, K.; Murugesan, T.; Hussain, M. A critical review on TiO<sub>2</sub> based photocatalytic CO<sub>2</sub> reduction system: Strategies to improve efficiency. *J. CO<sub>2</sub> Util.* **2018**, *26*, 98–122. [[CrossRef](#)]
16. Shayegan, Z.; Lee, C.; Haghighat, F. TiO<sub>2</sub> photocatalyst for removal of volatile organic compounds in gas phase—A review. *Chem. Eng. J.* **2018**, *334*, 2408–2439. [[CrossRef](#)]
17. Chen, D.; Cheng, Y.; Zhou, N.; Chen, P.; Wang, Y.; Li, K.; Huo, S.; Cheng, P.; Peng, P.; Zhang, R.; et al. Photocatalytic degradation of organic pollutants using TiO<sub>2</sub>-based photocatalysts: A review. *J. Clean. Prod.* **2020**, *268*, 121725. [[CrossRef](#)]
18. Reddy, P.V.L.; Kavitha, B.; Reddy, P.A.K.; Kim, K.H. TiO<sub>2</sub>-based photocatalytic disinfection of microbes in aqueous media: A review. *Environ. Res.* **2017**, *154*, 296–303. [[CrossRef](#)]

19. Hadjiivanov, K.; Klissurski, D.G. Surface chemistry of titania (anatase) and titania-supported catalysts. *Chem. Soc. Rev.* **1996**, *25*, 61–69. [[CrossRef](#)]
20. Dahl, M.; Liu, Y.; Yin, Y. Composite Titanium Dioxide Nanomaterials. *Chem. Rev.* **2014**, *114*, 9853–9889. [[CrossRef](#)]
21. Fernández-García, M.; Rodríguez, J.A. Metal Oxide Nanoparticles. In *Encyclopedia of Inorganic Chemistry*; John Wiley & Sons, Ltd.: Hoboken, NJ, USA, 2009.
22. Myakonkaya, O.; Hu, Z.; Nazar, M.F.; Eastoe, J. Recycling Functional Colloids and Nanoparticles. *Chem. Eur. J.* **2010**, *16*, 11784–11790. [[CrossRef](#)]
23. Argyle, M.D.; Bartholomew, C.H. Heterogeneous Catalyst Deactivation and Regeneration: A Review. *Catalysts* **2015**, *5*, 145–269. [[CrossRef](#)]
24. Shan, A.Y.; Ghazi, T.I.M.; Rashid, S.A. Immobilisation of titanium dioxide onto supporting materials in heterogeneous photocatalysis: A review. *Appl. Catal. A Gen.* **2010**, *389*, 1–8. [[CrossRef](#)]
25. Gil, A.; Gándia, L.M.; Vicente, M.A. Recent Advances in the Synthesis and Catalytic Applications of Pillared Clays. *Catal. Rev.* **2000**, *42*, 145–212. [[CrossRef](#)]
26. Serwicka, E.M.; Bahranowski, K. Environmental catalysis by tailored materials derived from layered minerals. *Catal. Today* **2004**, *90*, 85–92. [[CrossRef](#)]
27. Centi, G.; Perathoner, S. Catalysis by layered materials: A review. *Microporous Mesoporous Mater.* **2008**, *107*, 3–15. [[CrossRef](#)]
28. Zhou, C.H. An overview on strategies towards clay-based designer catalysts for green and sustainable catalysis. *Appl. Clay Sci.* **2011**, *53*, 87–96. [[CrossRef](#)]
29. Liu, J.; Zhang, G. Recent advances in synthesis and applications of clay-based photocatalysts: A review. *Phys. Chem. Chem. Phys.* **2014**, *16*, 8178–8192. [[CrossRef](#)]
30. Szczepanik, B. Photocatalytic degradation of organic contaminants over clay-TiO<sub>2</sub> nanocomposites: A review. *Appl. Clay Sci.* **2017**, *141*, 227–239. [[CrossRef](#)]
31. Mishra, A.; Mehta, A.; Basu, S. Clay supported TiO<sub>2</sub> nanoparticles for photocatalytic degradation of environmental pollutants: A Review. *J. Environ. Chem. Eng.* **2018**, *6*, 6088–6107. [[CrossRef](#)]
32. Deeppracha, S.; Vibulyaseak, K.; Ogawa, M. Complexation of TiO<sub>2</sub> with clays and clay minerals for hierarchically designed functional hybrids. In *Advanced Supramolecular Nanoarchitectonics*, 1st ed.; Ariga, K., Aono, M., Eds.; Elsevier: Amsterdam, The Netherlands, 2019; pp. 125–150.
33. Ruiz-Hitzky, E.; Aranda, P.; Akkari, M.; Khaorapapong, N.; Ogawa, M. Photoactive nanoarchitectures based on clays incorporating TiO<sub>2</sub> and ZnO nanoparticles. *Beilstein J. Nanotechnol.* **2019**, *10*, 1140–1156. [[CrossRef](#)] [[PubMed](#)]
34. Gil, A.; Vicente, M.A. Progress and perspectives on pillared clays applied in energetic and environmental remediation processes. *Curr. Opin. Green Sustain. Chem.* **2020**, *21*, 56–63. [[CrossRef](#)]
35. Schoonheydt, R.A.; Johnston, C.T.; Bergaya, F. Clay minerals and their surfaces. In *Developments in Clay Science*; Schoonheydt, R., Johnston, C.T., Bergaya, F., Eds.; Elsevier: Amsterdam, The Netherlands, 2018; Volume 9, pp. 1–21.
36. Ariga, K.; Aono, M. Introduction: Nanoarchitectonics for Materials Innovation. In *Manipulation of Nanoscale Materials: An Introduction to Nanoarchitectonics*; RSC: Cambridge, UK, 2012; pp. 1–3.
37. Vaughan, D.E.W. Pillared clays—A historical perspective. *Catal. Today* **1988**, *2*, 187–198. [[CrossRef](#)]
38. Bergaya, F.; Lagaly, G. General Introduction: Clays, Clay Minerals, and Clay Science. In *Developments in Clay Science*, 2nd ed.; Bergaya, F., Lagaly, G., Eds.; Elsevier: Amsterdam, The Netherlands, 2013; Volume 5A, pp. 1–19.
39. Brigatti, M.F.; Galan, E.; Theng, B.K.G. Structure and mineralogy of clay minerals. In *Developments in Clay Science*, 2nd ed.; Bergaya, F., Lagaly, G., Eds.; Elsevier: Amsterdam, The Netherlands, 2013; Volume 5A, pp. 21–81.
40. Sparks, D.L. Inorganic soil components. In *Environmental Soil Chemistry*, 2nd ed.; Sparks, D.L., Ed.; Academic Press: Burlington, MA, USA, 2003; pp. 43–73.
41. Galan, E. Properties and applications of palygorskite-sepiolite clays. *Clay Miner.* **1996**, *31*, 443–453. [[CrossRef](#)]
42. Steudel, A.; Emmerich, K. Strategies for the successful preparation of homoionic smectites. *Appl. Clay Sci.* **2018**, *75–76*, 13–21. [[CrossRef](#)]
43. Zhang, H.; Banfield, J.F. Thermodynamic analysis of phase stability of nanocrystalline titania. *J. Mater. Chem.* **1998**, *8*, 2073–2076. [[CrossRef](#)]
44. Sterte, J. Synthesis and properties of titanium oxide cross-linked montmorillonite. *Clays Clay Miner.* **1986**, *34*, 658–664. [[CrossRef](#)]
45. Yamanaka, S.; Nishihara, T.; Hattori, M.; Suzuki, Y. Preparation and properties of titania pillared clay. *Mater. Chem. Phys.* **1987**, *17*, 87–101. [[CrossRef](#)]
46. Bernier, A.; Admaiai, L.F.; Grange, P. Synthesis and characterization of titanium pillared clay. Influence of the temperature of preparation. *Appl. Catal.* **1991**, *77*, 269–281. [[CrossRef](#)]
47. Lin, J.T.; Jong, S.J.; Cheng, S. A new method for preparing microporous titanium pillared clays. *Microporous Mater.* **1993**, *1*, 287–290. [[CrossRef](#)]
48. Bahranowski, K.; Dula, R.; Komorek, J.; Romotowski, T.; Serwicka, E.M. Preparation, physicochemical and catalytic properties of vanadium doped alumina and titania-pillared montmorillonites. *Stud. Surf. Sci. Catal.* **1995**, *91*, 747–754.
49. Kooli, F.; Bovey, J.; Jones, W. Dependence of the properties of titanium-pillared clays on the host matrix: A comparison of montmorillonite, saponite and rectorite pillared materials. *J. Mater. Chem.* **1997**, *7*, 153–158. [[CrossRef](#)]

50. Long, R.Q.; Yang, R.T. Selective catalytic reduction of NO with ammonia over V<sub>2</sub>O<sub>5</sub> doped TiO<sub>2</sub> pillared clay catalysts. *Appl. Catal. B-Environ.* **2000**, *24*, 13–21. [[CrossRef](#)]
51. Yuan, P.; Yin, X.; He, H.; Yang, D.; Wang, L.; Zhu, J. Investigation on the delaminated-pillared structure of TiO<sub>2</sub>-PILC synthesized by TiCl<sub>4</sub> hydrolysis method. *Microporous Mesoporous Mater.* **2006**, *93*, 240–247. [[CrossRef](#)]
52. Damardji, B.; Khalaf, H.; Duclaux, L.; David, B. Preparation of TiO<sub>2</sub>-pillared montmorillonite as photocatalyst Part I. Microwave calcination, characterisation, and adsorption of a textile azo dye. *Appl. Clay Sci.* **2009**, *44*, 201–205. [[CrossRef](#)]
53. Chmielarz, L.; Piwowarska, Z.; Kuśtrowski, P.; Węgrzyn, A.; Gil, B.; Kowalczyk, A.; Dudek, B.; Dziembaj, R.; Michalik, M. Comparison study of titania pillared interlayered clays and porous clay heterostructures modified with copper and iron as catalysts of the DeNO<sub>x</sub> process. *Appl. Clay Sci.* **2011**, *53*, 164–173. [[CrossRef](#)]
54. Bahranowski, K.; Włodarczyk, W.; Wisła-Walsh, E.; Gawęł, A.; Matusik, J.; Klimek, A.; Gil, B.; Michalik-Zym, A.; Dula, R.; Socha, R.P.; et al. [Ti,Zr]-pillared montmorillonite—A new quality with respect to Ti- and Zr-pillared clays. *Microporous Mesoporous Mater.* **2015**, *202*, 155–164. [[CrossRef](#)]
55. Butman, M.F.; Ovchinnikov, N.L.; Karasev, N.S.; Kochkina, N.E.; Agafonov, A.V.; Vinogradov, A.V. Photocatalytic and adsorption properties of TiO<sub>2</sub>-pillared montmorillonite obtained by hydrothermally activated intercalation of titanium polyhydroxo complexes. *Beilstein J. Nanotechnol.* **2018**, *9*, 364–378. [[CrossRef](#)]
56. González, B.; Trujillano, R.; Vicente, M.A.; Rives, V.; Korili, S.A.; Gil, A. Photocatalytic degradation of trimethoprim on doped Ti-pillared montmorillonite. *Appl. Clay Sci.* **2019**, *167*, 43–49. [[CrossRef](#)]
57. Chauhan, M.; Saini, V.K.; Suthar, S. Ti-pillared montmorillonite clay for adsorptive removal of amoxicillin, imipramine, diclofenac-sodium, and paracetamol from water. *J. Hazard. Mater.* **2020**, *399*, 122832. [[CrossRef](#)]
58. Yoneyama, H.; Haga, S.; Yamanaka, S. Photocatalytic activities of microcrystalline titania incorporated in sheet silicates of clay. *J. Phys. Chem.* **1989**, *93*, 4833–4837. [[CrossRef](#)]
59. Del Castillo, H.L.; Grange, P. Preparation and catalytic activity of titanium pillared montmorillonite. *Appl. Catal. A-Gen.* **1993**, *103*, 23–34. [[CrossRef](#)]
60. Del Castillo, H.L.; Gil, A.; Grange, P. Influence of the nature of titanium alkoxide and of the acid of hydrolysis in the preparation of titanium-pillared montmorillonites. *J. Phys. Chem. Sol.* **1997**, *58*, 1053–1062. [[CrossRef](#)]
61. Ooka, C.; Akita, S.; Ohashi, Y.; Horiuchi, T.; Suzuki, K.; Komai, S.; Yoshida, H.; Hattori, T. Crystallization of hydrothermally treated TiO<sub>2</sub> pillars in pillared montmorillonite for improvement of the photocatalytic activity. *J. Mater. Chem.* **1999**, *100*, 2943–2952. [[CrossRef](#)]
62. Valverde, J.L.; Sánchez, P.; Dorado, F.; Asencio, I.; Romero, A. Preparation and characterization of Ti-pillared clays using Ti alkoxides. Influence of the synthesis parameters. *Clays Clay Miner.* **2003**, *51*, 41–51. [[CrossRef](#)]
63. Ooka, C.; Yoshida, H.; Suzuki, K.; Hattori, T. Highly hydrophobic TiO<sub>2</sub> pillared clay for photocatalytic degradation of organic compounds in water. *Microporous Mesoporous Mater.* **2004**, *67*, 143–150. [[CrossRef](#)]
64. Sun, S.; Jiang, Y.; Yu, L.; Li, F.; Yang, Z.; Hou, T.; Hu, D.; Xia, M. Enhanced photocatalytic activity of microwave treated TiO<sub>2</sub> pillared montmorillonite. *Mater. Chem. Phys.* **2006**, *98*, 377–381. [[CrossRef](#)]
65. Rezala, H.; Khalaf, H.; Valverde, J.L.; Romero, A.; Molinari, A.; Maldotti, A. Photocatalysis with Ti-pillared clays for the oxofunctionalization of alkylaromatics by O<sub>2</sub>. *Appl. Catal. A-Gen.* **2009**, *352*, 234–242. [[CrossRef](#)]
66. Chen, D.; Zhu, Q.; Zhou, F.; Deng, X.; Li, F. Synthesis and photocatalytic performances of the TiO<sub>2</sub> pillared montmorillonite. *J. Hazard. Mater.* **2012**, *235–236*, 186–193. [[CrossRef](#)]
67. Sahel, K.; Bouhent, M.; Belkhadem, F.; Ferchichi, M.; Dappozze, F.; Guillard, C.; Figueras, F. Photocatalytic degradation of anionic and cationic dyes over TiO<sub>2</sub> P25, and Ti-pillared clays and Ag-doped Ti-pillared clays. *Appl. Clay Sci.* **2014**, *95*, 205–210. [[CrossRef](#)]
68. Kang, L.; Liu, H.; He, H.; Yang, C. Oxidative desulfurization of dibenzothiophene using molybdenum catalyst supported on Ti-pillared montmorillonite and separation of sulfones by filtration. *Fuel* **2018**, *234*, 1229–1237. [[CrossRef](#)]
69. Fatimah, I.; Nurillahi, R.; Sahroni, I.; Muraza, O. TiO<sub>2</sub>-pillared saponite and photosensitization using a ruthenium complex for photocatalytic enhancement of the photodegradation of bromophenol blue. *Appl. Clay Sci.* **2019**, *183*, 105302. [[CrossRef](#)]
70. Yoda, S.; Sakurai, Y.; Endo, A.; Miyata, T.; Yanagishita, H.; Otake, K.; Tsuchiya, T. Synthesis of titania pillared montmorillonite via intercalation of titanium alkoxide dissolved in supercritical carbon dioxide. *J. Mater. Chem.* **2004**, *14*, 2763–2767. [[CrossRef](#)]
71. Einaga, H. Hydrolysis of titanium(IV) in aqueous (Na,H)Cl solution. *J. Chem. Soc. Dalton Trans.* **1979**, *12*, 1917–1919. [[CrossRef](#)]
72. Comba, P.; Merbach, A. The titanyl question revisited. *Inorg. Chem.* **1987**, *26*, 1315–1323. [[CrossRef](#)]
73. Vicente, M.A.; Bañares-Muñoz, M.A.; Toranzo, R.; Gandía, L.M.; Gil, A. Influence of the Ti precursor on the properties of Ti-pillared smectites. *Clay Miner.* **2001**, *36*, 125–138. [[CrossRef](#)]
74. Binitha, N.N.; Sugunan, S. Preparation, characterization and catalytic activity of titania pillared montmorillonite clays. *Microporous Mesoporous Mater.* **2006**, *93*, 82–89. [[CrossRef](#)]
75. Ming-Yuan, H.; Zhonghui, L.; Enze, M. Acidic and hydrocarbon catalytic properties of pillared clay. *Catal. Today* **1988**, *2*, 321–338. [[CrossRef](#)]
76. Yang, G.; Lan, X.; Zhuang, J.; Ma, D.; Zhou, L.; Liu, X.; Han, X.; Bao, X. Acidity and defect sites in titanium silicalite catalyst. *Appl. Catal. A-Gen.* **2008**, *337*, 58–65. [[CrossRef](#)]
77. Lambert, J.-F.; Poncelet, G. Acidity in pillared clays: Origin and catalytic manifestations. *Top. Catal.* **1997**, *4*, 43–56. [[CrossRef](#)]
78. Gil, A.; Korili, S.A.; Vicente, M.A. Recent advances in the control and characterization of the porous structure of pillared clay catalysts. *Catal. Rev.* **2008**, *50*, 153–221. [[CrossRef](#)]

79. Gil, A.; Del Castillo, H.L.; Masson, J.; Court, J.; Grange, P. Selective dehydration of 1-phenylethanol to 3-oxa-2,4-diphenylpentane on titanium pillared montmorillonite. *J. Mol. Catal. A-Chem.* **1996**, *107*, 185–190. [[CrossRef](#)]
80. Swarnakar, R.; Brandt, K.B.; Kydd, R.A. Catalytic activity of Ti- and Al-pillared montmorillonite and beidellite for cumene cracking and hydrocracking. *Appl. Catal. A-Gen.* **1996**, *142*, 61–71. [[CrossRef](#)]
81. Belkhadem, F.; Clacens, J.-M.; Bengueddach, A.; Figueras, F. Acidity and Catalytic Properties for the alkylation of aromatics of PILCs with mixed oxide pillars prepared from two different bentonites. *Appl. Catal. A-Gen.* **2006**, *298*, 188–193. [[CrossRef](#)]
82. Han, L.; Cai, S.; Gao, M.; Hasegawa, J.; Wang, P.; Zhang, J.; Shi, L.; Zhang, D. Selective Catalytic Reduction of NO<sub>x</sub> with NH<sub>3</sub> by Using Novel Catalysts: State of the Art and Future Prospects. *Chem. Rev.* **2019**, *119*, 10916–10976. [[CrossRef](#)] [[PubMed](#)]
83. Gholami, F.; Tomas, M.; Gholami, Z.; Vakili, M. Technologies for the nitrogen oxides reduction from flue gas: A review. *Sci. Total Environ.* **2020**, *714*, 136712. [[CrossRef](#)]
84. Serwicka, E.M. Clays as catalysts for the removal of nitrogen oxides. *Pol. J. Chem.* **2001**, *75*, 307–328.
85. Grzybek, T. Layered clays as SCR deNO<sub>x</sub> catalysts. *Catal. Today* **2007**, *119*, 125–132. [[CrossRef](#)]
86. Yang, R.; Chen, J.; Kikkinides, E.; Cheng, L.; Cichanowicz, J. Pillared Clays as Superior Catalysts for Selective Catalytic Reduction of Nitric Oxide with Ammonia. *Ind. Eng. Chem. Res.* **1992**, *31*, 1440–1445. [[CrossRef](#)]
87. Bahranowski, K.; Janas, J.; Machej, T.; Serwicka, E.M.; Vartikian, L. Vanadium-Doped Titania-Pillared Montmorillonite Clay as a Catalyst for Selective Catalytic Reduction of NO by Ammonia. *Clay Miner.* **1997**, *32*, 665–672. [[CrossRef](#)]
88. Bahranowski, K.; Serwicka, E.M. ESR study of vanadium-doped alumina- and titania-pillared montmorillonites. *Coll. Surf.* **1993**, *72*, 153–160. [[CrossRef](#)]
89. Bahranowski, K.; Labanowska, M.; Serwicka, E.M. ESR characterization of catalytically active V centres supported on alumina-, titania- and zirconia pillared montmorillonite clay. *Appl. Magn. Reson.* **1996**, *10*, 477–490. [[CrossRef](#)]
90. Long, R.Q.; Yang, R.T. Catalytic Performance and Characterization of VO<sup>2+</sup>-Exchanged Titania-Pillared Clays for Selective Catalytic Reduction of Nitric Oxide with Ammonia. *J. Catal.* **2000**, *196*, 73–85. [[CrossRef](#)]
91. Chae, H.J.; Nam, I.S.; Ham, S.W.; Hong, S.B. Characteristics of vanadia on the surface of V<sub>2</sub>O<sub>5</sub>/Ti-PILC catalyst for the reduction of NO<sub>x</sub> by NH<sub>3</sub>. *Appl. Catal. B-Environ.* **2004**, *5*, 117–126. [[CrossRef](#)]
92. Lai, J.-K.; Wachs, I.E. A Perspective on the Selective Catalytic Reduction (SCR) of NO with NH<sub>3</sub> by Supported V<sub>2</sub>O<sub>5</sub>-WO<sub>3</sub>/TiO<sub>2</sub> Catalysts. *ACS Catal.* **2018**, *8*, 6537–6551. [[CrossRef](#)]
93. Zang, S.; Zhang, G.; Qiu, W.; Song, L.; Zhang, R.; He, H. Resistance to SO<sub>2</sub> poisoning of V<sub>2</sub>O<sub>5</sub>/TiO<sub>2</sub>-PILC catalyst for the selective catalytic reduction of NO by NH<sub>3</sub>. *Chin. J. Catal.* **2016**, *37*, 888–897. [[CrossRef](#)]
94. Del Castillo, H.L.; Gil, A.; Grange, P. Selective catalytic reduction of NO by NH<sub>3</sub> on titanium pillared montmorillonite. *Catal. Lett.* **1996**, *36*, 237–239. [[CrossRef](#)]
95. Del Castillo, H.L.; Gil, A.; Grange, P. Preparation and characterization of sulfated titanium-modified pillared montmorillonite. *Catal. Lett.* **1997**, *43*, 133–137.
96. Khalfallah Boudali, L.; Ghorbel, A.; Grange, P. Selective catalytic reduction of NO by NH<sub>3</sub> on sulfated titanium-pillared clay. *Catal. Lett.* **2003**, *86*, 251–256.
97. Khalfallah Boudali, L.; Ghorbel, A.; Grange, P.; Figueras, F. Selective catalytic reduction of NO with ammonia over V<sub>2</sub>O<sub>5</sub> supported sulfated titanium-pillared clay catalysts: Influence of V<sub>2</sub>O<sub>5</sub> content. *Appl. Catal. B-Environ.* **2005**, *59*, 105–111. [[CrossRef](#)]
98. Khalfallah Boudali, L.; Ghorbel, A.; Grange, P. SCR of NO by NH<sub>3</sub> over V<sub>2</sub>O<sub>5</sub> supported sulfated Ti-pillared clay: Reactivity and reducibility of catalysts. *Appl. Catal. A-Gen.* **2006**, *305*, 7–14. [[CrossRef](#)]
99. Khalfallah Boudali, L.; Ghorbel, A.; Grange, P. Characterization and reactivity of WO<sub>3</sub>-V<sub>2</sub>O<sub>5</sub> supported on sulfated titanium pillared clay catalysts for the SCR-NO reaction. *C. R. Chim.* **2009**, *12*, 779–786. [[CrossRef](#)]
100. Arfaoui, J.; Boudali, L.K.; Ghorbel, A.; Delahay, G. Effect of vanadium on the behaviour of unsulfated and sulfated Ti-pillared clay catalysts in the SCR of NO by NH<sub>3</sub>. *Catal. Today* **2009**, *142*, 234–238. [[CrossRef](#)]
101. Arfaoui, J.; Boudali, L.K.; Ghorbel, A.; Delahay, G. Influence of the nature of titanium source and of vanadia content on the properties of titanium-pillared montmorillonite. *J. Phys. Chem. Sol.* **2008**, *69*, 1121–1124. [[CrossRef](#)]
102. Cheng, J.; Song, Y.; Ye, Q.; Cheng, S.; Kang, T.; Dai, H. A mechanistic investigation on the selective catalytic reduction of NO with ammonia over the V-Ce/Ti-PILC catalysts. *Mol. Catal.* **2018**, *445*, 111–123. [[CrossRef](#)]
103. Liu, Z.; Zhang, S.; Li, J.; Zhu, J.; Ma, L. Novel V<sub>2</sub>O<sub>5</sub>-CeO<sub>2</sub>/TiO<sub>2</sub> catalyst with low vanadium loading for the selective catalytic reduction of NO<sub>x</sub> by NH<sub>3</sub>. *Appl. Catal. B-Environ.* **2014**, *158–159*, 11–19. [[CrossRef](#)]
104. Cai, M.; Bian, X.; Xie, F.; Wu, W.; Cen, P. Preparation and Performance of Cerium-Based Catalysts for Selective Catalytic Reduction of Nitrogen Oxides: A Critical Review. *Catalysts* **2021**, *11*, 361. [[CrossRef](#)]
105. Cheng, J.; Ye, Q.; Zheng, C.; Cheng, S.; Kang, T.; Dai, H. Effect of ceria loading on Zr-pillared clay catalysts for selective catalytic reduction of NO with NH<sub>3</sub>. *New J. Chem.* **2019**, *43*, 10850–10858. [[CrossRef](#)]
106. Cheng, L.S.; Yang, R.T.; Chen, N. Iron Oxide and Chromia Supported on Titania-Pillared Clay for Selective Catalytic Reduction of Nitric Oxide with Ammonia. *J. Catal.* **1996**, *164*, 70–81. [[CrossRef](#)]
107. Yang, R.T.; Li, W.B. Ion-Exchanged Pillared Clays: A New Class of Catalysts for Selective Catalytic Reduction of NO by Hydrocarbons and by Ammonia. *J. Catal.* **1995**, *155*, 414–417. [[CrossRef](#)]
108. Long, R.Q.; Yang, R.T. Selective catalytic reduction of nitrogen oxides by ammonia over Fe<sup>3+</sup>-exchanged TiO<sub>2</sub>-pillared clay catalysts. *J. Catal.* **1999**, *186*, 254–268. [[CrossRef](#)]

109. Long, R.Q.; Yang, R.T. Acid- and base-treated Fe<sup>3+</sup>-TiO<sub>2</sub>-pillared clays for selective catalytic reduction of NO by NH<sub>3</sub>. *Catal. Lett.* **1999**, *59*, 39–44. [[CrossRef](#)]
110. Long, R.Q.; Yang, R.T. FTIR and kinetic studies of the mechanism of Fe<sup>3+</sup>-exchanged TiO<sub>2</sub>-pillared clay catalyst for selective catalytic reduction of NO with ammonia. *J. Catal.* **2000**, *190*, 22–31. [[CrossRef](#)]
111. Long, R.Q.; Yang, R.T.; Zammit, K.D. Superior Pillared Clay Catalysts for Selective Catalytic Reduction of Nitrogen Oxides for Power Plant Emission Control. *J. Air Waste Manag. Assoc.* **2000**, *50*, 436–442. [[CrossRef](#)] [[PubMed](#)]
112. Long, R.Q.; Yang, R.T. The promoting role of rare earth oxides on Fe-exchanged TiO<sub>2</sub>-pillared clay for selective catalytic reduction of nitric oxide by ammonia. *Appl. Catal. B-Environ.* **2000**, *27*, 87–95. [[CrossRef](#)]
113. Chmielarz, L.; Kuśtrowski, P.; Zbroja, M.; Łasocha, W.; Dziembaj, R. Selective reduction of NO with NH<sub>3</sub> over pillared clays modified with transition metals. *Catal. Today* **2004**, *90*, 43–49. [[CrossRef](#)]
114. Chmielarz, L.; Piwowarska, Z.; Kuśtrowski, P.; Gil, B.; Adamski, A.; Dudek, B.; Michalik, M. Porous clay heterostructures (PCHs) intercalated with silica-titania pillars and modified with transition metals as catalysts for the DeNO<sub>x</sub> process. *Appl. Catal. B-Environ.* **2009**, *91*, 449–459. [[CrossRef](#)]
115. Galarneau, A.; Barodawalla, A.; Pinnavaia, T.J. Porous clay heterostructures formed by gallery-templated synthesis. *Nature* **1995**, *374*, 529–531. [[CrossRef](#)]
116. Xu, D.; Wu, W.; Wang, P.; Deng, J.; Yan, T.; Zhang, D. Boosting the Alkali/Heavy Metal Poisoning Resistance for NO Removal by Using Iron-Titanium Pillared Montmorillonite Catalysts. *J. Hazard. Mater.* **2020**, *399*, 122947. [[CrossRef](#)] [[PubMed](#)]
117. Mrad, R.; Aissat, A.; Cousin, R.; Courcot, D.; Siffert, S. Catalysts for NO<sub>x</sub> selective catalytic reduction by hydrocarbons (HC-SCR). *Appl. Catal. A-Gen.* **2015**, *504*, 542–548.
118. Yahiro, H.; Iwamoto, M. Copper ion-exchanged zeolite catalysts in deNO<sub>x</sub> reaction. *Appl. Catal. A-Gen.* **2001**, *222*, 163–181. [[CrossRef](#)]
119. Yang, R.T.; Tharappiwattananon, N.; Long, R.Q. Ion-exchanged pillared clays for selective catalytic reduction of NO by ethylene in the presence of oxygen. *Appl. Catal. B-Environ.* **1998**, *19*, 289–304. [[CrossRef](#)]
120. Valverde, J.L.; Lucas, A.D.; Sánchez, P.; Dorado, F.; Romero, A. Cation exchanged and impregnated Ti-pillared clays for selective catalytic reduction of NO<sub>x</sub> by propylene. *Appl. Catal. B-Environ.* **2003**, *43*. [[CrossRef](#)]
121. Bahranowski, K.; Dula, R.; Łabanowska, M.; Serwicka, E.M. ESR Study of Cu Centers Supported on Al-, Ti-, and Zr-Pillared Montmorillonite Clays. *Appl. Spectrosc.* **1996**, *50*, 1439–1445. [[CrossRef](#)]
122. Bahranowski, K.; Kielski, A.; Serwicka, E.M.; Wisła-Walsh, E.; Wodnicka, K. Influence of doping with copper on the texture of pillared montmorillonite catalysts. *Microporous Mesoporous Mater.* **2000**, *41*, 201–215. [[CrossRef](#)]
123. Li, X.; Lu, G.; Qu, Z.; Zhang, D.; Liu, S. The role of titania pillar in copper-ion exchanged titania pillared clays for the selective catalytic reduction of NO by propylene. *Appl. Catal. A-Gen.* **2011**, *398*, 82–87. [[CrossRef](#)]
124. Lu, G.; Li, X.; Qu, Z.; Zhao, Q.; Zhao, L.; Chen, G. Copper-ion exchanged Ti-pillared clays for selective catalytic reduction of NO by propylene. *Chem. Eng. J.* **2011**, *168*, 1128–1133. [[CrossRef](#)]
125. Dong, S.; Su, Y.; Liu, X.; Li, Q.; Yuan, M.; Zhou, H.; Deng, W. Experimental study on selective catalytic reduction of NO by C<sub>3</sub>H<sub>6</sub> over Fe/Ti-PILC catalysts. *J. Fuel Chem. Technol.* **2018**, *46*, 1231–1239. [[CrossRef](#)]
126. Qian, W.; Su, Y.; Yang, X.; Yuan, M.; Deng, W.; Zhao, B. Experimental study on selective catalytic reduction of NO with propene over iron based catalysts supported on aluminum pillared clays. *J. Fuel Chem. Technol.* **2017**, *45*, 1499–1507. [[CrossRef](#)]
127. Wen, N.; Dong, S.; Su, Y.; Deng, W.; Zhao, B. Effect of synthesis parameters on catalytic performance of Fe/Ti-PILC catalysts for SCR-C<sub>3</sub>H<sub>6</sub> and in situ DRIFTS study. *J. Environ. Chem. Eng.* **2020**, *8*, 104555. [[CrossRef](#)]
128. Chmielarz, L.; Kuśtrowski, P.; Zbroja, M.; Rafalska-Łasocha, A.; Dudek, B.; Dziembaj, R. SCR of NO by NH<sub>3</sub> on alumina or titania-pillared montmorillonite various modified with Cu or Co Part I. General characterization and catalysts screening. *Appl. Catal. B-Environ.* **2003**, *45*, 103–116. [[CrossRef](#)]
129. Shen, B.; Yao, Y.; Ma, H.; Liu, T. Ceria Modified MnO<sub>x</sub>/TiO<sub>2</sub>-Pillared Clays Catalysts for the Selective Catalytic Reduction of NO with NH<sub>3</sub> at Low Temperature. *Chin. J. Catal.* **2011**, *32*, 1803–1811. [[CrossRef](#)]
130. Shen, B.X.; Ma, H.; Yao, Y. Mn-CeO<sub>x</sub>/Ti-PILCs for selective catalytic reduction of NO with NH<sub>3</sub> at low temperature. *J. Environ. Sci.* **2012**, *24*, 499–506. [[CrossRef](#)]
131. Wang, Z.; Jiao, M.; Chen, Z.; He, H.; Liu, L. Effects of montmorillonite and anatase TiO<sub>2</sub> support on CeO<sub>2</sub> catalysts during NH<sub>3</sub>-SCR reaction. *Microporous Mesoporous Mater.* **2021**, *320*, 111072. [[CrossRef](#)]
132. Luo, S.; Zhou, W.; Xie, A.; Wu, F.; Yao, C.; Li, X.; Zuo, S.; Liu, T. Effect of MnO<sub>2</sub> polymorphs structure on the selective catalytic reduction of NO<sub>x</sub> with NH<sub>3</sub> over TiO<sub>2</sub>-Palygorskite. *Chem. Eng. J.* **2016**, *286*, 291–299. [[CrossRef](#)]
133. Xie, W.; Zhang, G.; Mua, B.; Tang, Z.; Zhang, J. The promoting effect of palygorskite on CeO<sub>2</sub>-WO<sub>3</sub>-TiO<sub>2</sub> catalyst for the selective catalytic reduction of NO<sub>x</sub> with NH<sub>3</sub>. *Appl. Clay Sci.* **2020**, *192*, 105641. [[CrossRef](#)]
134. Soni, V.; Singh, P.; Shree, V.; Goel, V. Effects of VOCs on Human Health. In *Air Pollution and Control. Energy, Environment, and Sustainability*; Sharma, N., Agarwal, A., Eastwood, P., Gupta, T., Singh, A., Eds.; Springer: Singapore, 2018; pp. 119–142.
135. Gelles, T.; Krishnamurthy, A.; Adebayo, B.; Rownaghi, A.; Rezaei, F. Abatement of Gaseous Volatile Organic Compounds: A Materials Perspective. *Catal. Today* **2019**, *350*, 3–18. [[CrossRef](#)]
136. Guo, Y.; Wen, M.; Li, G.; An, T. Recent advances in VOC elimination by catalytic oxidation technology onto various nanoparticles catalysts: A critical review. *Appl. Catal. B-Environ.* **2021**, *281*, 119447. [[CrossRef](#)]

137. Li, J.; Hu, M.; Zuo, S.; Wang, X. Catalytic combustion of volatile organic compounds on pillared interlayered clay (PILC)-based catalysts. *Curr. Opin. Chem. Eng.* **2018**, *20*, 93–98. [[CrossRef](#)]
138. Liang, X.; Qi, F.; Liu, P.; Wei, G.; Su, X.; Ma, L.; He, H.; Lin, X.; Xi, Y.; Zhu, J.; et al. Performance of Ti-pillared montmorillonite supported Fe catalysts for toluene oxidation: The effect of Fe on catalytic activity. *Appl. Clay Sci.* **2016**, *132–133*, 96–104. [[CrossRef](#)]
139. Napruszewska, B.; Michalik-Zym, A.; Rogowska, M.; Bielańska, E.; Rojek, W.; Gawęł, A.; Wójcik-Bania, M.; Bahranowski, K.; Serwicka, E.M. Novel Montmorillonite/TiO<sub>2</sub>/MnAl-Mixed Oxide Composites Prepared from Inverse Microemulsions as Combustion Catalysts. *Materials* **2017**, *10*, 1326. [[CrossRef](#)]
140. Bahranowski, K.; Gawęł, A.; Klimek, A.; Michalik-Zym, A.; Napruszewska, B.D.; Nattich-Rak, M.; Rogowska, M.; Serwicka, E.M. Influence of purification method of Na-montmorillonite on textural properties of clay mineral composites with TiO<sub>2</sub> nanoparticles. *Appl. Clay Sci.* **2017**, *140*, 75–80. [[CrossRef](#)]
141. Michalik-Zym, A.; Dula, R.; Duraczyńska, D.; Kryściak-Czerwenka, J.; Machej, T.; Socha, R.P.; Włodarczyk, W.; Gawęł, A.; Matusik, J.; Bahranowski, K.; et al. Active, selective and robust Pd and/or Cr catalysts supported on Ti-, Zr- or [Ti,Zr]-pillared montmorillonites for destruction of chlorinated volatile organic compounds. *Appl. Catal. B-Environ.* **2015**, *174–175*, 293–307. [[CrossRef](#)]
142. Bahranowski, K.; Gawęł, A.; Janik, R.; Komorek, J.; Machej, T.; Michalik, A.; Serwicka, E.M.; Włodarczyk, W. Catalytic Combustion of Trichloroethylene over Pd-Doped Ti-Pillared Montmorillonites. *Pol. J. Chem.* **2003**, *77*, 675–682.
143. Zuo, S.; Ding, M.; Tong, J.; Feng, L.; Qi, C. Study on the preparation and characterization of a titanium-pillared clay-supported CrCe catalyst and its application to the degradation of a low concentration of chlorobenzene. *Appl. Clay Sci.* **2015**, *105–106*, 118–123. [[CrossRef](#)]
144. He, X.; Tang, A.; Yang, H.; Ouyang, J. Synthesis and catalytic activity of doped TiO<sub>2</sub>-palygorskite composites. *Appl. Clay Sci.* **2011**, *53*, 80–84. [[CrossRef](#)]
145. Huang, Q.; Zuo, S.; Zhou, R. Catalytic performance of pillared interlayered clays (PILCs) supported CrCe catalysts for deep oxidation of nitrogen-containing VOCs. *Appl. Catal. B-Environ.* **2010**, *95*, 327–334. [[CrossRef](#)]
146. Shi, Z.; Huang, Q.; Yang, P.; Zhou, R. The catalytic performance of Ti-PILC supported CrO<sub>x</sub>-CeO<sub>2</sub> catalysts for n-butylamine oxidation. *J. Porous Mater.* **2015**, *22*, 739–747. [[CrossRef](#)]
147. Luttrell, T.; Halpegamage, S.; Tao, J.; Kramer, A.; Sutter, E.; Batzill, M. Why is anatase a better photocatalyst than rutile?—Model studies on epitaxial TiO<sub>2</sub> films. *Sci. Rep.* **2014**, *4*, 4043. [[CrossRef](#)]
148. Praneeth, N.V.S.; Paria, S. Clay-semiconductor nanocomposites for photocatalytic applications. In *Clay Minerals: Properties, Occurrence and Uses*; Sen, T.K., Ed.; Nova Science Publishers: Rourkela, India, 2017; Chapter 5; pp. 144–184.
149. Baloyi, J.; Ntho, T.; Moma, J. Synthesis and application of pillared clay heterogeneous catalysts for wastewater treatment: A review. *RSC Adv.* **2018**, *8*, 5197–5211. [[CrossRef](#)]
150. Tanguay, J.F.; Suib, S.L.; Coughlin, R.W. Dichloromethane photodegradation using titanium catalysts. *J. Catal.* **1989**, *117*, 335–347. [[CrossRef](#)]
151. Ding, Z.; Zhu, H.Y.; Lu, G.Q.; Greenfield, P.F. Photocatalytic Properties of Titania Pillared Clays by Different Drying Methods. *J. Colloid Interface Sci.* **1999**, *209*, 193–199. [[CrossRef](#)]
152. Yoshida, H.; Kawase, T.; Miyashita, Y.; Murata, C.; Ooka, C.; Hattori, T. Effect of Hydrothermal Treatment of Titania-pillared Montmorillonite for Photocatalytic Degradation of Dibutyl Phthalate in Water. *Chem. Lett.* **1999**, *28*, 715–716. [[CrossRef](#)]
153. Cheng, S. From layer compounds to catalytic materials. *Catal. Today* **1999**, *49*, 303–312. [[CrossRef](#)]
154. Boretti, A.; Rosa, L. Reassessing the projections of the World Water Development Report. *NPJ Clean Water* **2019**, *2*, 15. [[CrossRef](#)]
155. Perathoner, S.; Centi, G. Catalytic Wastewater Treatment Using Pillared Clays. In *Pillared Clays and Related Catalysts*; Gil, A., Korilli, S.A., Trujillano, R., Vicente, M.A., Eds.; Springer: New York, NY, USA, 2010; pp. 167–200.
156. Reza, K.M.; Kurny, A.; Gulshan, F. Parameters affecting the photocatalytic degradation of dyes using TiO<sub>2</sub>: A review. *Appl. Water Sci.* **2017**, *7*, 1569–1578. [[CrossRef](#)]
157. Awate, S.; Suzuki, K. Enhanced Adsorption Capacity and Photo-Catalytic Oxidative Activity of Dyes in Aqueous Medium by Hydrothermally Treated Titania Pillared Clay. *Adsorption* **2001**, *7*, 319–326. [[CrossRef](#)]
158. Sun, Z.; Chen, Y.; Ke, Q.; Yang, Y.; Yuan, J. Photocatalytic degradation of a cationic azo dye by TiO<sub>2</sub>/bentonite nanocomposite. *J. Photochem. Photobiol. A Chem.* **2002**, *149*, 169–174. [[CrossRef](#)]
159. Zhu, H.Y.; Orthman, J.A.; Li, J.Y.; Zhao, J.C.; Churchman, G.J.; Vansant, E.F. Novel Composites of TiO<sub>2</sub>(Anatase) and Silicate Nanoparticles. *Chem. Mater.* **2002**, *14*, 5037–5044. [[CrossRef](#)]
160. Li, J.; Chen, C.; Zhao, J.; Zhu, H.; Orthman, J. Photodegradation of dye pollutants on TiO<sub>2</sub> nanoparticles dispersed in silicate under UV-VIS irradiation. *Appl. Catal. B-Environ.* **2002**, *37*, 331–338. [[CrossRef](#)]
161. Djellabi, R.; Ghorab, M.F.; Cerrato, G.; Morandi, S.; Gatto, S.; Oldani, V.; Di Michele, A.; Bianchi, C.L. Photoactive TiO<sub>2</sub>-montmorillonite composite for degradation of organic dyes in water. *J. Photochem. Photobiol. A Chem.* **2014**, *295*, 57–63. [[CrossRef](#)]
162. Damardji, B.; Khalaf, H.; Duclaux, L.; David, B. Preparation of TiO<sub>2</sub>-pillared montmorillonite as photocatalyst Part II. Photocatalytic degradation of a textile azo dye. *Appl. Clay Sci.* **2009**, *45*, 98–104. [[CrossRef](#)]
163. Miao, S.; Liu, Z.; Han, B.; Zhang, J.; Yu, X.; Du, J.; Sun, Z. Synthesis and characterization of TiO<sub>2</sub>-montmorillonite nanocomposites and their application for removal of methylene blue. *J. Mater. Chem.* **2006**, *16*, 579–584. [[CrossRef](#)]
164. Liu, S.; Yang, J.H.; Choy, J.H. Microporous SiO<sub>2</sub>-TiO<sub>2</sub> nanosols pillared montmorillonite for photocatalytic decomposition of methyl orange. *J. Photochem. Photobiol. A Chem.* **2006**, *179*, 75–80. [[CrossRef](#)]

165. Zhang, G.K.; Ding, X.M.; He, F.S.; Yu, X.Y.; Zhou, J.; Hu, Y.J.; Xie, J.W. Low-temperature synthesis and photocatalytic activity of TiO<sub>2</sub> pillared montmorillonite. *Langmuir* **2008**, *24*, 1026–1030. [[CrossRef](#)] [[PubMed](#)]
166. Liu, J.; Dong, M.; Zuo, S.; Yu, Y. Solvothermal preparation of TiO<sub>2</sub>/montmorillonite and photocatalytic activity. *Appl. Clay Sci.* **2009**, *43*, 156–159. [[CrossRef](#)]
167. Ding, X.; An, T.; Li, G.; Zhang, S.; Chen, J.; Yuan, J.; Zhao, H.; Chen, H.; Sheng, G.; Fu, J. Preparation and characterization of hydrophobic TiO<sub>2</sub> pillared clay: The effect of acid hydrolysis catalyst and doped Pt amount on photocatalytic activity. *J. Colloid Interface Sci.* **2008**, *320*, 501–507. [[CrossRef](#)] [[PubMed](#)]
168. Meng, X.; Qian, Z.; Wang, H.; Gao, X.; Zhang, S.; Yang, M. Sol-gel immobilization of SiO<sub>2</sub>/TiO<sub>2</sub> on hydrophobic clay and its removal of methyl orange from water. *J. Sol-Gel Sci. Technol.* **2008**, *46*, 195–200. [[CrossRef](#)]
169. Dvininov, E.; Popovici, E.; Pode, R.; Cocheci, L.; Barvinschi, P.; Nica, V. Synthesis and characterization of TiO<sub>2</sub>-pillared Romanian clay and their application for azoic dyes photodegradation. *J. Hazard. Mater.* **2009**, *167*, 1050–1056. [[CrossRef](#)]
170. Lin, J.J.; Cheng, I.J.; Wang, R.; Lee, R.J. Tailoring Basal Spacings of Montmorillonite by Poly(oxyalkylene)diamine Intercalation. *Macromolecules* **2001**, *34*, 8832–8834. [[CrossRef](#)]
171. Chen, D.; Du, G.; Zhu, Q.; Zhou, F. Synthesis and characterization of TiO<sub>2</sub> pillared montmorillonites: Application for methylene blue degradation. *J. Colloid Interface Sci.* **2013**, *409*, 151–157. [[CrossRef](#)]
172. Yang, S.; Liang, G.; Gu, A.; Mao, H. Synthesis of TiO<sub>2</sub> pillared montmorillonite with ordered interlayer mesoporous structure and high photocatalytic activity by an intra-gallery templating method. *Mater. Res. Bull.* **2013**, *48*, 3948–3954. [[CrossRef](#)]
173. Letaief, S.; Ruiz-Hitzky, E. Silica-clay nanocomposites. *Chem. Commun.* **2003**, 2996–2997. [[CrossRef](#)]
174. Belver, C.; Bedia, J.; Rodriguez, J.J. Titania-clay heterostructures with solar photocatalytic applications. *Appl. Catal. B-Environ.* **2015**, *176–177*, 278–287. [[CrossRef](#)]
175. Huang, S.; Lu, X.; Li, Z.; Ravishankar, H.; Wang, J.; Wang, X. A biomimetic approach towards the synthesis of TiO<sub>2</sub> /carbon-clay as a highly recoverable photocatalyst. *J. Photochem. Photobiol. A Chem.* **2018**, *351*, 131–138. [[CrossRef](#)]
176. Huo, M.; Guo, H.; Jiang, Y.; Ju, H.; Xue, B.; Li, F. A facile method of preparing sandwich layered TiO<sub>2</sub> in between montmorillonite sheets and its enhanced UV-light photocatalytic activity. *J. Photochem. Photobiol. A Chem.* **2018**, *358*, 121–129. [[CrossRef](#)]
177. Liu, J.; Li, X.; Zuo, S.; Yu, Y. Preparation and photocatalytic activity of silver and TiO<sub>2</sub> nanoparticles/montmorillonite composites. *Appl. Clay Sci.* **2007**, *37*, 275–280. [[CrossRef](#)]
178. Li, J.; Wang, W. A study of photodegradation of sulforhodamine B on Au-TiO<sub>2</sub>/bentonite under UV and visible light irradiation. *Solid State Sci.* **2009**, *11*, 2037–2043. [[CrossRef](#)]
179. Zhang, G.; Ding, X.; Hu, Y.; Huang, B.; Zhang, X.; Qin, X.; Zhou, J.; Xie, J. Photocatalytic degradation of 4BS dye by N, S-codoped TiO<sub>2</sub> pillared montmorillonite photocatalysts under visible-light irradiation. *J. Phys. Chem. C* **2008**, *112*, 17994–17997. [[CrossRef](#)]
180. Chen, K.; Li, J.; Li, J.; Zhang, Y.; Wang, W. Synthesis and characterization of TiO<sub>2</sub>-montmorillonites doped with vanadium and/or carbon and their application for the photodegradation of sulphorhodamine B under UV-vis irradiation. *Colloids Surf. A Physicochem. Eng. Asp.* **2010**, *360*, 47–56. [[CrossRef](#)]
181. Belver, C.; Bedia, J.; Alvarez-Montero, M.A.; Rodriguez, J.J. Solar photocatalytic purification of water with Ce-doped TiO<sub>2</sub> /clay heterostructures. *Catal.Today* **2016**, *266*, 36–45. [[CrossRef](#)]
182. Lettieri, S.; Pavone, M.; Fioravanti, A.; Santamaria Amato, L.; Maddalena, P. Charge Carrier Processes and Optical Properties in TiO<sub>2</sub> and TiO<sub>2</sub>-Based Heterojunction Photocatalysts: A Review. *Materials* **2021**, *14*, 1645. [[CrossRef](#)]
183. Mishra, A.; Mehta, A.; Kainth, S.; Basu, S. Effect of g-C<sub>3</sub>N<sub>4</sub> loading on TiO<sub>2</sub>/Bentonite nanocomposites for efficient heterogeneous photocatalytic degradation of industrial dye under visible light. *J. Alloys Compd.* **2018**, *764*, 406–415. [[CrossRef](#)]
184. Daniel, L.M.; Frost, R.L.; Zhu, H.Y. Synthesis and characterisation of clay-supported titania photocatalysts. *J. Colloid Interface Sci.* **2007**, *316*, 72–79. [[CrossRef](#)] [[PubMed](#)]
185. Ma, J.; Jia, Y.; Jing, Y.; Sun, J.; Yao, Y. Synthesis and photocatalytic activity of TiO<sub>2</sub>-hectorite composites. *Appl. Clay Sci.* **2009**, *46*, 114–116. [[CrossRef](#)]
186. Deepracha, S.; Bureekaew, S.; Ogawa, M. Synergy effects of the complexation of a titania and a smectite on the film formation and its photocatalyst' performance. *Appl. Clay Sci.* **2019**, *169*, 129–134. [[CrossRef](#)]
187. You, R.; Chen, J.; Hong, M.; Li, J.; Hong, X. Facile Synthesis of g-C<sub>3</sub>N<sub>4</sub>/TiO<sub>2</sub>/Hectorite Z-Scheme Composite and Its Visible Photocatalytic Degradation of Rhodamine B. *Materials* **2020**, *13*, 5304. [[CrossRef](#)] [[PubMed](#)]
188. Machado, L.C.R.; Torchia, C.B.; Lago, R.M. Floating photocatalysts based on TiO<sub>2</sub> supported on high surface area exfoliated vermiculite for water decontamination. *Catal. Commun.* **2006**, *7*, 538–541. [[CrossRef](#)]
189. Chong, M.N.; Vimonses, V.; Lei, S.; Jin, B.; Chow, C.; Saint, C. Synthesis and characterisation of novel titania impregnated kaolinite nano-photocatalyst. *Microporous Mesoporous Mater.* **2009**, *117*, 233–242. [[CrossRef](#)]
190. Vimonses, V.; Chong, M.N.; Jin, B. Evaluation of the physical properties and photodegradation ability of titania nanocrystalline impregnated onto modified kaolin. *Microporous Mesoporous Mater.* **2010**, *132*, 201–209. [[CrossRef](#)]
191. Zhang, Y.; Gan, H.; Zhang, G. A novel mixed-phase TiO<sub>2</sub>/kaolinite composites and their photocatalytic activity for degradation of organic contaminants. *Chem. Eng. J.* **2011**, *172*, 936–943. [[CrossRef](#)]
192. Kutláková, K.M.; Tokarský, J.; Kovář, P.; Vojtěšková, S.; Kovářová, A.; Smetana, B.; Kukutschová, J.; Čapková, P.; Matějka, V. Preparation and characterization of photoactive composite kaolinite/TiO<sub>2</sub>. *J. Hazard. Mater.* **2011**, *188*, 212–220. [[CrossRef](#)]

193. Barbosa, L.V.; Marçal, L.; Nassar, E.J.; Calefi, P.S.; Vicente, M.A.; Trujillano, R.; Rives, V.; Gil, A.; Korili, S.A.; Ciuffi, K.J. Kaolinite-titanium oxide nanocomposites prepared via sol-gel as heterogeneous photocatalysts for dyes degradation. *Catal. Today* **2015**, *246*, 133–142. [[CrossRef](#)]
194. Mishra, A.; Mehta, A.; Sharma, M.; Basu, S. Enhanced heterogeneous photodegradation of VOC and dye using microwave synthesized TiO<sub>2</sub>/Clay nanocomposites: A comparison study of different type of clays. *J. Alloys Compd.* **2017**, *694*, 574–580. [[CrossRef](#)]
195. Wu, A.; Wang, D.; Wei, C.; Zhang, X.; Liu, Z.; Feng, P.; Oua, X.; Qianga, Y.; Garcia, C.; Niu, J. A comparative photocatalytic study of TiO<sub>2</sub> loaded on three natural clays with different morphologies. *Appl. Clay Sci.* **2019**, *183*, 105352. [[CrossRef](#)]
196. Bel Hadjltaief, H.; Ben Zina, M.; Galvez, M.E.; Da Costa, P. Photocatalytic degradation of methyl green dye in aqueous solution over natural clay-supported ZnO–TiO<sub>2</sub> catalysts. *J. Photochem. Photobiol. A Chem.* **2016**, *315*, 25–33. [[CrossRef](#)]
197. Jaramillo-Fierro, X.; González, S.; Jaramillo, H.A.; Medina, F. Synthesis of the ZnTiO<sub>3</sub>/TiO<sub>2</sub> Nanocomposite Supported in Ecuadorian Clays for the Adsorption and Photocatalytic Removal of Methylene Blue Dye. *Nanomaterials* **2020**, *10*, 1891. [[CrossRef](#)] [[PubMed](#)]
198. Li, C.; Wang, J.; Feng, S.; Yang, Z.; Ding, S. Low-temperature synthesis of heterogeneous crystalline TiO<sub>2</sub>–halloysite nanotubes and their visible light photocatalytic activity. *J. Mater. Chem. A* **2013**, *1*, 8045–8054. [[CrossRef](#)]
199. Li, C.; Wang, J.; Guo, H.; Ding, S. Low temperature synthesis of polyaniline–crystalline TiO<sub>2</sub>–halloysite composite nanotubes with enhanced visible light photocatalytic activity. *J. Colloid Interface Sci.* **2015**, *458*, 1–13. [[CrossRef](#)] [[PubMed](#)]
200. Du, Y.; Zheng, P. Adsorption and photodegradation of methylene blue on TiO<sub>2</sub>–halloysite adsorbents. *Korean J. Chem. Eng.* **2014**, *31*, 2051–2056. [[CrossRef](#)]
201. Zheng, P.; Du, Y.; Chang, P.R.; Ma, X. Amylose–halloysite–TiO<sub>2</sub> composites: Preparation, characterization and photodegradation. *Appl. Surf. Sci.* **2015**, *329*, 256–261. [[CrossRef](#)]
202. Aranda, P.; Kun, R.; Martin-Luengo, M.A.; Letaief, S.; Dékány, I.; Ruiz-Hitzky, E. Titania-sepiolite nanocomposites prepared by a surfactant templating colloidal route. *Chem. Mater.* **2008**, *20*, 84–91. [[CrossRef](#)]
203. Bouna, L.; Rhouta, B.; Amjoud, M.; Maury, F.; Lafont, M.C.; Jada, A.; Senocq, F.; Daoudi, L. Synthesis, characterization and photocatalytic activity of TiO<sub>2</sub> supported natural palygorskite microfibers. *Appl. Clay Sci.* **2011**, *52*, 301–311. [[CrossRef](#)]
204. Stathatos, E.; Papoulis, D.; Aggelopoulos, C.A.; Panagiotaras, D.; Nikolopoulou, A. TiO<sub>2</sub>/palygorskite composite nanocrystalline films prepared by surfactant templating route: Synergistic effect to the photocatalytic degradation of an azo-dye in water. *J. Hazard. Mater.* **2012**, *211–212*, 68–76. [[CrossRef](#)] [[PubMed](#)]
205. Zhang, Y.; Wang, D.; Zhang, G. Photocatalytic degradation of organic contaminants by TiO<sub>2</sub>/sepiolite composites prepared at low temperature. *Chem. Eng. J.* **2011**, *173*, 1–10. [[CrossRef](#)]
206. Zhou, F.; Yan, C.; Wang, H.; Zhou, S.; Komarneni, S. Sepiolite-TiO<sub>2</sub> nanocomposites for photocatalysis: Synthesis by microwave hydrothermal treatment versus calcination. *Appl. Clay Sci.* **2017**, *146*, 246–253. [[CrossRef](#)]
207. Zhou, F.; Yan, C.; Liang, T.; Sun, Q.; Wang, H. Photocatalytic degradation of Orange G using sepiolite-TiO<sub>2</sub> nanocomposites: Optimization of physicochemical parameters and kinetics studies. *Chem. Eng. Sci.* **2018**, *183*, 231–239. [[CrossRef](#)]
208. Zhao, D.; Zhou, J.; Liu, N. Characterization of the structure and catalytic activity of copper modified palygorskite/TiO<sub>2</sub> (Cu<sup>2+</sup>-PG/TiO<sub>2</sub>) catalysts. *Mater. Sci. Eng. A* **2006**, *431*, 256–262. [[CrossRef](#)]
209. Zhao, D.; Zhou, J.; Liu, N. Surface characteristics and photoactivity of silver-modified palygorskite clays coated with nanosized titanium dioxide particles. *Mater. Charact.* **2017**, *58*, 249–255. [[CrossRef](#)]
210. Zhang, L.; Lv, F.; Zhang, W.; Li, R.; Zhong, H.; Zhao, Y.; Zhang, Y.; Wang, X. Photo degradation of methyl orange by attapulgite–SnO<sub>2</sub>–TiO<sub>2</sub> nanocomposites. *J. Hazard. Mater.* **2009**, *171*, 294–300. [[CrossRef](#)] [[PubMed](#)]
211. Zhang, J.; Zhang, L.; Zhou, S.; Chen, H.; Zhao, Y.; Wang, X. Exceptional visible-light-induced photocatalytic activity of attapulgite–BiOBr–TiO<sub>2</sub> nanocomposites. *Appl. Clay Sci.* **2014**, *90*, 135–140. [[CrossRef](#)]
212. Chen, D.; Du, Y.; Zhu, H.; Deng, Y. Synthesis and characterization of a microfibrillar TiO<sub>2</sub>–CdS/palygorskite nanostructured material with enhanced visible-light photocatalytic activity. *Appl. Clay Sci.* **2014**, *87*, 285–291. [[CrossRef](#)]
213. Liu, R.; Ji, Z.; Wang, J.; Zhang, J. Solvothermal synthesized Ag-decorated TiO<sub>2</sub>/sepiolite composite with enhanced UV–vis and visible light photocatalytic activity. *Microporous Mesoporous Mater.* **2018**, *266*, 268–275. [[CrossRef](#)]
214. Kuang, M.; Zhang, J.; Wang, W.; Chen, J.; Cao, Y.; Wang, J.; Ji, Z. Ternary Ag-deposited TiO<sub>2</sub>/palygorskite composites with synergistic effect for enhanced photocatalytic activity. *Solid State Sci.* **2019**, *97*, 106015. [[CrossRef](#)]
215. Li, Y.; Sun, H.; Peng, T.; You, H.; Qin, Y.; Zeng, L. Effects of muscovite matrix on photocatalytic degradation in TiO<sub>2</sub>/muscovite nanocomposites. *Appl. Clay Sci.* **2019**, *179*, 105155. [[CrossRef](#)]
216. Li, Y.; Sun, H.; Peng, T.; You, H.; Zeng, L.; Qin, Y. Preparation and Visible Photocatalytic Properties of N-Doped TiO<sub>2</sub>/Muscovite Nanocomposites. *Clays Clay Miner.* **2021**, *69*, 254–262. [[CrossRef](#)]
217. Bruce, R.M.; Santodonato, J.; Neal, M.W. Summary Review of the Health Effects Associated With Phenol. *Toxicol. Ind. Health* **1987**, *3*, 535–568. [[CrossRef](#)] [[PubMed](#)]
218. Ilisz, I.; Dombi, A.; Mogyorósi, K.; Dékány, I. Photocatalytic water treatment with different TiO<sub>2</sub> nanoparticles and hydrophilic/hydrophobic layer silicate adsorbents. *Colloids Surf. A Physicochem. Eng. Asp.* **2004**, *230*, 89–97. [[CrossRef](#)]
219. Pichat, P.; Khalaf, H.; Tabet, D.; Houari, M.; Saidi, M. Ti-montmorillonite as photocatalyst to remove 4-chlorophenol in water and methanol in air. *Environ. Chem. Lett.* **2005**, *2*, 191–194. [[CrossRef](#)]

220. Zhu, H.Y.; Li, J.Y.; Zhao, J.C.; Churchman, G.J. Photocatalysts prepared from layered clays and titanium hydrate for degradation of organic pollutants in water. *Appl. Clay Sci.* **2005**, *28*, 79–88. [[CrossRef](#)]
221. Kun, R.; Mogyorosi, K.; Dékány, I. Synthesis and structural and photocatalytic properties of TiO<sub>2</sub>/montmorillonite nanocomposites. *Appl. Clay Sci.* **2006**, *32*, 99–110. [[CrossRef](#)]
222. Ménesi, J.; Körösi, L.; Bazsó, É.; Zöllmer, V.; Richardt, A.; Dékány, I. Photocatalytic oxidation of organic pollutants on titania–clay composites. *Chemosphere* **2008**, *70*, 538–542. [[CrossRef](#)] [[PubMed](#)]
223. Chen, J.; Liu, X.; Li, G.; Nie, X.; An, T.; Zhang, S.; Zhao, H. Synthesis and characterization of novel SiO<sub>2</sub> and TiO<sub>2</sub> co-pillared montmorillonite composite for adsorption and photocatalytic degradation of hydrophobic organic pollutants in water. *Catal. Today* **2011**, *164*, 364–369. [[CrossRef](#)]
224. Manova, E.; Aranda, P.; Angeles Martín-Luengo, M.; Letaief, S.; Ruiz-Hitzky, E. New titania-clay nanostructured porous materials. *Microporous Mesoporous Mater.* **2010**, *131*, 252–260. [[CrossRef](#)]
225. Yang, X.; Zhu, H.; Liu, J.; Gao, X.; Martens, W.N.; Frost, R.L.; Shen, Y.; Yuan, Z. A mesoporous structure for efficient photocatalysts: Anatase nanocrystals attached to leached clay layers. *Microporous Mesoporous Mater.* **2008**, *112*, 32–44. [[CrossRef](#)]
226. Xuzhuang, Y.; Yang, D.; Huaiyong, Z.; Jiangwen, L.; Martins, W.N.; Frost, R.; Daniel, L.; Yuenian, S. Mesoporous Structure with Size Controllable Anatase Attached on Silicate Layers for Efficient Photocatalysis. *J. Phys. Chem. C* **2009**, *113*, 8243–8248. [[CrossRef](#)]
227. Décsiné Gombos, E.; Krakkó, D.; Záray, G.; Illés, Á.; Dóbe, S.; Szegedi, Á. Laponite immobilized TiO<sub>2</sub> catalysts for photocatalytic degradation of phenols. *J. Photochem. Photobiol. A: Chem.* **2020**, *387*, 112045. [[CrossRef](#)]
228. Carriazo, J.G.; Moreno-Forero, M.; Molina, R.A.; Moreno, S. Incorporation of titanium and titanium–iron species inside a smectite-type mineral for photocatalysis. *Appl. Clay Sci.* **2010**, *50*, 401–408. [[CrossRef](#)]
229. Zhang, L.; Liu, J.; Tang, C.; Lv, J.; Zhong, H.; Zhao, Y.; Wang, X. Palygorskite and SnO<sub>2</sub>–TiO<sub>2</sub> for the photodegradation of phenol. *Appl. Clay Sci.* **2011**, *51*, 68–73.
230. Rath, B.S.; Kumar, P.S.; Show, P.L. A Review on Effective Removal of Emerging Contaminants from Aquatic Systems: Current Trends and Scope for Further Research. *J. Hazard. Mater.* **2021**, *409*, 124413. [[CrossRef](#)]
231. Ooka, C.; Yoshida, H.; Horio, M.; Suzuki, K.; Hattori, T. Adsorptive and photocatalytic performance of TiO<sub>2</sub> pillared montmorillonite in degradation of endocrine disruptors having different hydrophobicity. *Appl. Catal. B-Environ.* **2003**, *41*, 313–321. [[CrossRef](#)]
232. Sasai, R.; Watanabe, R.; Yamada, T. Preparation and characterization of titania- and organo-pillared clay hybrid photocatalysts capable of oxidizing aqueous bisphenol A under visible light. *Appl. Clay Sci.* **2014**, *93–94*, 72–77. [[CrossRef](#)]
233. Belver, C.; Bedia, J.; Rodriguez, J.J. Zr-doped TiO<sub>2</sub> supported on delaminated clay materials for solar photocatalytic treatment of emerging pollutants. *J. Hazard. Mater.* **2017**, *322*, 233–242. [[CrossRef](#)]
234. Tobajas, M.; Belver, C.; Rodriguez, J.J. Degradation of emerging pollutants in water under solar irradiation using novel TiO<sub>2</sub>-ZnO/clay nanoarchitectures. *Chem. Eng. J.* **2017**, *309*, 596–606. [[CrossRef](#)]
235. Belver, C.; Hinojosa, M.; Bedia, J.; Tobajas, M.; Alvarez, M.; Rodríguez-González, V.; Rodriguez, J. Ag-Coated Heterostructures of ZnO-TiO<sub>2</sub>/Delaminated Montmorillonite as Solar Photocatalysts. *Materials* **2017**, *10*, 960. [[CrossRef](#)] [[PubMed](#)]
236. Vaizogullar, A.İ. TiO<sub>2</sub>/ZnO Supported on Sepiolite: Preparation, Structural Characterization, and Photocatalytic Degradation of Flumequine Antibiotic in Aqueous Solution. *Chem. Eng. Commun.* **2017**, *204*, 689–697. [[CrossRef](#)]
237. Li, C.; Sun, Z.; Zhang, W.; Yu, C.; Zheng, S. Highly efficient g-C<sub>3</sub>N<sub>4</sub>/TiO<sub>2</sub>/kaolinite composite with novel three-dimensional structure and enhanced visible light responding ability towards ciprofloxacin and *S. aureus*. *Appl. Catal. B-Environ.* **2018**, *220*, 272–282. [[CrossRef](#)]
238. Hu, X.; Sun, Z.; Song, J.; Zhang, G.; Li, C.; Zheng, S. Synthesis of novel ternary heterogeneous BiOCl/TiO<sub>2</sub>/sepiolite composite with enhanced visible-light-induced photocatalytic activity towards tetracycline. *J. Colloid Interface Sci.* **2019**, *533*, 238–250. [[CrossRef](#)]
239. Belessi, V.; Lambropoulou, D.; Konstantinou, I.; Katsoulidis, A.; Pomonis, P.; Petridis, D.; Albanis, T. Structure and photocatalytic performance of TiO<sub>2</sub>/clay nanocomposites for the degradation of dimethachlor. *Appl. Catal. B-Environ.* **2007**, *73*, 292–299. [[CrossRef](#)]
240. Paul, B.; Martens, W.N.; Frost, R.L. Immobilised anatase on clay mineral particles as a photocatalyst for herbicides degradation. *Appl. Clay Sci.* **2012**, *57*, 49–54. [[CrossRef](#)]
241. Belver, C.; Han, C.; Rodriguez, J.J.; Dionysiou, D.D. Innovative W-doped titanium dioxide anchored on clay for photocatalytic removal of atrazine. *Catal. Today* **2017**, *280*, 21–28. [[CrossRef](#)]
242. Feroso, J.; Sánchez, B.; Suarez, S. Air purification applications using photocatalysis. In *Nanostructured Photocatalysts*; Boukherroub, R., Ogale, S.B., Robertson, N., Eds.; Elsevier: Amsterdam, The Netherlands, 2020; pp. 99–128.
243. Ooka, C. Effect of surface hydrophobicity of TiO<sub>2</sub>-pillared clay on adsorption and photocatalysis of gaseous molecules in air. *Appl. Catal. A-Gen.* **2004**, *260*, 47–53. [[CrossRef](#)]
244. Kibanova, D.; Cervini-Silva, J.; Destailats, H. Efficiency of Clay–TiO<sub>2</sub> Nanocomposites on the Photocatalytic Elimination of a Model Hydrophobic Air Pollutant. *Environ. Sci. Technol.* **2009**, *43*, 1500–1506. [[CrossRef](#)]
245. Kibanova, D.; Trejo, M.; Destailats, H.; Cervini-Silva, J. Synthesis of hectorite-TiO<sub>2</sub> and kaolinite-TiO<sub>2</sub> nanocomposites with photocatalytic activity for the degradation of model air pollutants. *Appl. Clay Sci.* **2009**, *42*, 563–568. [[CrossRef](#)]

246. Kibanova, D.; Sleiman, M.; Cervini-Silva, J.; Destailats, H. Adsorption and photocatalytic oxidation of formaldehyde on a clay-TiO<sub>2</sub> composite. *J. Hazard. Mater.* **2012**, *211*, 233–239. [[CrossRef](#)] [[PubMed](#)]
247. Lim, M.; Zhou, Y.; Wood, B.; Wang, L.Z.; Rudolph, V.; Lu, G.Q. (Max). Highly Thermostable Anatase Titania-Pillared Clay for the Photocatalytic Degradation of Airborne Styrene. *Environ. Sci. Technol.* **2009**, *43*, 538–543. [[CrossRef](#)]
248. Papoulis, D.; Komarneni, S.; Panagiotaras, D.; Stathatos, E.; Toli, D.; Christoforidis, K.C.; Fernández-García, M.; Li, H.; Yin, S.; Sato, T. Halloysite–TiO<sub>2</sub> nanocomposites: Synthesis, characterization and photocatalytic activity. *Appl. Catal. B-Environ.* **2013**, *132*, 416–422. [[CrossRef](#)]
249. Papoulis, D.; Komarneni, S.; Panagiotaras, D.; Nikolopoulou, A.; Christoforidis, K.; Fernández-García, M.; Li, H.; Shu, Y.; Sato, T. Palygorskite–TiO<sub>2</sub> nanocomposites: Part 2. photocatalytic activities in decomposing air and organic pollutants. *Appl. Clay Sci.* **2013**, *83*, 198–202. [[CrossRef](#)]
250. Papoulis, D.; Komarneni, S.; Panagiotaras, D.; Stathatos, E.; Christoforidis, K.C.; Fernández-García, M.; Li, H.; Shu, Y.; Sato, T.; Katsuki, H. Three-phase nanocomposites of two nanoclays and TiO<sub>2</sub>: Synthesis, characterization and photocatalytic activities. *Appl. Catal. B Environ.* **2014**, *147*, 526–533. [[CrossRef](#)]
251. Liu, R.; Wang, J.; Zhang, J.; Xie, S.; Wang, X.; Ji, Z. Honeycomb-like micro-mesoporous structure TiO<sub>2</sub>/sepiolite composite for combined chemisorption and photocatalytic elimination of formaldehyde. *Microporous Mesoporous Mater.* **2017**, *248*, 234–245. [[CrossRef](#)]
252. Portela, R.; Jansson, I.; Suárez, S.; Villarroel, M.; Sánchez, B.; Avila, P. Natural silicate-TiO<sub>2</sub> hybrids for photocatalytic oxidation of formaldehyde in gas phase. *Chem. Eng. J.* **2017**, *310*, 560–570. [[CrossRef](#)]
253. Zhang, G.; Wang, H.; Guo, S.; Wang, J.; Liu, J. Synthesis of Cu/TiO<sub>2</sub>/organo-attapulgite fiber nanocomposite and its photocatalytic activity for degradation of acetone in air. *Appl. Surf. Sci.* **2016**, *362*, 257–264. [[CrossRef](#)]
254. Suárez, S.; Coronado, J.M.; Portela, R.; Martín, J.C.; Yates, M.; Avila, P.; Sánchez, B. On the Preparation of TiO<sub>2</sub>–Sepiolite Hybrid Materials for the Photocatalytic Degradation of TCE: Influence of TiO<sub>2</sub> Distribution in the Mineralization. *Environ. Sci. Technol.* **2008**, *42*, 5892–5896. [[CrossRef](#)] [[PubMed](#)]
255. Hewer, T.L.R.; Suárez, S.; Coronado, J.M.; Portela, R.; Avila, P.; Sanchez, B. Hybrid photocatalysts for the degradation of trichloroethylene in air. *Catal. Today* **2009**, *143*, 302–308. [[CrossRef](#)]
256. Suárez, S.; Hewer, T.L.R.; Portela, R.; Hernández-Alonso, M.D.; Freire, R.S.; Sánchez, B. Behaviour of TiO<sub>2</sub>–SiMgO<sub>x</sub> hybrid composites on the solar photocatalytic degradation of polluted air. *Appl. Catal. B-Environ.* **2011**, *101*, 176–182. [[CrossRef](#)]
257. Chen, J.; Li, G.; He, Z.; An, T. Adsorption and degradation of model volatile organic compounds by a combined titania–montmorillonite–silica photocatalyst. *J. Hazard. Mater.* **2011**, *190*, 416–423. [[CrossRef](#)]
258. Ma, J.; Zhu, C.; Lu, J.; Liu, H.; Huang, L.; Chen, T.; Chen, D. Catalytic degradation of gaseous benzene by using TiO<sub>2</sub>/goethite immobilized on palygorskite: Preparation, characterization and mechanism. *Solid State Sci.* **2015**, *49*, 1–9. [[CrossRef](#)]
259. Russell, H.S.; Frederickson, L.B.; Hertel, O.; Ellerman, T.; Jensen, S.S. A Review of Photocatalytic Materials for Urban NO<sub>x</sub> Remediation. *Catalysts* **2021**, *11*, 675. [[CrossRef](#)]
260. Nikolopoulou, A.; Papoulis, D.; Komarneni, S.; Tsolis-Katagas, P.; Panagiotaras, D.; Kacandes, G.H.; Zhang, P.; Yin, S.; Sato, T. Solvothermal preparation of TiO<sub>2</sub>/saponite nanocomposites and photocatalytic activity. *Appl. Clay Sci.* **2009**, *46*, 363–368. [[CrossRef](#)]
261. Papoulis, D.; Komarneni, S.; Nikolopoulou, A.; Tsolis-Katagas, P.; Panagiotaras, D.; Kacandes, H.G.; Zhang, P.; Yin, S.; Sato, T.; Katsuki, H. Palygorskite- and Halloysite-TiO<sub>2</sub> nanocomposites: Synthesis and photocatalytic activity. *Appl. Clay Sci.* **2010**, *50*, 118–124. [[CrossRef](#)]
262. Papoulis, D.; Somalaki, K.; Todorova, N.; Trapalis, C.; Panagiotaras, D.; Sygkridou, D.; Stathos, E.; Gianni, E.; Mavrikos, A.; Komarneni, S. Sepiolite/TiO<sub>2</sub> and metal ion modified sepiolite/TiO<sub>2</sub> nanocomposites: Synthesis, characterization and photocatalytic activity in abatement of NO<sub>x</sub> gases. *Appl. Clay Sci.* **2019**, *179*, 105156. [[CrossRef](#)]
263. Todorova, N.; Giannakopoulou, T.; Karapati, S.; Petridis, D.; Vaimakis, T.; Trapalis, C. Composite TiO<sub>2</sub>/clays materials for photocatalytic NO<sub>x</sub> oxidation. *Appl. Surf. Sci.* **2014**, *319*, 113–120.
264. Bloh, J.Z.; Folli, A.; Macphee, D.E. Photocatalytic NO<sub>x</sub> abatement: Why the selectivity matters. *RSC Adv.* **2014**, *4*, 45726–45734. [[CrossRef](#)]